The Slow Drift Motions of Offshore Structures

by

Ole Johannes Emmerhoff

Sivilingeniør, Norwegian Institute of Technology (NTH), 1989

Submitted to the Department of Ocean Engineering
in partial fulfillment of the requirements for the degree of

Doctor of Philosophy in Hydrodynamics

at the

MASSACHUSETTS INSTITUTE OF TECHNOLOGY

September 1994

Author .....
Department of Ocean Engineering
9 September, 1994

Certified by .....
Paul D. Sclavounos
Professor of Ocean Engineering
Thesis Supervisor

Accepted by .....
A. Douglas Carmichael
Chairman, Departmental Committee on Graduate Students

The Slow Drift Motions of Offshore Structures

by

Ole Johannes Emmerhoff

Submitted to the Department of Ocean Engineering
on 9 September, 1994, in partial fulfillment of the
requirements for the degree of
Doctor of Philosophy in Hydrodynamics

Abstract

The large amplitude surge-sway-yaw 'slow-drift' motions of a floating body constrained by weak restoring forces in random waves are considered. A multiple time scales approximation is employed to separate the fast time scale associated with the linear motions from the slowly varying motions. The ideal fluid free surface flow is approximated by a perturbation series expansion for small slow-drift velocities and wave-steepness, and is solved around the instantaneous position of the body. The linear zero-speed and forward-speed velocity potentials are solved for arrays of vertical cylinders, using exact interaction theory. The horizontal mean drift forces and the wave-drift damping are obtained, and results for realistic configurations are compared with well-established methods.

The surge-sway-yaw equations of the slow-drift motions are solved numerically in the time domain under the influence of short-crested, random waves, including viscous forces. The random wave-signal is generated by the filtering of white Gaussian noise. The slowly-varying forces are obtained using the Newman approximation and double summations of time series. The use of a robust random number generator and the Fast Fourier Transform allows for efficient simulations of long records of the slow-drift motions, and the study of its statistical parameters. The sensitivity upon the simulation length, transients, drag-coefficient and directional spreading are demonstrated.

Thesis Supervisor: Paul D. Sclavounos
Title: Professor of Ocean Engineering

Acknowledgments

I wish to thank my advisor Professor Paul D. Sclavounos for all that he has taught me through these years at MIT. I will always remember his patience, encouragement and generosity. I am also very thankful for the encouragement and valuable comments I received from the committee members, Professor J. H. Milgram and Professor J. N. Newman.

I am most thankful to my wife Cheryl for her unconditional love and care. She was always by my side and made this work possible. Our son Kurt Aron came with joy, happiness and wisdom.

I am grateful to my parents, Anders and Ruth, and my sisters Karoline and Anne Berit and my brother Reinert, and their families, for their unending support and encouragement.

My thanks are extended to the people of the 'free surface group', who created a friendly environment to work in. And many thanks to the 'basketball-boys' for all the fun games we had on the court. It was good to get the mind off hydrodynamics and on to something more mindless.

The financial support was provided by the MIT Sea Grant College Program and by a consortium of industrial sponsors of the SWIM (Slow Wave Induced Motion) Project, consisting of Aker, Amoco, Conoco, Norsk Hydro, Norwegian Contractors, Saga, Statoil and Veritas Research. Their support is greatly appreciated.

Contents

List of Figures

Chapter 1

Introduction

The purpose of this thesis was to develop a method for evaluating the slow-drift motions of floating offshore structures.

Floating production systems have become a very important part of the exploration and extraction of hydrocarbons from the sea-bottom, and are considered the only feasible solution for safe and cost efficient oil and gas production at large depth. Unlike gravity platforms, such systems undergo large excursions from their mean position, due to the influence of wind, waves and current. It is vital for the design of moorings and riser systems that the magnitude of the motions are predicted well and that they are kept within preset bounds.

The motions of moored floating platforms in deep water are typically characterized by two distinct time-scales; the fast and the slow time-scales. The former is of the order of 10 seconds, which is the dominant period in the wave-spectrum. The slow time-scale is defined by the natural period of the system, which is an order of magnitude larger than the wave-frequency due to relatively large mass of the system and weak restoring forces. The fast-scale motions are typically much smaller than the slow-scale (slow-drift) motions, which are caused by slowly varying forces from the environments. A major contribution comes from the second-order difference frequency forces, which are due to the interactions of waves with nearly equal frequencies. The wind and current do also contribute to the excitation of the system. The resonant slow-drift motions are only bounded by the relevant hydrodynamic damp-

ing of the system. The damping is due to both ideal fluid effects and the damping associated with the viscosity of the fluid. Ideal fluid effects are dominated by the wave-drift damping, which is linear in the slow-drift velocity and second-order in the wave-amplitude. The viscous forces mainly arise from the flow-separation around the structure and also by the non-linear forces on the mooring lines. The main part of this thesis is devoted to the second-order forces, in particular the wave-drift damping. Viscous effects are included via a Morison type force in the simulations of motions.

A large number of articles have been devoted to the second-order wave forces which do not depend on the forward-speed. A partial list of studies includes, Pinkster and Van Oortmerssen (1977), Faltinsen and Løken (1978), Molin (1978), Ogilvie (1983), Eatock Taylor and Hung (1985), Korsmeyer, Lee, Newman and Sclavounos (1988), Sclavounos (1988), Chau (1989), Nielsen, Herfjord and Løken (1990), Kim and Yue (1990) and Lee, Newman, Kim and Yue (1991).

The wave-drift damping is defined as the damping force proportional to the forward speed U and the wave-amplitude squared for small U. The relevance of the damping term was first introduced by Wichers and Sluijs (1979) upon their experiments of the extinction rate of ship model motions in calm water and in waves. Several theoretical studies have followed, where the diffraction problem has been studied with a small forward translation of the body. The derivative of the resulting mean force with respect to U is either derived analytically (Nossen, Grue & Palm 1991; Newman 1993) or by numerical differentiation from computations with small forward speed (Zhao & Faltinsen 1989). The wave-drift damping is derived analytically in the present study. Except for Newman (1993), the above studies accounted for the forward speed in a quasi-steady manner, by considering the added resistance of the body in waves due to a small forward translation. In Newman (1993), the wave-drift damping was derived from a perturbation analysis where the low-frequency body oscillations were superposed on the diffraction field. The results for the wave-drift damping was found to be identical to results of the present study. The wave-drift damping moment due to a slow yaw rotation is of similar interest as the wave-drift damping due to a slow translation. The effects of a slow yaw rotation was stud-

ied in Newman (1993) and Palm & Grue (1994). The slow-drift motion in all three horizontal modes of motion (surge, sway and yaw) are included in the present study.

The motions of floating structures in real sea-states are considered random processes, due to the random excitation and damping of the system. It is therefore necessary to get sufficient information about the statistical properties of the motions in order to predict extreme motions. There exist statistical models, based on the statistical properties of the driving forces of the system (Johnsen & Naess, 1991). The applicability of the models are limited, however, due to simplifications of the physical model and the complications of solving the Fokker-Planck (-Kolmogorov) equation for multi degree-of-freedom systems. Slow-drift motions in the frequency domain are also used in the design of floating production systems. A major limitation of this method is that it accepts only linear terms in the motions, which excludes, for example, responses to Morison type drag forces. The use of time-simulations combined with statistical models have proven valuable in the predictions of extreme motions, due to their flexibility with respect to non-linearities in the physical model. The slow time-scale of the slow-drift motions require however that the length of the simulations are very long, in order to obtain useful information about the statistical properties. The hydrodynamic forces are obtained from time-series of the frequency-domain forces, since the direct solution of the linear and second-order problem in the time-domain would lead to a prohibitive computational task.

In the current study, an efficient routine has been developed for the simulation of the slow-drift motions. Realizations of the random wave-elevation is achieved by the filtering of white Gaussian noise and the second-order forces are evaluated by the use of products of single Fast Fourier Transforms.

Chapter 2 formulates the boundary value problem of a general body with a slow translation in surge and sway and slow rotation in yaw. A perturbation expansion is proposed in the small wave-amplitude A and the surge-sway-yaw slow-drift velocities U, V and Ω, respectively.

Chapter 3 derives the analytic solutions of the linear zero-speed and forward-speed potentials for arrays of vertical cylinders, employing the theory of Linton &

Evans. The body is allowed to oscillate about its mean position with small amplitude (linear) motions in surge, sway and yaw.

Chapter 4 presents the hydrodynamic forces on the body in regular waves. The expressions for the linear and second-order mean forces are first obtained by pressure integration. The wave-drift damping is obtained by the momentum conservation, and the proof of a conservation law, which enables the far-field expressions to be evaluated on the body, is presented.

Chapter 5 illustrates the forces and motions in the frequency-domain of a few geometries.

Chapter 6 presents the equations of the slow-drift motions in the time-domain. The methodology of generating the random wave-elevation and second-order forces are also presented.

Chapter 7 illustrates the results of time-simulations of a platform in a real sea-state. The sensitivities of several parameters upon the slow-drift motions are studied.

Chapter 8 gives an overview of the thesis and compares the method with previous studies. Some extensions of the present method are discussed.

Chapter 2

Mathematical formulation

This chapter derives the leading order boundary value problem for a structure undergoing large-amplitude translations in surge and sway and rotations in yaw due to the interactions with gravity waves. The structure is free to oscillate at the wave-frequency in all six degrees of freedom about the instantaneous slow-drift position.

An inertial Cartesian coordinate system $\boldsymbol{X} = (X, Y, Z)$ is defined at the mean undisturbed position of the structure, with the Z-axis pointing upwards and the $Z = 0$ plane coinciding with the calm water surface. A second Cartesian system $\boldsymbol{x} = (x, y, z)$ is fixed on the mean slow-drift position of the structure. The vector $\boldsymbol{X}_\circ = (X_\circ(t), Y_\circ(t), 0)$ defines the position of the origin of the slow-drift frame relative to the inertial frame. The respective slow-drift velocity $\boldsymbol{u}$ and rotation $\boldsymbol{\Omega}$ are defined by

$$\begin{aligned} \boldsymbol{u} \equiv (u, v, 0)^T &= \left(\frac{\mathrm{d}X_\circ(t)}{\mathrm{d}t}, \frac{\mathrm{d}Y_\circ(t)}{\mathrm{d}t}, 0 \right)^T, \\ \boldsymbol{\Omega} \equiv (0, 0, \Omega)^T &= \left(0, 0, \frac{\mathrm{d}\Theta(t)}{\mathrm{d}t} \right)^T. \end{aligned} \tag{2.1}$$

The coordinates in the slow-drift system are related to the inertial coordinates by

$$\boldsymbol{x} = [S](\boldsymbol{X} - \boldsymbol{X}_\circ) \tag{2.2}$$

$$\boldsymbol{X} = \boldsymbol{X}_\circ + [S]^T \boldsymbol{x} \tag{2.3}$$

where $[S]$ is the transformation matrix defined by

$$[S] = \begin{bmatrix} \cos\Theta & \sin\Theta & 0 \\ -\sin\Theta & \cos\Theta & 0 \\ 0 & 0 & 1 \end{bmatrix}, \tag{2.4}$$

which has the property $[S]^{-1} = [S]^T$.

The boundary value problem will be formulated in the slow-drift coordinate system (x, y, z). Denoting by $\boldsymbol{U} = (U, V, 0)^T$ the slow-drift velocities along the (x, y, z) axis, it follows that

$$\boldsymbol{u} = [S]^T \boldsymbol{U}. \tag{2.5}$$

The slow-drift yaw rotation velocity $\boldsymbol{\Omega}$ is the same for both coordinate systems.

In the two following sections, the boundary value problem for small wave amplitudes and slow-drift velocities will be derived to leading order.

2.1 Free surface conditions

Assume irrotational flow and introduce a velocity potential $\Phi(\boldsymbol{X}, t)$ satisfying the Laplace equation

$$\nabla^2\Phi = 0 \tag{2.6}$$

and the nonlinear free-surface condition

$$\frac{\mathrm{d}^2\Phi}{\mathrm{d}t^2} + g\Phi_z + 2\nabla\Phi \cdot \frac{\mathrm{d}\nabla\Phi}{\mathrm{d}t} + \tfrac{1}{2}\nabla\Phi \cdot \nabla(\nabla\Phi \cdot \nabla\Phi) = 0 \tag{2.7}$$

enforced on the exact position of the free surface $z = \zeta(X, Y, t)$ defined by

$$\zeta = -\frac{1}{g}\left(\frac{\mathrm{d}\Phi}{\mathrm{d}t} + \tfrac{1}{2}\nabla\Phi \cdot \nabla\Phi\right)_{z=\zeta}, \tag{2.8}$$

where g is the acceleration of gravity and all time derivatives are understood with respect to the inertial frame.

Let $\phi(\boldsymbol{x}, t) = \Phi(\boldsymbol{X}, t)$ be the velocity potential with respect to the body fixed coordinates. Time derivatives between the two coordinate systems are related by the Galilean transformation

$$\frac{d\Phi}{dt} = \left[\frac{\partial}{\partial t} - \boldsymbol{f}\cdot\Delta\right]\phi, \tag{2.9}$$

where

$$\boldsymbol{f}\cdot\Delta \;\equiv\; (U - \Omega y)\frac{\partial}{\partial x} + (V + \Omega x)\frac{\partial}{\partial y}. \tag{2.10}$$

The time derivative on the left hand side of equation (2.9) is with respect to the inertial reference frame. The substitution of $\phi(\boldsymbol{x}, t) = \Phi(\boldsymbol{X}, t)$ and the Galilean transformation into equations (2.7)-(2.8) allows us to express the boundary-value problem with respect to the body fixed coordinates.

Two independently small parameters are introduced, the characteristic wave slope δ and the slow-drift parameter τ_j. The latter represents the slow-drift velocities and is defined as: $\tau_1 = \omega_0 U/g$, $\tau_2 = \omega_0 V/g$ and $\tau_3 = \omega_0 \Omega d/g$, where ω_0 is a typical wave frequency and d is a typical spacing between the cylinders. In the following equations, terms that contain τ_j must be summed over $j = 1, 2, 3$. Small values of τ_j correspond to small slow-drift velocities relative to the phase velocity g/ω_0 of the wave. The characteristic frequency for all three modes of the slowly varying motions is an order of magnitude smaller than ω_0, and terms proportional to $\mathrm{d}U/\mathrm{d}t$, $\mathrm{d}V/\mathrm{d}t$ and $\mathrm{d}\Omega/\mathrm{d}t$ are therefore neglected in the following analysis. Interactions among the slow-drift velocities, of $O(\tau_i\tau_j)$ are also neglected.

Assume the existence of a perturbation series expansion for the velocity potential and the wave elevation,

$$\phi(\boldsymbol{x},t) = \underbrace{\phi_{01}(\boldsymbol{x},t)}_{O(\tau_j)} + \underbrace{\phi_{10}(\boldsymbol{x},t)}_{O(\delta)} + \underbrace{\phi_{11}(\boldsymbol{x},t)}_{O(\delta\tau_j)} + \underbrace{\phi_{20}(\boldsymbol{x},t)}_{O(\delta^2)} + \underbrace{\phi_{21}(\boldsymbol{x},t)}_{O(\delta^2\tau_j)} + \cdots \tag{2.11}$$

$$\zeta(x,y,t) = \underbrace{\zeta_{10}(x,y,t)}_{O(\delta)} + \underbrace{\zeta_{11}(x,y,t)}_{O(\delta\tau_j)} + \underbrace{\zeta_{20}(x,y,t)}_{O(\delta^2)} + \underbrace{\zeta_{21}(x,y,t)}_{O(\delta^2\tau_j)} + \cdots \tag{2.12}$$

The first index in the velocity potentials and wave elevations corresponds to δ and the second to τ_j. A Taylor expansion of the right-hand side of (2.8) about the $z = 0$ plane and substitution of (2.11) and (2.12) in both sides of the equation, leads to the following definition for the two first wave elevations ζ_{ij}:

$$\zeta_{10} = -\frac{1}{g}\left(\frac{\partial\phi_{10}}{\partial t}\right)_{z=0} \tag{2.13}$$

$$\zeta_{11} = -\frac{1}{g}\left(\frac{\partial\phi_{11}}{\partial t} - \boldsymbol{f}\cdot\Delta\phi_{10} + \nabla\phi_{10}\cdot\nabla\phi_{01}\right)_{z=0}. \tag{2.14}$$

A similar Taylor series expansion of the free-surface condition (2.7) combined with the Galilean transformation (2.9) and the wave elevations (2.13), (2.14) leads to a sequence of free-surface boundary conditions for the velocity potentials ϕ_{ij} applied on the $z = 0$ plane:

$$\frac{\partial\phi_{01}}{\partial z} = 0, \tag{2.15}$$

$$\frac{\partial^2\phi_{10}}{\partial t^2} + g\frac{\partial\phi_{10}}{\partial z} = 0, \tag{2.16}$$

$$\frac{\partial^2\phi_{11}}{\partial t^2} + g\frac{\partial\phi_{11}}{\partial z} = 2\boldsymbol{f}\cdot\Delta\frac{\partial\phi_{10}}{\partial t} + \frac{\partial\phi_{10}}{\partial t}\frac{\partial^2\phi_{01}}{\partial z^2} - 2\nabla\phi_{01}\cdot\frac{\partial\nabla\phi_{10}}{\partial t}, \tag{2.17}$$

$$g\frac{\partial\bar{\phi}_{20}}{\partial z} = -\overline{\frac{\partial}{\partial t}(\nabla\phi_{10}\cdot\nabla\phi_{10})} + \overline{\frac{1}{g}\frac{\partial\phi_{10}}{\partial t}\frac{\partial}{\partial z}\left[\frac{\partial^2\phi_{10}}{\partial t^2} + g\frac{\partial\phi_{10}}{\partial z}\right]}, \tag{2.18}$$

where $\boldsymbol{f}\cdot\Delta$ is defined in equation (2.10), $\bar{\phi}_{20}$ is the steady part of ϕ_{20} and the over bar means average with respect to time.

The double-body potential ϕ_{01} is the leading order approximation for the steady flow for small τ_j. ϕ_{10} and ϕ_{11} are linear in δ and represent the zero speed potential and its leading forward speed correction, respectively. It would in principal be necessary to include both of the second order potentials ϕ_{20} and ϕ_{21} in the analysis in order to calculate the leading order exciting forces and damping coefficients in the slow time scale. In a narrow banded sea-state, however, we can make use of the Newman approximation for the slowly varying forces and thereby avoid solving for the time varying parts of the potentials ϕ_{20} and ϕ_{21}. Only the steady part of ϕ_{20} will be included, which appears in the expressions for the wave-drift damping forces. Terms of $O(\tau_j^2)$ may contribute to the slowly varying forces for finite values of τ_j, but are not considered in this study. Terms of $O(\delta\tau_j^2)$ do not contribute to the leading order forces in the slow time scale.

2.2 Body boundary conditions

The free-surface conditions (2.15)-(2.17) must be supplemented by a corresponding sequence of boundary conditions satisfied by the velocity potentials ϕ_{ij} on the body boundary. The conditions are derived along similar lines to Ogilvie (1983) and Sclavounos (1994).

The body boundary condition, which states that the normal velocity of the fluid must equal the normal velocity of the body boundary enforced on the exact position of the body, is written

$$\boldsymbol{N}\cdot\nabla\Phi = \boldsymbol{N}\cdot\boldsymbol{V}_b, \tag{2.19}$$

where $\boldsymbol{N} = (N_1, N_2, N_3)$ is a unit normal vector to the body surface pointing out of the fluid domain and $\boldsymbol{V}_b$ is the velocity of the body boundary. The equation is given

with respect to the inertial system. We will derive the boundary conditions for ϕ_{ij} in the slow-drift frame of reference, and must therefore define the normal vector and the velocity of the body boundary with respect to this frame.

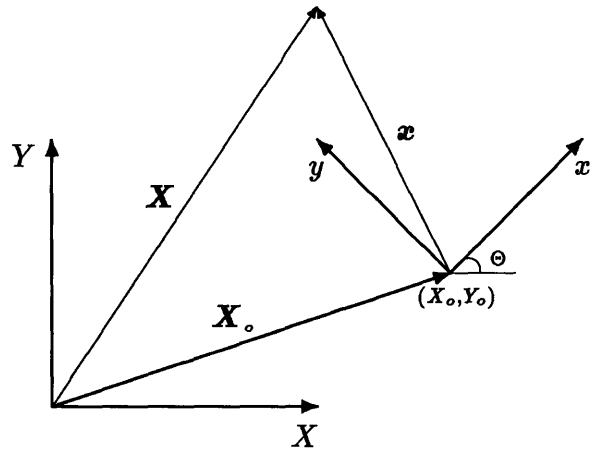

Figure 2-1: Definition of inertial and slow-drift coordinate-systems

Let $\boldsymbol{X}$ be the position of a point on the body relative to the inertial frame and $\boldsymbol{x}$ the corresponding point relative to the slow-drift frame, see Figure 2-1. If the point denoted by $\boldsymbol{x}$ moves in some prescribed way, we find the corresponding time derivative of $\boldsymbol{X}$ using equation (2.3):

$$\boldsymbol{V}_b = \dot{\boldsymbol{X}} = \dot{\boldsymbol{X}}_o + [S]^T\dot{\boldsymbol{x}} + \Omega\boldsymbol{k} \times (\boldsymbol{X} - \boldsymbol{X}_o), \tag{2.20}$$

where $\boldsymbol{k}$ is the unit vector in the z-direction and the dot $(\cdot)$ denotes differentiation with respect to time. In order to write $\boldsymbol{V}_b$ which is given with respect to the inertial frame in terms of the slow-drift coordinates, we use the relation

$$\boldsymbol{V}_b = [S]^T\boldsymbol{v}_b, \tag{2.21}$$

where $\boldsymbol{v}_b$ is the velocity of the body in terms of the slow-drift coordinates. Trans-

forming equation (2.20) into the slow-drift frame then gives

$$\boldsymbol{v}_b = \dot{\boldsymbol{x}} + \boldsymbol{U} + \Omega \boldsymbol{k} \times \boldsymbol{x}, \tag{2.22}$$

where $\boldsymbol{U}$ is defined in equation (2.5). Going back to equation (2.19), we have that $\boldsymbol{N} \cdot \nabla\Phi = \boldsymbol{N} \cdot \boldsymbol{V}_b$ on the body boundary with respect to the inertial frame. Since these are scalar quantities, we also have

$$\boldsymbol{n} \cdot \nabla\phi = \boldsymbol{n} \cdot \boldsymbol{v}_b, \tag{2.23}$$

on the body with respect to the slow-drift frame. $\boldsymbol{n} = (n_1, n_2, n_3)$ is here the unit normal vector in the slow-drift frame.

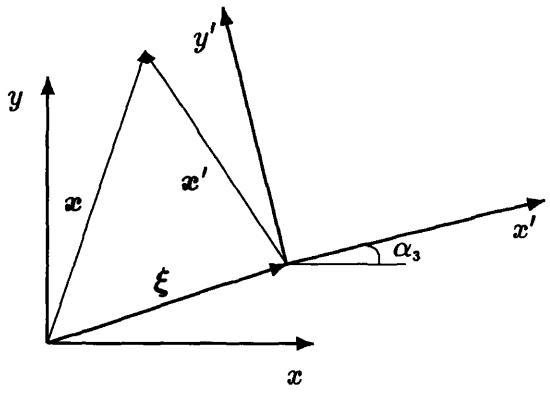

Figure 2-2: Definition of slow-drift and body-fixed coordinate-systems

We now want to expand the quantity $(\nabla\phi - \boldsymbol{v}_b)$ in a Taylor series about the slow-drift frame, since the body undergoes small amplitude oscillations $\boldsymbol{\xi} = (\xi_1, \xi_2, \xi_3)$ along the (x, y, z) axis and the small amplitude rotations $\boldsymbol{\alpha} = (\alpha_1, \alpha_2, \alpha_3)$ about the (x, y, z) axis, respectively of $O(\delta)$. Define $\boldsymbol{x}' = (x', y', z')$ to be a point on the body in the body fixed coordinate system, see Figure 2-2, and $\boldsymbol{n}'$ the corresponding unit normal vector. The equations for $\boldsymbol{x}$ and $\boldsymbol{n}$ with respect to the body-fixed frame are

then

$$\boldsymbol{x} = \boldsymbol{x}' + \boldsymbol{\xi} + \boldsymbol{\alpha} \times \boldsymbol{x}', \tag{2.24}$$

$$\boldsymbol{n} = \boldsymbol{n}' + \boldsymbol{\alpha} \times \boldsymbol{n}', \tag{2.25}$$

where we have neglected terms of $O(\delta^2)$. Applying the vector form of Taylor's theorem for $(\nabla\phi - \boldsymbol{v}_b)$ in equation (2.23), where the distance between the 'exact' body surface and the slow-drift surface is given by $\boldsymbol{x} - \boldsymbol{x}'$, leads to the following expression for the boundary conditions in the slow-drift frame

$$\begin{aligned}(\boldsymbol{n}' + \boldsymbol{\alpha} \times \boldsymbol{n}' + \cdots) \cdot (\nabla\phi + [(\boldsymbol{x} - \boldsymbol{x}') \cdot \nabla]\nabla\phi + \cdots) \; = \\ (\boldsymbol{n}' + \boldsymbol{\alpha} \times \boldsymbol{n}' + \cdots) \cdot (\dot{\boldsymbol{\xi}} + \dot{\boldsymbol{\alpha}} \times \boldsymbol{x}' + \boldsymbol{U} + \Omega\boldsymbol{k} \times \boldsymbol{x}),\end{aligned} \tag{2.26}$$

where equations (2.22), (2.24) and (2.25) were used. The boundary conditions for the potentials ϕ_{ij} can now be derived from equation (2.26) by expanding quantities that depend on the small parameters δ and τ_j. The expansion for ϕ is given in equation (2.11) and the linear motions $\boldsymbol{\xi}$ and $\boldsymbol{\alpha}$ by equation (4.21). Collecting terms of the same order gives the following set of boundary conditions for ϕ_{01}, ϕ_{10} and ϕ_{11}:

$O(\tau_j)$:

$$\begin{aligned}\boldsymbol{n} \cdot \nabla\phi_{01} &= \boldsymbol{n} \cdot (\boldsymbol{U} + \Omega\boldsymbol{k} \times \boldsymbol{x}), \\ &\Updownarrow \\ \frac{\partial\phi_{01}}{\partial n} &= Un_1 + Vn_2 + \Omega(xn_2 - yn_1).\end{aligned} \tag{2.27}$$

$O(\delta)$:

$$\begin{aligned}\boldsymbol{n} \cdot \nabla\phi_{10} &= \boldsymbol{n} \cdot (\dot{\boldsymbol{\xi}}^{(0)} + \dot{\boldsymbol{\alpha}}^{(0)} \times \boldsymbol{x}), \\ &\Updownarrow\end{aligned}$$

$$\frac{\partial \phi_{10}}{\partial n} = \dot{\xi}_j^{(0)} n_j + \dot{\alpha}_j^{(0)} (\boldsymbol{x} \times \boldsymbol{n})_j. \tag{2.28}$$

$O(\delta\tau_j)$:

$$\begin{aligned} \boldsymbol{n} \cdot \nabla \phi_{11} &= \boldsymbol{n} \cdot (-[(\boldsymbol{\xi}^{(0)} + \boldsymbol{\alpha}^{(0)} \times \boldsymbol{x}) \cdot \nabla] \nabla \phi_{01} + \dot{\boldsymbol{\xi}}^{(1)} + \dot{\boldsymbol{\alpha}}^{(1)} \times \boldsymbol{x}) \\ &\quad -\boldsymbol{\alpha}^{(0)} \times \boldsymbol{n} \cdot (\nabla \phi_{01} - \boldsymbol{U} - \Omega \boldsymbol{k} \times \boldsymbol{x}), \\ &\Updownarrow \\ \frac{\partial \phi_{11}}{\partial n} &= \dot{\xi}_j^{(1)} n_j + \dot{\alpha}_j^{(1)} (\boldsymbol{x} \times \boldsymbol{n})_j + \boldsymbol{\xi}^{(0)} \cdot (m_1, m_2, m_3) + \boldsymbol{\alpha}^{(0)} \cdot (m_4, m_5, m_6), \end{aligned} \tag{2.29}$$

where

$$(m_1, m_2, m_3) = -[(\boldsymbol{n} \cdot \nabla) \nabla \phi_{01}], \tag{2.30}$$

$$(m_4, m_5, m_6) = -[(\boldsymbol{n} \cdot \nabla)(\boldsymbol{x} \times \nabla \phi_{01}] + [\boldsymbol{n} \times (\boldsymbol{U} + \Omega \boldsymbol{k} \times \boldsymbol{x})]. \tag{2.31}$$

$O(\delta^2)$:

$$\begin{aligned} \boldsymbol{n} \cdot \nabla \bar{\phi}_{20} &= -\overline{\boldsymbol{\alpha} \times \boldsymbol{n} \cdot \nabla \phi_{10}} - \overline{\boldsymbol{n} \cdot [(\boldsymbol{\xi} + \boldsymbol{\alpha} \times \boldsymbol{x}) \cdot \nabla] \nabla \phi_{10}} + \overline{\boldsymbol{\alpha} \times \boldsymbol{n} \cdot (\dot{\boldsymbol{\xi}} + \dot{\boldsymbol{\alpha}} \times \boldsymbol{x})}, \\ &\Updownarrow \\ \frac{\partial \bar{\phi}_{20}}{\partial n} &= \overline{\boldsymbol{\alpha} \times \boldsymbol{n} \cdot [\dot{\boldsymbol{\xi}} + \dot{\boldsymbol{\alpha}} \times \boldsymbol{x} - \nabla \phi_{10}]} - \overline{\boldsymbol{n} \cdot [(\boldsymbol{\xi} + \boldsymbol{\alpha} \times \boldsymbol{x}) \cdot \nabla] \nabla \phi_{10}}. \end{aligned} \tag{2.32}$$

The primes on $\boldsymbol{n}$ and $\boldsymbol{x}$ have been left out in the above equations. All the above quantities are to be evaluated in the frame of reference which follows the slow-drift motions of the body.

The notation (2.30)-(2.31) was introduced by Ogilvie & Tuck (1969), and are referred to as the *m-terms*. The *m-terms* are due to the interactions between the linear body motions and the steady flow. Some algebra was required to obtain (2.30)-(2.31) from (2.29), and is shown in Appendix B.

Except for differences of notation the boundary conditions for ϕ_{11} are identical to equation (2.37) of Sclavounos (1994). The boundary conditions for $\bar{\phi}_{20}$ are identical to equation (12) of Grue and Palm (1993).

In addition to the free-surface and the body boundary conditions, the potentials ϕ_{ij} also satisfy proper radiation conditions in the far-field, and the bottom boundary condition

$$\frac{\partial \phi_{ij}}{\partial n} = 0, \qquad \text{on } z = -h, \tag{2.33}$$

where h is the water-depth.

Chapter 3

Explicit solution of the boundary value problem for vertical cylinders

This Chapter derives the solution of the boundary value problem presented in Chapter 2 for an array of vertical circular cylinders extending from the free-surface to the sea-bottom. The structure is subject to a regular incident wave with amplitude A,

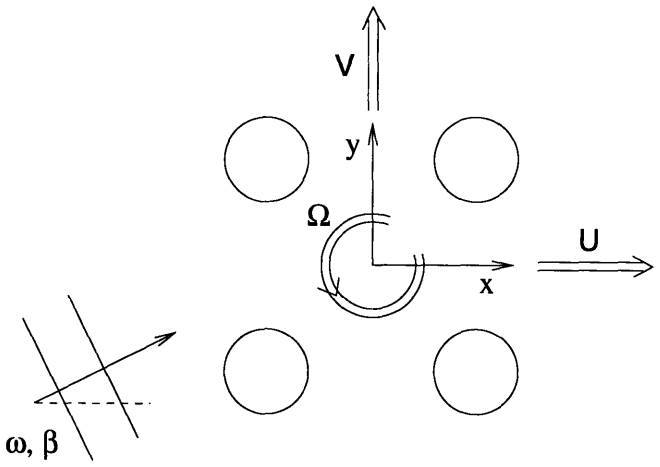

Figure 3-1: The slow-drift velocities U, V and Ω for an array of cylinders, subject to a regular wave with frequency ω_0 and direction β

absolute frequency ω_0 and wave-number κ. The angle of incidence is β relative to the x-axis in the slow-drift frame, see Figure 3-1. The structure is free to respond with small linear motions in surge, sway and yaw about its instantaneous slow-drift position at the encounter frequency ω.

Section 3.1 presents the solution of the zero-speed potential ϕ_{10}, using the method of Linton & Evans (1990), which solves the diffraction problem for an array of cylinders accounting for all interactions effects between the cylinders. The method is here extended to include the radiation potential.

The analytic solution of the forward-speed potential ϕ_{11} is derived in Section 3.2, which involves the ν-derivative and the Weber-transform of ϕ_{10} as particular solutions of the free-surface condition, and wave-maker theory for the body boundary conditions.

3.1 The zero-speed potential ϕ_{10}

The boundary value problem for the potential ϕ_{10} is identical to the problem of a freely floating body oscillating about its mean position with small amplitude motions. The slow-drift velocities U and V are present only via the frequency of the oscillations

$$\omega = \omega_0 - \kappa U \cos\beta - \kappa V \sin\beta. \tag{3.1}$$

The linearity of the zero-speed problem allows the decomposition of ϕ_{10} into a diffraction part and a radiation part. The diffraction part consists of an incident wave and the scattering of the restrained body, while the radiation part consists of the radiating waves due to the forced motions in otherwise calm water. The time-dependence of all linear quantities are assumed to be time-harmonic, and we can therefore write the

potential ϕ_{10} as

$$\begin{aligned} \phi_{10} &= \mathrm{Re}\left[\varphi\, e^{i\omega t}\right] \\ &\equiv \mathrm{Re}\left[\frac{igA}{\omega_0}(\varphi_D + \varphi_R)\, e^{i\omega t}\right], \end{aligned} \tag{3.2}$$

where the factor igA/ω_0 has been factored out in order to make the diffraction and radiation potentials non-dimensional. Write the diffraction potential as a sum of the incident wave and the scattered wave,

$$\varphi_D = \varphi_I + \varphi_S, \tag{3.3}$$

and the radiation potential as a sum of the forced motion potentials for the different modes of motion,

$$\varphi_R = \nu \sum_{i=1,2,6} \bar{\xi}_i^{(0)} \varphi_R^i, \tag{3.4}$$

where $\nu = \omega_0^2/g$ and $\bar{\xi}_i^{(0)}$ is the non-dimensional linear motion amplitude, defined in Section 4.2. Substituting equations (3.2) - (3.4) for ϕ_{10} in the boundary conditions (2.16) and (2.28), results in the following boundary conditions for φ_D and φ_R^i:

$$-\nu\varphi_D + \frac{\partial \varphi_D}{\partial z} = 0, \qquad \text{on } z = 0, \tag{3.5}$$

$$\frac{\partial \varphi_D}{\partial n} = 0, \qquad \text{on } S_B, \tag{3.6}$$

$$-\nu\varphi_R^i + \frac{\partial \varphi_R^i}{\partial z} = 0, \qquad \text{on } z = 0, \tag{3.7}$$

$$\frac{\partial \varphi_R^i}{\partial n} = n_i, \qquad \text{on } S_B, \tag{3.8}$$

where $\boldsymbol{n} = (n_1, n_2, 0)$ is the unit normal vector on the body pointing out of the fluid domain, and $n_6 = xn_2 - yn_1$.

A local frame of reference (x_j, y_j, z_j) is defined at the center of cylinder j, and is

related to the slow-drift frame as follows

$$\begin{aligned} x &= \bar{x}_j + x_j \\ y &= \bar{y}_j + y_j \\ z &= z_j \end{aligned} \tag{3.9}$$

as illustrated in Figure 3-2, and with the corresponding cylindrical coordinates (r_j, θ_j) defined by: $x_j = r_j \cos\theta_j$ and $y_j = r_j \sin\theta_j$. In the following analysis, the z-dependence

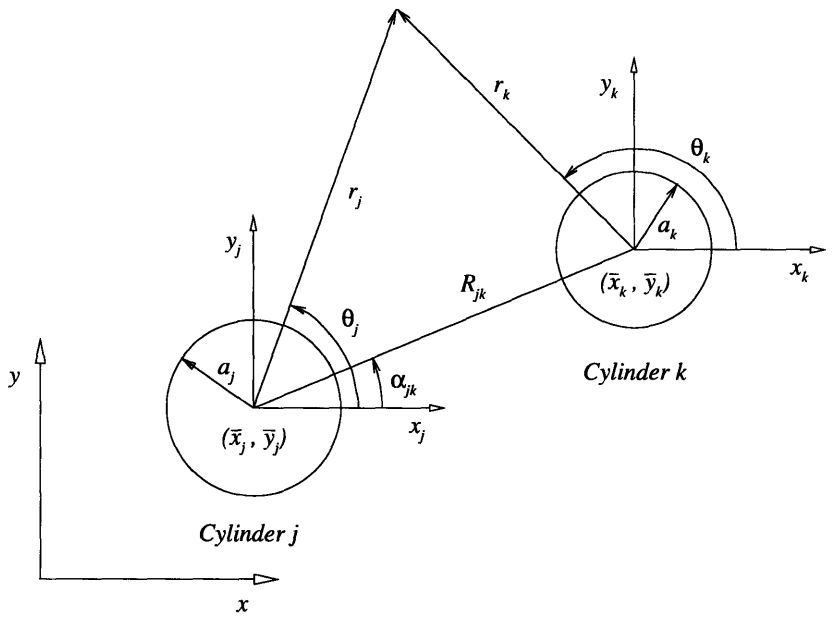

Figure 3-2: Configuration of the cylinders

of all potentials will be represented by a complete set of orthogonal functions, defined as

$$f_0(z_j) = \left(\frac{2\kappa}{\kappa h / \cosh^2 \kappa h + \nu/\kappa} \right)^{1/2} \frac{\cosh \kappa(z_j + h)}{\cosh \kappa h} \tag{3.10}$$

$$f_n(z_j) = \left(\frac{2k_n}{k_n h / \cos^2 k_n h - \nu/k_n} \right)^{1/2} \frac{\cos k_n(z_j + h)}{\cos k_n h}, \quad n = 1, ..., \infty, \tag{3.11}$$

with the following orthogonality properties,

$$\int_{-h}^{0} f_0(z_j) f_0(z_j) \mathrm{d}z_j = 1, \tag{3.12}$$

$$\int_{-h}^{0} f_n(z_j) f_n(z_j) \mathrm{d}z_j = 1, \tag{3.13}$$

$$\int_{-h}^{0} f_m(z_j) f_n(z_j) \mathrm{d}z_j = 0, \text{ if } m \neq n, \ m = 0, ..., \infty, \ n = 0, ..., \infty, \tag{3.14}$$

where k_n is defined as the successive solutions of $k_n \tan k_n h = -\nu$, $n = 1, ..., \infty$.

3.1.1 Diffraction

The incident wave potential φ_I, expressed in terms of the slow-drift coordinates (x, y, z) and the local coordinates (x_j, y_j, z_j), respectively, is written

$$\begin{aligned} \varphi_I &= \frac{\cosh \kappa(z+h)}{\cosh \kappa h} \mathrm{e}^{-\mathrm{i}\kappa(x\cos\beta + y\sin\beta)} \\ &= \frac{\cosh \kappa(z_j+h)}{\cosh \kappa h} \mathrm{e}^{-\mathrm{i}\kappa(\bar{x}_j\cos\beta + \bar{y}_j\sin\beta) - \mathrm{i}\kappa r_j\cos(\theta_j-\beta)} \\ &= I_j f_0(z_j) \sum_{m=-\infty}^{\infty} (-\mathrm{i})^m J_m(\kappa r_j) \mathrm{e}^{\mathrm{i}m(\theta_j-\beta)}, \end{aligned} \tag{3.15}$$

$$I_j = \left(\frac{\kappa h / \cosh^2 \kappa h + \nu/\kappa}{2\kappa} \right)^{1/2} \mathrm{e}^{-\mathrm{i}\kappa(\bar{x}_j\cos\beta + \bar{y}_j\sin\beta)}, \tag{3.16}$$

where I_j includes the 'phase-factor' associated with cylinder j and a factor to cancel the square-root term in the definition of $f_0(z_j)$ in equation (3.10). $J_m(\kappa r_j)$ is the Bessel-function of first kind. The derivation of the scattering potential φ_S, using the method of Linton & Evans (1990), follows.

The general solution of Laplace's equation given the homogeneous free-surface condition in equation (3.5) and outgoing waves at infinity, is of the form:

$$f_0(z_j) \sum_{m=-\infty}^{\infty} a_{m0}^j H_m^{(2)}(\kappa r_j) \mathrm{e}^{\mathrm{i}m\theta_j} + \sum_{n=1}^{\infty} f_n(z_j) \sum_{m=-\infty}^{\infty} a_{mn}^j K_m(k_n r_j) \mathrm{e}^{\mathrm{i}m\theta_j}, \tag{3.17}$$

where a^j_{mn} are unknown coefficients determined by the body boundary conditions, $H^{(2)}_m(\kappa r_j)$ is the Hankel-function of second order and $K_m(k_n r_j)$ is the modified Bessel function. The boundary condition for φ_S, equation (3.6), is such that the second term in equation (3.17) is exactly zero. The waves associated with the scattering from cylinder j can thus be written

$$\varphi^j_S \;=\; f_0(z_j) \sum_{m=-\infty}^{\infty} A^j_{Dm} Z^j_m H^{(2)}_m(\kappa r_j) \mathrm{e}^{\mathrm{i}m\theta_j}, \tag{3.18}$$

where $Z^j_m = J'_m(\kappa a_j)/H^{(2)\prime}_m(\kappa a_j)$ is multiplied to simplify the algebra and A^j_{Dm} are the interaction coefficients to be determined by the body boundary conditions. The total diffraction potential φ_D, written as the sum of the incident wave potential φ_I and the scattering potentials φ^j_S from all cylinders, is written

$$\varphi_D \;=\; \varphi_I + \sum_{j=1}^{N} \varphi^j_S. \tag{3.19}$$

Using Graf's theorem for Bessel-functions (Abramowitz & Stegun, page 363, equation 9.1.79.), we can write equation (3.19) in terms of the coordinates (r_k, θ_k) and then apply the boundary conditions which are

$$\frac{\partial \varphi_D}{\partial r_k} \;=\; 0 \qquad\qquad \text{on } r_k = a_k, \quad k = 1, ..., N. \tag{3.20}$$

Some algebra leads to the following equations, which determine the interaction coefficients A^k_{Dm}:

$$A^k_{Dm} + \underbrace{\sum_{j=1}^{N}}_{\neq k} \sum_{n=-\infty}^{\infty} A^j_{Dn} Z^j_n \, \mathrm{e}^{\mathrm{i}(n-m)\alpha_{jk}} H^{(2)}_{n-m}(\kappa R_{jk}) \;=\; -I_k \mathrm{e}^{-\mathrm{i}m(\pi/2+\beta)},$$

$$k = 1, \ldots, N, \;\; m = -\infty, \ldots, \infty, \tag{3.21}$$

where N is the number of cylinders. Equations (3.18), (3.19) and (3.21) can be used to write φ_D in terms of the coordinates (r_j, θ_j, z_j). Some algebra leads to the following

simple expression:

$$\varphi_D = f_0(z_j) \sum_{m=-\infty}^{\infty} A^j_{Dm} [Z^j_m H^{(2)}_m(\kappa r_j) - J_m(\kappa r_j)] \, e^{im\theta_j}, \tag{3.22}$$

where the use of Graf's theorem requires that $r_j < R_{jk}$ for any j and k.

3.1.2 Extension of the method by Linton & Evans

The determination of a linear potential with more general body boundary conditions than φ_S, requires new sets of interactions coefficients, which will be discussed next. Consider the generalized radiation velocity potential χ, subject to the Laplace equation and the boundary conditions on $z = 0$ and on each cylinder j, respectively

$$-\nu\chi + \frac{\partial \chi}{\partial z} = 0, \tag{3.23}$$

$$\frac{\partial \chi}{\partial r_j} = u^j(\theta_j, z), \tag{3.24}$$

where $u^j(\theta_j, z)$ admits the Fourier decomposition

$$u^j(\theta_j, z) = \sum_{m=-\infty}^{\infty} u^j_m(z) \, e^{im\theta_j}. \tag{3.25}$$

The solution of this boundary-value problem will be carried out by extending the Linton & Evans interaction theory to the radiation problem. Only the wavelike interactions between the cylinders will be accounted for, while interactions arising from the non-wavelike components (the evanescent terms) of the radiation solution around each cylinder will be omitted. These components are omitted since the non-wavelike components are associated only with the near-field of the cylinders, which generally are configured with relatively wide spacing.

The potential χ may be decomposed into two components. The first component is the sum of wave disturbances 'radiated' from single cylinders acting as wavemakers,

and is subject to the boundary condition (3.24) on cylinder j. This component is free of interaction effects and around cylinder j is defined by

$$\chi_0^j = f_0(z_j) \sum_{m=-\infty}^{\infty} \beta_{m0}^j H_m^{(2)}(\kappa r_j)\, e^{im\theta_j} + \sum_{n=1}^{\infty} f_n(z_j) \sum_{m=-\infty}^{\infty} \beta_{mn}^j K_m(k_n r_j)\, e^{im\theta_j}. \quad (3.26)$$

The coefficient β_{mn}^j is obtained by combining equations (3.24) - (3.26); multiplying by $f_0(z_j)$, $f_n(z_j)$ and integrating over z from $-h$ to 0. This gives

$$\beta_{m0}^j = \frac{1}{\kappa H_m^{(2)\prime}(\kappa a_j)} \int_{-h}^{0} u_m^j(z) f_0(z_j) dz, \quad (3.27)$$

$$\beta_{mn}^j = \frac{1}{k_n K_m'(k_n a_j)} \int_{-h}^{0} u_m^j(z) f_n(z_j) dz, \quad n = 1, ..., \infty. \quad (3.28)$$

The second component consists of the 'diffracted' wave disturbance around cylinder j due to the waves 'radiated' by the other cylinders and may be expressed in the form

$$\chi_1^j = f_0(z_j) \sum_{m=-\infty}^{\infty} C_m^j Z_m^j H_m^{(2)}(\kappa r_j) e^{im\theta_j}, \quad (3.29)$$

where C_m^j are unknown interaction coefficients and the interaction of the evanescent terms are omitted. The total potential χ, may therefore be written as the sum of all radiated and diffracted wave disturbances, or

$$\chi = \sum_{j=1}^{N} (\chi_0^j + \chi_1^j). \quad (3.30)$$

The unknown interaction coefficients C_m^j may be determined by enforcing a homogeneous boundary condition on each cylinder for the velocity potential χ_1. Expressing χ_1 in terms of the coordinates of cylinder j requires the use of Graf's addition theorem for Bessel functions. Algebra analogous to that in Linton & Evans leads to the

following system of equations for the coefficients C_m^k

$$C_m^k + \underbrace{\sum_{j=1}^{N}}_{\neq k} \sum_{n=-\infty}^{\infty} (C_n^j Z_n^j + \beta_n^j)\, \mathrm{e}^{\mathrm{i}(n-m)\alpha_{jk}} H_{n-m}^{(2)}(\kappa R_{jk}) \;=\; 0,$$

$$k = 1, \ldots, N, \;\; m = -\infty, \ldots, \infty. \tag{3.31}$$

Following the determination of the 'radiation' interaction coefficients C_m^j, Graf's addition theorem and equation (3.31) allow the total potential χ around cylinder j to be expressed in the form

$$\begin{aligned} \chi \;=\; & f_0(z_j) \sum_{m=-\infty}^{\infty} [(C_m^j Z_m^j + \beta_m^j)\, H_m^{(2)}(\kappa r_j) - C_m^j J_m(\kappa r_j)]\, \mathrm{e}^{\mathrm{i}m\theta_j} + \\ & \sum_{n=1}^{\infty} f_n(z_j) \sum_{m=-\infty}^{\infty} \beta_{mn}^j K_m(k_n r_j)\, \mathrm{e}^{\mathrm{i}m\theta_j}, \end{aligned} \tag{3.32}$$

where $r_j < R_{jk}$ for any j and k.

3.1.3 Radiation

In the special case where χ and $u_m^j(z)$ are given by $\chi = \varphi_R^i$ and $u_m^j(z) = n_j$, cf equations (3.7) and (3.8), then equation (3.32) supplies the solution to the surge, sway and yaw radiation potentials and is given by

$$\begin{aligned} \varphi_R^i \;=\; & \sum_{m=-\infty}^{\infty} [(A_{Rm}^{ij} Z_m^j + \beta_m^{ij})\, H_m^{(2)}(\kappa r_j) - A_{Rm}^{ij} J_m(\kappa r_j)]\, \mathrm{e}^{\mathrm{i}m\theta_j} + \\ & \sum_{n=1}^{\infty} f_n(z_j) \sum_{m=-\infty}^{\infty} \beta_{mn}^{ij} K_m(k_n r_j)\, \mathrm{e}^{\mathrm{i}m\theta_j}, \end{aligned} \tag{3.33}$$

where the interaction coefficients A^{ik}_{Rm} must satisfy the following equations:

$$A^{ik}_{Rm} + \underbrace{\sum_{j=1}^{N}}_{\neq k} \sum_{n=-\infty}^{\infty} A^{ij}_{Rn} Z^j_n \, \mathrm{e}^{\mathrm{i}(n-m)\alpha_{jk}} H^{(2)}_{n-m}(\kappa R_{jk}) \;=$$

$$- \underbrace{\sum_{j=1}^{N}}_{\neq k} \left[\beta^{ij}_{10} \, \mathrm{e}^{\mathrm{i}(n-1)\alpha_{jk}} H^{(2)}_{n-1}(\kappa R_{jk}) + \beta^{ij}_{-10} \, \mathrm{e}^{\mathrm{i}(n+1)\alpha_{jk}} H^{(2)}_{n+1}(\kappa R_{jk}) \right],$$

$$k = 1, \ldots, N, \;\; m = -\infty, \ldots, \infty. \qquad (3.34)$$

The coefficients β^{ij}_{mn} are evaluated using equations (3.27), (3.28) and (3.8), with the components of n_i given by

$$n_1 = -\cos\theta_j, \qquad (3.35)$$

$$n_2 = -\sin\theta_j, \qquad (3.36)$$

$$n_6 = -\bar{x}_j \sin\theta_j + \bar{y}_j \cos\theta_j. \qquad (3.37)$$

Employing the identities $\cos\theta_j \equiv \frac{1}{2}(\mathrm{e}^{\mathrm{i}\theta_j} + \mathrm{e}^{-\mathrm{i}\theta_j})$ and $\sin\theta_j \equiv -\frac{\mathrm{i}}{2}(\mathrm{e}^{\mathrm{i}\theta_j} - \mathrm{e}^{-\mathrm{i}\theta_j})$, the coefficients β^{ij}_{mn} for $n = 0, 1, ..., \infty$ are written

$$\begin{aligned}
\beta^{1j}_{\pm 1n} &= \pm\beta_{1n}, \\
\beta^{2j}_{\pm 1n} &= -\mathrm{i}\beta_{1n}, \\
\beta^{6j}_{\pm 1n} &= -(\mathrm{i}\bar{x}_j \pm \bar{y}_j)\beta_{1n}, \\
\beta^{ij}_{mn} &= 0, \qquad |m| \neq 1, \;\; i = 1, 2, 6,
\end{aligned} \qquad (3.38)$$

where

$$\beta_{10} = \frac{\frac{1}{2}\sqrt{2}\,\nu}{\kappa^{\frac{5}{2}} H_1'(\kappa a_j)\sqrt{\kappa h / \cosh^2 \kappa h + \nu/\kappa}}, \qquad (3.39)$$

$$\beta_{1n} = -\frac{\frac{1}{2}\sqrt{2}\,(-1)^n \nu}{k_n^{\frac{5}{2}} K_1'(k_n a_j)\sqrt{k_n h / \cos^2 k_n h - \nu/k_n}}, \;\; n = 1, ..., \infty. \qquad (3.40)$$

3.2 The forward-speed potential ϕ_{11}

The potential ϕ_{11} is linear in the slow-drift velocities U, V and Ω and is the leading order correction to ϕ_{10}. The boundary conditions for ϕ_{11} on the free-surface and on the body-boundary are given by equations (2.17), and (2.29), respectively, and will in the following section be derived with respect to the local frame of reference on each cylinder in regular waves. The consecutive sections present the solution of the boundary value problem.

3.2.1 Boundary conditions in the local frame

From the free-surface condition in equation (2.17) and the harmonic time dependence of ϕ_{10} in equation (3.2), we can deduce that ϕ_{11} must be of the form

$$\phi_{11} = \mathrm{Re}\left[\psi\, \mathrm{e}^{\mathrm{i}\omega t}\right]. \tag{3.41}$$

In order to evaluate the time-derivative of ϕ_{11} correctly to order $\delta\tau_j$, consider the time-derivative of ϕ as follows,

$$\begin{aligned}
\frac{\partial \phi}{\partial t} &= \mathrm{Re}\,\frac{\partial}{\partial t}\left[\phi_{01} + (\varphi + \psi + \cdots)\mathrm{e}^{\mathrm{i}\omega t} + \cdots\right] \\
&= \mathrm{Re}\left[\left(\mathrm{i}\omega(\varphi + \psi + \cdots) + \frac{\mathrm{d}\Theta}{\mathrm{d}t}\frac{\partial}{\partial \Theta}(\varphi + \psi + \cdots)\right)\mathrm{e}^{\mathrm{i}\omega t} + \cdots\right] \\
&= \mathrm{Re}\,[(\underbrace{\mathrm{i}\omega_0\varphi}_{O(\delta)} + \underbrace{\mathrm{i}\omega_0\psi - \mathrm{i}\kappa(U\cos\beta + V\sin\beta)\varphi - \Omega\frac{\partial \varphi}{\partial \beta}}_{O(\delta\tau_j)})\mathrm{e}^{\mathrm{i}\omega t}] + o(\delta\tau_j),
\end{aligned} \tag{3.42}$$

where the frequency of encounter ω is given by equation (3.1). Notice that time is present both via the harmonic term $\mathrm{e}^{\mathrm{i}\omega t}$ and the angle of rotation $\Theta(t)$. The term

$\partial/\partial\Theta$ was replaced by $-\partial/\partial\beta$ in the above equation, since $\Theta + \beta = \beta_0$ is constant with respect to time, where β_0 is the angle between the wave-heading and the inertial X-axis. Using equations (2.17), (3.2), (3.41) and (3.42), the free surface boundary condition for ψ in terms of the slow-drift frame, is then written

$$\begin{aligned} -\nu\psi + \frac{\partial\psi}{\partial z} &= 2\mathrm{i}\frac{\omega_0}{g}U\frac{\partial\varphi}{\partial x} + 2\mathrm{i}\frac{\omega_0}{g}V\frac{\partial\varphi}{\partial y} + 2\mathrm{i}\frac{\omega_0}{g}\Omega\frac{\partial\varphi}{\partial\Theta} - 2\mathrm{i}\frac{\omega_0}{g}\nabla\phi_{01}\cdot\nabla\varphi \\ &\quad -2\kappa\frac{\omega_0}{g}U\cos\beta\varphi - 2\kappa\frac{\omega_0}{g}V\sin\beta\varphi - 2\mathrm{i}\frac{\omega_0}{g}\Omega\frac{\partial\varphi}{\partial\beta}. \end{aligned} \tag{3.43}$$

The decomposition of φ into a diffraction potential φ_D and a radiation potential φ_R, cf equation (3.2), suggests the equivalent decomposition of ψ, written as

$$\psi = \frac{\mathrm{i}gA}{\omega_0}(\psi_D + \psi_R). \tag{3.44}$$

The radiation potential ψ_R is proportional to the linear motions. As will be seen later in this chapter, one part of ψ_R will be proportional to $\partial\bar{\xi}_i^{(0)}/\partial\beta$, such that ψ_R will be written

$$\psi_R = \nu\sum_{i=1,2,6}\left(\bar{\xi}_i^{(0)}\psi_R^i + \frac{\partial\bar{\xi}_i^{(0)}}{\partial\beta}\psi_R^{\beta i} + \bar{\xi}_i^{(1)}\varphi_R^i\right). \tag{3.45}$$

The potentials φ_D and φ_R are given with respect to the local coordinates (x_j, y_j, z_j) on cylinder j. It is therefore appropriate to define the potential $\psi^j(x_j, y_j, z_j) = \psi(x, y, z)$ and translate the boundary conditions for ψ into the local frame in terms of ψ^j. From equation (3.9) we can infer that differentiation with respect to x, y and z in the slow-drift frame are identical to differentiation with respect to x_j, y_j and z_j, respectively in the local frame. The corresponding relations for the cylindrical coordinates (R, Θ) in the slow-drift frame and (r_j, θ_j) in the local frame, are given by

$$R\frac{\partial\psi}{\partial R} = \bar{x}_j\frac{\partial\psi^j}{\partial x_j} + \bar{y}_j\frac{\partial\psi^j}{\partial y_j} + r_j\frac{\partial\psi^j}{\partial r_j}, \tag{3.46}$$

$$\frac{\partial\psi}{\partial\Theta} = \bar{x}_j\frac{\partial\psi^j}{\partial y_j} - \bar{y}_j\frac{\partial\psi^j}{\partial x_j} + \frac{\partial\psi^j}{\partial\theta_j}. \tag{3.47}$$

Equation (3.46) will not be used in this analysis, but is included for the sake of completeness. The boundary conditions for ψ_D^j, ψ_R^{ij} and $\psi_R^{\beta ij}$ on the free-surface and on the body can now be obtained from equations (3.43), (3.44), (3.45), (3.47) and (2.17), and are as follows:

$$-\nu\psi_D + \frac{\partial\psi_D}{\partial z} = f_D \tag{3.48}$$

$$\frac{\partial\psi_D}{\partial n} = 0 \tag{3.49}$$

$$-\nu\psi_R^i + \frac{\partial\psi_R^i}{\partial z} = f_R \tag{3.50}$$

$$\frac{\partial\psi_R^i}{\partial n} = \frac{m_i}{\mathrm{i}\omega_0} \tag{3.51}$$

$$-\nu\psi_R^{\beta i} + \frac{\partial\psi_R^{\beta i}}{\partial z} = 2\mathrm{i}\frac{\omega_0}{g}\Omega\varphi_R^i \tag{3.52}$$

$$\frac{\partial\psi_R^{\beta i}}{\partial n} = 0 \tag{3.53}$$

where

$$\begin{aligned} f_D = {} & 2\mathrm{i}\frac{\omega_0}{g}(U - \bar{y}_j\Omega)\frac{\partial\varphi_D}{\partial x_j} + 2\mathrm{i}\frac{\omega_0}{g}(V + \bar{x}_j\Omega)\frac{\partial\varphi_D}{\partial y_j} + 2\mathrm{i}\frac{\omega_0}{g}\Omega\frac{\partial\varphi_D}{\partial\theta_j} \\ & -2\frac{\omega_0}{g}(\kappa U\cos\beta + \kappa V\sin\beta)\varphi_D + 2\mathrm{i}\frac{\omega_0}{g}\Omega\frac{\partial\varphi_D}{\partial\beta} - 2\mathrm{i}\frac{\omega_0}{g}\nabla\phi_{01}\cdot\nabla\varphi_D, \end{aligned} \tag{3.54}$$

$$\begin{aligned} f_R = {} & 2\mathrm{i}\frac{\omega_0}{g}(U - \bar{y}_j\Omega)\frac{\partial\varphi_R^i}{\partial x_j} + 2\mathrm{i}\frac{\omega_0}{g}(V + \bar{x}_j\Omega)\frac{\partial\varphi_R^i}{\partial y_j} + 2\mathrm{i}\frac{\omega_0}{g}\Omega\frac{\partial\varphi_R^i}{\partial\theta_j} \\ & -2\frac{\omega_0}{g}(\kappa U\cos\beta + \kappa V\sin\beta)\varphi_R^i - 2\mathrm{i}\frac{\omega_0}{g}\nabla\phi_{01}\cdot\nabla\varphi_R^i. \end{aligned} \tag{3.55}$$

3.2.2 Outline of solution

The solution for the potentials ψ_D^j, ψ_R^{ij} and $\psi_R^{\beta ij}$ are simplified by considering the potential Ψ^j with the following boundary conditions:

$$-\nu\Psi^j + \frac{\partial\Psi^j}{\partial z_j} = L\varphi + c_6\nabla\phi_{01}\cdot\nabla\varphi, \tag{3.56}$$

$$\frac{\partial\Psi^j}{\partial r_j} = v(z_j), \tag{3.57}$$

where

$$L = c_1 + c_2\frac{\partial}{\partial x_j} + c_3\frac{\partial}{\partial y_j} + c_4\frac{\partial}{\partial\theta_j} + c_5\frac{\partial}{\partial\beta}. \tag{3.58}$$

The constants c_1 - c_6 and $v(z_j)$ must be determined by inspection of equations (3.48) - (3.55) for the potentials ψ_D^j, ψ_R^{ij} and $\psi_R^{\beta ij}$, respectively. The determination of Ψ^j can be decomposed into a sequence of problems, and is written as a sum of the individual potentials Ψ_1^j, Ψ_2^j and Ψ_3^j. The two first potentials combined satisfy the free-surface condition in equation (3.56), but do not satisfy the body-boundary conditions. The potential Ψ_3^j corrects for the normal velocities that are induced by the solutions of Ψ_1^j and Ψ_2^j on the body-boundary and ensures that the condition in equation (3.57) is satisfied. Ψ_1^j, Ψ_2^j and Ψ_3^j are thus subject to the following boundary conditions:

$$-\nu\Psi_1^j + \frac{\partial\Psi_1^j}{\partial z_j} = L\varphi, \tag{3.59}$$

$$\frac{\partial\Psi_1^j}{\partial r_j} = v_1(z_j) \tag{3.60}$$

$$-\nu\Psi_2^j + \frac{\partial\Psi_2^j}{\partial z_j} = c_6\nabla\phi_{01}\cdot\nabla\varphi, \tag{3.61}$$

$$\frac{\partial\Psi_2^j}{\partial r_j} = v_2(z_j), \tag{3.62}$$

$$-\nu\Psi_3^j + \frac{\partial\Psi_3^j}{\partial z_j} = 0, \tag{3.63}$$

$$\frac{\partial \Psi_3^j}{\partial r_j} = v(z_j) - v_1(z_j) - v_2(z_j), \tag{3.64}$$

where $v_1(z_j)$ and $v_2(z_j)$ are the normal velocities induced by Ψ_1^j and Ψ_2^j, respectively and are given by equation (3.81).

The particular solution of Ψ_1^j can be found by inspection. Take first the ν-derivative of the linear zero-speed free-surface condition and then apply the linear operator L:

$$-\nu\varphi + \frac{\partial \varphi}{\partial z} = 0 \tag{3.65}$$

$$\Downarrow$$

$$-\nu\frac{\partial \varphi}{\partial \nu} + \frac{\partial^2 \varphi}{\partial \nu \partial z_j} = \varphi \tag{3.66}$$

$$\Downarrow$$

$$-\nu L\frac{\partial \varphi}{\partial \nu} + L\frac{\partial^2 \varphi}{\partial \nu \partial z_j} = L\varphi \tag{3.67}$$

$$\Updownarrow$$

$$-\nu\Psi_1^j + \frac{\partial \Psi_1^j}{\partial z} = L\varphi. \tag{3.68}$$

The above equations prove that the particular solution of equation (3.59) can be written

$$\Psi_1^j = L\frac{\partial \varphi}{\partial \nu}. \tag{3.69}$$

The determination of Ψ_2^j is simplified if only the far-field component is needed. This will be the case if conservation of momentum is used as in Section 4.3 in order to evaluate the slow-drift damping coefficient. Therefore, the remainder of this section seeks to determine the wavelike component of the potential Ψ_1^j, which are dominant in the far field.

In order to solve equation (3.61) we first expand Ψ_2^j in the Fourier series

$$\Psi_2^j = \sum_{m=-\infty}^{\infty} \Psi_{2m}^j e^{im\theta_j}, \tag{3.70}$$

and invoke the Weber transform pair for Ψ^j_{2m} (Davies 1978),

$$\tilde{\Psi}^j_{2m}(k) = \int_{a_j}^{\infty} r_j \mathrm{d}r_j \, \Psi^j_{2m}(r_j) W_m(kr_j), \tag{3.71}$$

$$\Psi^j_{2m}(r_j) = \int_0^{\infty} k \, \mathrm{d}k \, \tilde{\Psi}^j_{2m}(k) \frac{W_m(kr_j)}{[J'_m(ka_j)]^2 + [Y'_m(ka_j)]^2}, \tag{3.72}$$

where

$$W_m(kr_j) = Y'_m(ka_j)J_m(kr_j) - J'_m(ka_j)Y_m(kr_j). \tag{3.73}$$

The Weber transform exists here due to the rapid decay of $\nabla\phi_{01}$ as $r_j \to \infty$. This would not be the case with equation (3.59) because of the $1/\sqrt{r_j}$ decay of the forcing term in the free surface condition. The transformation of the Laplace equation, the free surface condition and the bottom boundary condition for Ψ^j_2, leads to the following set of equations for $\tilde{\Psi}^j_{2m}(k)$:

$$\begin{aligned} -k^2\tilde{\Psi}^j_{2m} + \frac{\partial^2\tilde{\Psi}^j_{2m}}{\partial z_j^2} &= 0, && \text{in the fluid,} \\ -\nu\tilde{\Psi}^j_{2m} + \frac{\partial\tilde{\Psi}^j_{2m}}{\partial z_j} &= \tilde{F}_m(k), && \text{on } z_j = 0, \\ \frac{\partial\tilde{\Psi}^j_{2m}}{\partial z_j} &= 0, && \text{on } z_j = -h, \end{aligned} \tag{3.74}$$

where

$$\begin{aligned} \tilde{F}(k) &= c_6 \int_{a_j}^{\infty} r_j \mathrm{d}r_j \, \nabla\phi_{01} \cdot \nabla\varphi \, W_m(kr_j) \\ &\equiv \sum_{m=-\infty}^{\infty} \tilde{F}_m(k) \mathrm{e}^{\mathrm{i}m\theta_j}, \end{aligned} \tag{3.75}$$

is the Weber transform of the right hand side of equation (3.61). The solution of the boundary value problem in equation (3.74) is obtained by standard methods, and is written

$$\tilde{\Psi}^j_{2m} = \frac{\cosh k(z_j + h)}{\cosh kh} \frac{\tilde{F}_m(k)}{k\tanh kh - \nu}. \tag{3.76}$$

The solution for Ψ^j_{2m} then follows upon substitution of $\tilde{\Psi}^j_{2m}$ into equation (3.72),

$$\Psi^j_{2m}(r_j) = \int_0^\infty \mathrm{d}k \, \frac{k\tilde{F}_m(k)}{k\tanh kh - \nu} \, \frac{W_m(kr_j)}{[J'_m(ka_j)]^2 + [Y'_m(ka_j)]^2} \frac{\cosh k(z_j + h)}{\cosh kh}, \quad (3.77)$$

with the path of integration intended above the pole at $k\tanh kh = \nu$, denoted by $k = \kappa$. The identity

$$\frac{W_m(kr_j)}{[J'_m(ka_j)]^2 + [Y'_m(ka_j)]^2} \equiv \frac{\mathrm{i}}{2}\left(\frac{H^{(1)}_m(kr_j)}{H^{(1)'}_m(ka_j)} - \frac{H^{(2)}_m(kr_j)}{H^{(2)'}_m(ka_j)}\right) \quad (3.78)$$

allows the deformation of the contour of integration in the upper/lower k-plane for

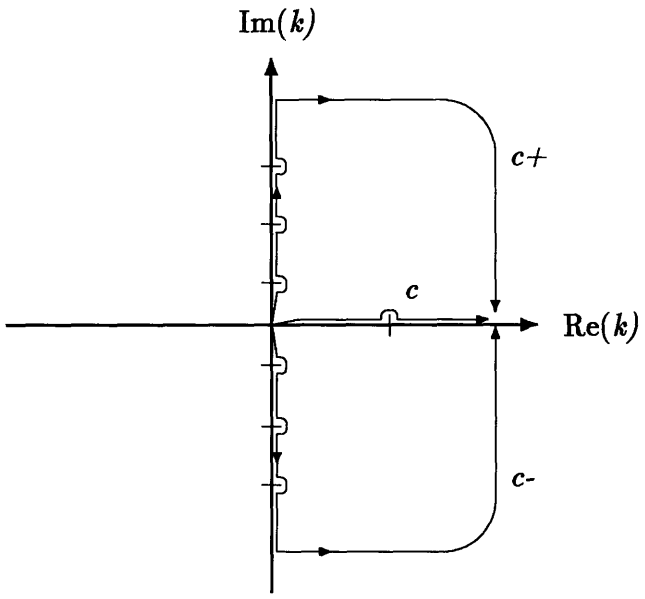

Figure 3-3: Path of integration in the complex k-plane

the first/second terms in (3.78), as illustrated in Figure 3-3. As $r \to \infty$, the wavelike contribution to Ψ^j_{2m} arises from the residue at $k = \kappa$, and takes the form

$$\Psi^j_2 = f_0(z_j) \sum_{m=-\infty}^{\infty} \gamma^j_m H^{(2)}_m(\kappa r_j) \mathrm{e}^{\mathrm{i}m\theta_j}, \quad (3.79)$$

$$\gamma^j_m = \frac{-\pi\sqrt{\frac{\kappa}{2}}\tilde{F}^j_m(\kappa)}{H^{(2)'}_m(\kappa a_j)\sqrt{\kappa h/\cosh^2 \kappa h + \nu/\kappa}}, \quad (3.80)$$

which represents outgoing waves satisfying the homogeneous free surface condition.

The solution of Ψ_3^j was derived in Section 3.1.2 with $\chi = \Psi_3^j$. The body-boundary condition for χ, cf equations (3.24) and (3.64), which includes contributions from Ψ_1^j and Ψ_2^j, is written

$$u(z_j) = v(z_j) - \frac{\partial}{\partial r_j} L \frac{\partial \varphi}{\partial \nu} - \kappa f_0(z_j) \sum_{m=-\infty}^{\infty} \gamma_m^j H_m^{(2)\prime}(\kappa a_j) \mathrm{e}^{\mathrm{i}m\theta_j}. \tag{3.81}$$

3.3 The potential $\bar{\phi}_{20}$

The boundary conditions for $\bar{\phi}_{20}$ in regular waves are here presented with respect to the slow-drift frame. The free-surface condition was given in Section 2.2 by equation (2.18) and the body-boundary condition by (2.32). The expressions for the potential ϕ_{10} and the linear motions $\boldsymbol{\xi}$, $\boldsymbol{\alpha}$ in regular waves with frequency ω are given by equations (3.2) and (4.20), respectively. Substituting for ϕ_{10} in equation (2.18) and taking the time-average, the first term on the right hand side is immediately found to be zero. By interchanging the order of differentiation and using the free-surface condition for ϕ_{10}, the first term inside the brackets of equation (2.18) is also found to vanish. Using equation (A.13), the free-surface condition for ϕ_{20} then takes the following form,

$$\frac{\partial \bar{\phi}_{20}}{\partial z} = -\frac{\omega_0}{2g} \mathrm{Im}\left(\varphi \frac{\partial^2 \varphi^*}{\partial z^2}\right). \tag{3.82}$$

The body-boundary conditions follow from equation (2.32) and are written,

$$\frac{\partial \bar{\phi}_{20}}{\partial n} = \tfrac{1}{2}\mathrm{Re}\left(\hat{\boldsymbol{\alpha}}^* \times \boldsymbol{n} \cdot [\mathrm{i}\omega(\hat{\boldsymbol{\xi}} + \hat{\boldsymbol{\alpha}} \times \boldsymbol{x}) - \nabla\varphi] - \boldsymbol{n} \cdot [(\hat{\boldsymbol{\xi}} + \hat{\boldsymbol{\alpha}} \times \boldsymbol{x}) \cdot \nabla]\nabla\varphi^*\right). \tag{3.83}$$

No attempt has been made in this thesis to solve the boundary value problem for $\bar{\phi}_{20}$ as presented above. The potential is however consistently included in the expressions for the wave-drift damping. The reader is referred to the paper by Grue & Palm (1993), where the effects of $\bar{\phi}_{20}$ are considered, without having to solve the boundary value problem.

Chapter 4

The hydrodynamic forces

The pressure in the fluid with respect to the slow-drift frame is provided by the Bernoulli's equation and is given by

$$p = -\rho\left(\frac{\partial\phi}{\partial t} - \boldsymbol{f}\cdot\Delta\phi + \tfrac{1}{2}\nabla\phi\cdot\nabla\phi + gz\right), \tag{4.1}$$

where $\boldsymbol{f}\cdot\Delta$ is defined by equation (2.9). From Bernoulli's equation and the expansion (2.11) for $\phi(\boldsymbol{x},t)$, it follows that the pressure in the fluid domain may be expanded in the form

$$p(\boldsymbol{x},t) = \underbrace{p_{00}(\boldsymbol{x})}_{O(1)} + \underbrace{p_{01}(\boldsymbol{x},t)}_{O(\tau_j)} + \underbrace{p_{10}(\boldsymbol{x},t)}_{O(\delta)} + \underbrace{p_{11}(\boldsymbol{x},t)}_{O(\delta\tau_j)} + \underbrace{p_{20}(\boldsymbol{x},t)}_{O(\delta^2)} + \underbrace{p_{21}(\boldsymbol{x},t)}_{O(\delta^2\tau_j)} + \cdots \tag{4.2}$$

where p_{00} is the hydrostatic, p_{10} the linear and p_{01} the pressure due to the double body flow. The remaining components are defined by the relations

$$p_{11} = -\rho\left[\frac{\partial\phi_{11}}{\partial t} - \boldsymbol{f}\cdot\Delta\phi_{10} + \nabla\phi_{10}\cdot\nabla\phi_{01}\right], \tag{4.3}$$

$$p_{20} = -\rho\left[\frac{\partial\phi_{20}}{\partial t} + \tfrac{1}{2}\nabla\phi_{10}\cdot\nabla\phi_{10}\right], \tag{4.4}$$

$$p_{21} = -\rho\left[\frac{\partial\phi_{st21}}{\partial t} - \boldsymbol{f}\cdot\Delta\phi_{20} + \nabla\phi_{01}\cdot\nabla\phi_{20} + \nabla\phi_{11}\cdot\nabla\phi_{10}\right]. \tag{4.5}$$

The hydrodynamic force experienced by the body may be obtained by integration of p_{ij} over its wetted surface or by the appropriate enforcement of the momentum conservation principle. It follows that the corresponding expansion of the force on the body becomes

$$\boldsymbol{F}(t) = \underbrace{\boldsymbol{F}_{10}(t)}_{O(\delta)} + \underbrace{\boldsymbol{F}_{11}(t)}_{O(\delta\tau_j)} + \underbrace{\boldsymbol{F}_{20}(t)}_{O(\delta^2)} + \underbrace{\boldsymbol{F}_{21}(t)}_{O(\delta^2\tau_j)} + \cdots . \tag{4.6}$$

Here $\boldsymbol{F}_{10}(t)$ is the linear exciting force for the fixed body and $\boldsymbol{F}_{11}(t)$ the leading order correction due to the slow-drift velocity τ_j. $\boldsymbol{F}_{20}(t)$ is the second order exciting force while $\boldsymbol{F}_{21}(t)$ is the corresponding correction due to the slow-drift velocity τ_j. In monochromatic waves, the forces $\boldsymbol{F}_{20}(t)$ and $\boldsymbol{F}_{21}(t)$ are the second-order mean drift force and wave-drift damping, respectively.

In the following section, the forces $\boldsymbol{F}_{ij}(t)$ are derived by pressure integration. The section thereafter derives expressions for the mean forces by the enforcement of the momentum conservation principle for arbitrary slow-drift velocities U and V, but with $\Omega = 0$.

4.1 Pressure integration

The forces on the body are here obtained by integration of the pressure over the wetted surface of the body. The body is allowed to oscillate with the small amplitude motions $\boldsymbol{\xi} = (\xi_1, \xi_2, 0)$ and rotation $\boldsymbol{\alpha} = (0, 0, \alpha_3)$. The expressions for the forces and moments on the body are written

$$\boldsymbol{F} = \int_{S_B} \mathcal{P}\,\boldsymbol{N}\,\mathrm{d}S, \tag{4.7}$$

$$\boldsymbol{M} = \int_{S_B} \mathcal{P}\,\boldsymbol{x} \times \boldsymbol{N}\,\mathrm{d}S, \tag{4.8}$$

where $\mathcal{P}$ is the pressure at the instantaneous position of the body and $\boldsymbol{N}$ the unit normal vector measured in the slow-drift frame. Due to the small amplitude motions $\boldsymbol{\xi}$ and $\boldsymbol{\alpha}$, the pressure $\mathcal{P}$ is expanded about the mean position of the slow-drift frame in a Taylor series, and is given by

$$\mathcal{P} = p|_{\bar{S}_B} + (\boldsymbol{\xi} + \boldsymbol{\alpha} \times \boldsymbol{X}) \cdot \nabla p|_{\bar{S}_B} + \cdots, \tag{4.9}$$

where $p|_{\bar{S}_B}$ is the pressure on the body evaluated in the slow-drift frame. The normal vector $\boldsymbol{N}$ and the position vector $\boldsymbol{x}$ in the slow-drift frame are transformed into the body-fixed frame as follows,

$$\boldsymbol{N} = \boldsymbol{n} + \boldsymbol{\alpha} \times \boldsymbol{x}, \tag{4.10}$$

$$\boldsymbol{x} = \boldsymbol{x}' + \boldsymbol{\xi} + \boldsymbol{\alpha} \times \boldsymbol{x}', \tag{4.11}$$

where $\boldsymbol{n}$ is the unit normal vector in the body-fixed frame and $\boldsymbol{x}'$ is defined in Figure 2-2. The linear forces and moments follow directly from equations (4.7) and (4.8) by

$$\boldsymbol{F}_{1_i} = \int_{\bar{S}_B} p_{1_i} \boldsymbol{n} \, \mathrm{d}S, \tag{4.12}$$

$$\boldsymbol{M}_{1_i} = \int_{\bar{S}_B} p_{1_i} \boldsymbol{x}' \times \boldsymbol{n} \, \mathrm{d}S, \tag{4.13}$$

for $i = 0, 1$. The time average of the second order forces are obtained by substituting the expressions for $\mathcal{P}$, $\boldsymbol{N}$ and $\boldsymbol{x}$ into equation (4.7) and (4.8) and taking the time average. The wetted surface S_B is divided into the mean wetted surface $\bar{S}_B$ and the surface between $z = 0$ and the wave run up. The integral over the latter surface is Taylor expanded about $z = 0$ and results in an integral along the mean water-line, denoted by c_w. The linear motions $\boldsymbol{\xi}$ and $\boldsymbol{\alpha}$ admit expansions in the slow-drift velocities as given by equation (4.21). Collecting terms of second order in the wave steepness δ and zero'th and first order in the slow-drift velocities τ_j, respectively gives

the following expressions for the mean forces and moments,

$$\bar{\boldsymbol{F}}_{20} = \int_{\bar{S}_B} \overline{\left[\left(p_{20} + (\boldsymbol{\xi}^{(0)} + \boldsymbol{\alpha}^{(0)} \times \boldsymbol{x}') \cdot \nabla p_{10}\right) \boldsymbol{n} + p_{10}\, \boldsymbol{\alpha}^{(0)} \times \boldsymbol{n}\right]} \, \mathrm{d}S + \frac{1}{2}\rho g \oint_{c_w} \overline{\zeta_{10}^2}\, \boldsymbol{n} \, \mathrm{d}l, \tag{4.14}$$

$$\bar{\boldsymbol{M}}_{20} = \int_{\bar{S}_B} \overline{\left[p_{20} + (\boldsymbol{\xi}^{(0)} + \boldsymbol{\alpha}^{(0)} \times \boldsymbol{x}') \cdot \nabla p_{10}\right]} (\boldsymbol{x}' \times \boldsymbol{n}) \, \mathrm{d}S + \int_{\bar{S}_B} \overline{\left[p_{10} \left(\boldsymbol{\xi}^{(0)} \times \boldsymbol{n} + \boldsymbol{\alpha}^{(0)} \times (\boldsymbol{x}' \times \boldsymbol{n})\right)\right]} \, \mathrm{d}S + \frac{1}{2}\rho g \oint_{c_w} \overline{\zeta_{10}^2} (\boldsymbol{x}' \times \boldsymbol{n}) \, \mathrm{d}l, \tag{4.15}$$

$$\bar{\boldsymbol{F}}_{21} = \int_{\bar{S}_B} \overline{\left[\left(p_{21} + (\boldsymbol{\xi}^{(0)} + \boldsymbol{\alpha}^{(0)} \times \boldsymbol{x}') \cdot \nabla p_{11}\right) \boldsymbol{n} + p_{11}\, \boldsymbol{\alpha}^{(0)} \times \boldsymbol{n}\right]} \, \mathrm{d}S + \int_{\bar{S}_B} \overline{\left[(\boldsymbol{\xi}^{(1)} + \boldsymbol{\alpha}^{(1)} \times \boldsymbol{x}') \cdot \nabla p_{10}\, \boldsymbol{n} + p_{10}\, \boldsymbol{\alpha}^{(1)} \times \boldsymbol{n}\right]} \, \mathrm{d}S + \rho g \oint_{c_w} \overline{\zeta_{10}\, \zeta_{11}}\, \boldsymbol{n} \, \mathrm{d}l, \tag{4.16}$$

$$\bar{\boldsymbol{M}}_{21} = \int_{\bar{S}_B} \overline{\left[p_{21} + (\boldsymbol{\xi}^{(0)} + \boldsymbol{\alpha}^{(0)} \times \boldsymbol{x}') \cdot \nabla p_{11}\right]} (\boldsymbol{x}' \times \boldsymbol{n}) \, \mathrm{d}S + \int_{\bar{S}_B} \overline{\left[(\boldsymbol{\xi}^{(1)} + \boldsymbol{\alpha}^{(1)} \times \boldsymbol{x}') \cdot \nabla p_{10} (\boldsymbol{x}' \times \boldsymbol{n})\right]} \, \mathrm{d}S + \int_{\bar{S}_B} \overline{\left[p_{11}\left(\boldsymbol{\xi}^{(0)} \times \boldsymbol{n} + \boldsymbol{\alpha}^{(0)} \times (\boldsymbol{x}' \times \boldsymbol{n})\right) + p_{10}\left(\boldsymbol{\xi}^{(1)} \times \boldsymbol{n} + \boldsymbol{\alpha}^{(1)} \times (\boldsymbol{x}' \times \boldsymbol{n})\right)\right]} \, \mathrm{d}S + \rho g \oint_{c_w} \overline{\zeta_{10}\, \zeta_{11}} (\boldsymbol{x}' \times \boldsymbol{n}) \, \mathrm{d}l, \tag{4.17}$$

where the following vector identity was used in the expressions for $\bar{\boldsymbol{M}}_{20}$ and $\bar{\boldsymbol{M}}_{21}$,

$$\begin{aligned} \boldsymbol{x}' \times (\boldsymbol{\alpha} \times \boldsymbol{n}) + (\boldsymbol{\alpha} \times \boldsymbol{x}') \times \boldsymbol{n} &= (\boldsymbol{\alpha} \cdot \boldsymbol{n})\, \boldsymbol{x}' - (\boldsymbol{\alpha} \cdot \boldsymbol{x}')\, \boldsymbol{n} \\ &= \boldsymbol{\alpha} \times (\boldsymbol{x}' \times \boldsymbol{n}). \end{aligned} \tag{4.18}$$

More detailed expressions for the linear and the mean-forces on a floating structure in monochromatic waves are given in Appendix A.

4.2 Linear motions

Due to the linear excitation from the ambient waves, the body will respond with the small amplitude motions $\xi_j(t)$ in mode j, where the index $j = 1,2,3$ refers to surge, sway and heave, respectively and rotations $\alpha_j(t)$, $j = 1,2,3$ about the corresponding axis. Only the surge, sway and yaw modes of motions are considered here. To simplify the notation in this section, the rotations $\alpha_j(t)$ are denoted by ξ_{j+3}. According to Newton's law, the motions can be determined by,

$$M_{ij}\frac{\mathrm{d}^2\xi_j(t)}{\mathrm{d}t^2} = F_i(t), \tag{4.19}$$

where $F_i(t)$ is the linear force in direction i. The linear forces are time-harmonic and the motions are therefore written,

$$\xi_j(t) = \mathrm{Re}\left(\hat{\xi}_j\,\mathrm{e}^{\mathrm{i}\omega t}\right). \tag{4.20}$$

Equation (4.19) will next be written with respect to the slow-drift frame. Time derivatives of a quantity in the slow-drift frame are given by equations (2.9) and (3.42). However, the term $\boldsymbol{f}\cdot\Delta$ in equation (2.9) equals zero since $\xi_j(t)$ is a function of time only. Expanding the linear force $F_i(t)$ in the slow-drift velocities, cf equations (A.1) and (A.2), suggests the following expansion for $\hat{\xi}_j$,

$$\hat{\xi}_j = \hat{\xi}_j^{(0)} + \hat{\xi}_j^{(1)} + O(\tau_j^2), \tag{4.21}$$

where $\hat{\xi}_j^{(0)}$ is the zero-speed linear motion and $\hat{\xi}_j^{(1)}$ is the correction due to the slow-drift velocities. Using the above equations, the equations of motion with respect to the slow-drift frame are now written,

$$M_{ij}\left[-\omega_0^2 + 2\omega_0\kappa(U\cos\beta + V\sin\beta) - 2\mathrm{i}\Omega\frac{\partial}{\partial\beta}\right]\left(\hat{\xi}_j^{(0)} + \hat{\xi}_j^{(1)} + \cdots\right) = F_i^{(0)} + F_i^{(1)} + \cdots. \tag{4.22}$$

Using the expressions for $F_i^{(0)}$ and $F_i^{(1)}$ in equations (A.3), (A.7), and consistently collecting terms of $O(1)$ and $O(\tau_j)$, respectively, the linear motions $\hat{\xi}_j^{(0)}$ and $\hat{\xi}_j^{(1)}$ are obtained from equation (4.22) as follows,

$$\left[-\omega_0^2\left(M_{ij}+A_{ij}^{(0)}\right)+\mathrm{i}\omega_0 B_{ij}^{(0)}+C_{ij}\right]\hat{\xi}_j^{(0)} \;=\; X_i^{(0)}, \tag{4.23}$$

$$\begin{aligned}\left[-\omega_0^2\left(M_{ij}+A_{ij}^{(0)}\right)+\mathrm{i}\omega_0 B_{ij}^{(0)}+C_{ij}\right]\hat{\xi}_j^{(1)} \;=\;& \\ X_i^{(1)}-\kappa\left[U\cos\beta+V\sin\beta\right]&\left[2\omega_0\left(M_{ij}+A_{ij}^{(0)}\right)-\mathrm{i}B_{ij}^{(0)}\right]\hat{\xi}_j^{(0)}+ \\ \left(\omega_0^2 A_{ij}^{(1)}-\mathrm{i}\omega_0 B_{ij}^{(1)}\right)&\hat{\xi}_j^{(0)}-\Omega\left[2\mathrm{i}\omega_0\left(M_{ij}+A_{ij}^{(0)}\right)+B_{ij}^{(0)}\right]\frac{\partial\hat{\xi}_j^{(0)}}{\partial\beta},\end{aligned} \tag{4.24}$$

where $\partial\hat{\xi}_j^{(0)}/\partial\beta$ is determined by,

$$\left[-\omega_0^2\left(M_{ij}+A_{ij}^{(0)}\right)+\mathrm{i}\omega_0 B_{ij}^{(0)}+C_{ij}\right]\frac{\partial\hat{\xi}_j^{(0)}}{\partial\beta} \;=\; \frac{\partial X_i^{(0)}}{\partial\beta}, \tag{4.25}$$

and the added-mass, damping-coefficients and the exciting forces are defined in Section A.1. The coefficients C_{ij} are the linear restoring coefficients, which for the horizontal modes of motion are due to external forces such as mooring lines.

4.3 The momentum conservation principle

As an alternative to the pressure integration over the wetted body surface, the horizontal mean forces on the body can be calculated using the momentum conservation principle. By this method, the force is expressed in terms of an integral of hydrodynamic quantities over a control-surface at some distance away from the body.

The momentum conservation principle is here first applied to a body undergoing arbitrary slow-drift motions in surge and sway in order to obtain the drift-forces of second-order in the wave-amplitude. The expressions are then perturbed in the

slow-drift velocities, assuming U and V are small, and expressions for the zero-speed drift force and the wave-drift damping are obtained. The angular velocity Ω of the slow-drift yaw-rotation is assumed to be equal to zero throughout this analysis.

The expressions for the mean drift-force in surge (1), sway (2) and yaw (6) were derived in Faltinsen (1990) and are written,

$$\bar{F}_i = -\iint_{S_\infty} [\overline{pn_i + \rho v_i v_n}]\, \mathrm{d}S, \qquad i = 1, 2, 6, \tag{4.26}$$

where the control-surface S_∞ was assumed fixed in space. The formula applies if S_∞ is fixed in the slow-drift frame of reference and the pressure p and the velocities v_i, v_n are given relative to this frame. The pressure is then given by equation (4.1) and the fluid velocities by,

$$v_1 = \frac{\partial \phi}{\partial x} - U, \tag{4.27}$$

$$v_2 = \frac{\partial \phi}{\partial y} - V, \tag{4.28}$$

$$v_6 = x v_2 - y v_1. \tag{4.29}$$

The unit normal vector $\boldsymbol{n} = (n_1, n_2, n_3)$ is pointing out of control-surface S_∞, while the yaw component n_6 is given by $n_6 = x n_2 - y n_1$. The control-surface is here taken to be a vertical circular cylinder centered at the origin of the slow-drift frame, with radius $R \to \infty$. Due to the oscillations of the wave-elevation, S_∞ is time-dependent. The control-surface is therefore written, $S_\infty = \bar{S}_\infty + \Delta S$, where $\bar{S}_\infty$ is the surface below $z = 0$ and ΔS the surface between $z = 0$ and the wave-elevation ζ. Assuming the wave-elevation is small, the integration along the z-axis on ΔS is expanded in a Taylor series about $z = 0$ as follows,

$$\begin{aligned} \iint_{\Delta S} (\star)\mathrm{d}S &= \int_{c_\infty} \int_0^\zeta (\star)\, \mathrm{d}z\, \mathrm{d}l \\ &= \int_{c_\infty} \left(\zeta(\star) + \tfrac{1}{2}\zeta^2 \frac{\partial(\star)}{\partial z} + \cdots \right)_{z=0} \mathrm{d}l, \end{aligned} \tag{4.30}$$

where $(\star)$ denotes the integrand in equation (4.26) and c_∞ the intersection between

S_∞ and $z = 0$. In order to obtain the drift-force correct to second-order in the wave-amplitude, the potential ϕ and the wave-elevation ζ are first expanded in the wave-steepness δ as follows,

$$\phi = \phi^{(0)} + \phi^{(1)} + \phi^{(2)} + o(\delta^2), \tag{4.31}$$

$$\zeta = \zeta^{(1)} + \zeta^{(2)} + o(\delta^2), \tag{4.32}$$

where the steady wave-elevation $\zeta^{(0)}$ was omitted assuming the steady potential $\phi^{(0)}$ can be represented by the double-body flow. Substituting the expression for ϕ into equations (4.1) and (4.27) - (4.29), and the expression for ζ into equation (4.30), the drift-forces in equation (4.26) of second-order in δ take the following form,

$$\begin{aligned}
\bar{F}_1 &= \rho \iint_{S_\infty} \left[\overline{\left(\phi_t - \boldsymbol{f}\cdot\Delta\phi + \tfrac{1}{2}\nabla\phi\cdot\nabla\phi + gz\right)n_1 - (\phi_x - U)(\phi_n - Un_1 - Vn_2)} \right] \mathrm{d}S \\
&= \rho \iint_{\bar{S}_\infty} \left[\overline{-(V/R)\phi_\odot^{(2)} + \tfrac{1}{2}\nabla\phi^{(1)}\cdot\nabla\phi^{(1)} n_1 - \phi_x^{(1)}\phi_n^{(1)}} \right] \mathrm{d}S - \\
&\quad \frac{\rho}{2g}\int_{c_\infty} \left[\overline{\phi_t^{(1)}\phi_t^{(1)} n_1 - 2(V/R)\phi_t^{(1)}\phi_\odot^{(1)}} \right] \mathrm{d}l - \rho \int_{c_\infty} \overline{\zeta^{(2)}} U(Un_1 + Vn_2)\mathrm{d}l + \\
&\quad \frac{\rho}{2g}\int_{c_\infty} \left[\overline{U^2\phi_x^{(1)}\phi_x^{(1)} n_1 + V^2\phi_y^{(1)}\phi_y^{(1)} n_1 - 2(V^2/R)\phi_\odot^{(1)}\phi_y^{(1)} + 2UV\phi_x^{(1)}\phi_x^{(1)} n_2} \right] \mathrm{d}l + o(\delta^2),
\end{aligned} \tag{4.33}$$

$$\begin{aligned}
\bar{F}_2 &= \rho \iint_{S_\infty} \left[\overline{\left(\phi_t - \boldsymbol{f}\cdot\Delta\phi + \tfrac{1}{2}\nabla\phi\cdot\nabla\phi + gz\right)n_2 - (\phi_y - V)(\phi_n - Un_1 - Vn_2)} \right] \mathrm{d}S \\
&= \rho \iint_{\bar{S}_\infty} \left[\overline{(U/R)\phi_\odot^{(2)} + \tfrac{1}{2}\nabla\phi^{(1)}\cdot\nabla\phi^{(1)} n_2 - \phi_y^{(1)}\phi_n^{(1)}} \right] \mathrm{d}S - \\
&\quad \frac{\rho}{2g}\int_{c_\infty} \left[\overline{\phi_t^{(1)}\phi_t^{(1)} n_2 + 2(U/R)\phi_t^{(1)}\phi_\odot^{(1)}} \right] \mathrm{d}l - \rho \int_{c_\infty} \overline{\zeta^{(2)}} V(Un_1 + Vn_2)\mathrm{d}l + \\
&\quad \frac{\rho}{2g}\int_{c_\infty} \left[\overline{U^2\phi_x^{(1)}\phi_x^{(1)} n_2 + V^2\phi_y^{(1)}\phi_y^{(1)} n_2 + 2(U^2/R)\phi_\odot^{(1)}\phi_x^{(1)} + 2UV\phi_y^{(1)}\phi_y^{(1)} n_1} \right] \mathrm{d}l + o(\delta^2),
\end{aligned} \tag{4.34}$$

$$\begin{aligned}
\bar{F}_6 &= -\rho \iint_{S_\infty} \overline{\left(x(\phi_y - V) - y(\phi_x - U)\right)(\phi_n - Un_1 - Vn_2)} \mathrm{d}S \\
&= -\rho \iint_{\bar{S}_\infty} \left[\overline{\phi_\odot^{(1)}\phi_n^{(1)} - (Un_1 + Vn_2)\phi_\odot^{(2)} + (yU - xV)\phi_n^{(2)}} \right] \mathrm{d}S +
\end{aligned}$$

$$\frac{\rho}{g}\int_{c_\infty}\left[\overline{\phi_t^{(1)}\left(U[-\phi_\odot^{(1)}n_1+\phi_n^{(1)}y]-V[\phi_\odot^{(1)}n_2+\phi_n^{(1)}x]\right)}\right]\mathrm{d}l+$$
$$\frac{\rho}{g}\int_{c_\infty}\left[\overline{U^2\phi_x^{(1)}(\phi_\odot^{(1)}n_1-\phi_n^{(1)}y)+V^2\phi_y^{(1)}(\phi_\odot^{(1)}n_2+\phi_n^{(1)}x)}\right]\mathrm{d}l+$$
$$\frac{\rho}{g}\int_{c_\infty}\left[\overline{UV\left(\phi_\odot^{(1)}[\phi_y^{(1)}n_1+\phi_x^{(1)}n_2]+\phi_n^{(1)}[\phi_x^{(1)}x-\phi_y^{(1)}y]\right)}\right]\mathrm{d}l+$$
$$\rho\int_{c_\infty}\overline{\zeta^{(2)}}(Un_1+Vn_2)(yU-xV)\,\mathrm{d}l+o(\delta^2). \tag{4.35}$$

Notice that in the integrand of equation (4.26) there are only terms of $O(\delta^2)$ on S_∞ and terms of $O(\delta)$ and $O(1)$ on ΔS. The steady double-body potential $\phi^{(0)}$ behaves like a dipole as $R\to\infty$ and does not contribute to the forces in the above expressions.

The drift-forces $\bar{F}_i$ are next expanded in U and V, assuming the slow-drift velocities are small. This allows the drift-forces in equations (4.33) - (4.35) to be expressed as a sum of the zero-speed drift-force D_i and the wave-drift damping coefficients B_{ij} as follows,

$$\bar{F}_i \;=\; D_i - B_{ij}U_j + O(U_j^2), \tag{4.36}$$

where $U_1 = U$ and $U_2 = V$. B_{ij} is defined as the leading order correction to the drift-force in direction i due to slow-drift motion in direction j. Expressions for B_{ij} are obtained by further expanding the potentials $\phi^{(1)}$ and $\phi^{(2)}$ in U_j, keeping terms of $O(U_j)$ only, and substituting into equations (4.33) - (4.35). To leading order, the potentials $\phi^{(1)}$ and $\phi^{(2)}$ are written,

$$\phi^{(1)} \;=\; \mathrm{Re}\left[(\varphi+\psi)\mathrm{e}^{\mathrm{i}\omega t}\right]+O(\delta U_j^2), \tag{4.37}$$
$$\phi^{(2)} \;=\; \bar{\phi}_{20}+O(\delta^2 U_j). \tag{4.38}$$

The potential ψ depends on the slow-drift velocities U, V and Ω, cf Section 3.2. Here shall be used a notation which allows explicit expressions for the wave-drift damping coefficients B_{ij}. Define,

$$\psi^U \;\equiv\; \psi|_{(U=1,V=0,\Omega=0)}, \tag{4.39}$$

$$\psi^V \equiv \psi|_{(U=0,V=1,\Omega=0)}, \tag{4.40}$$

where the subscripts on ψ denote the values of the slow-drift velocities to replace U, V and Ω in Section 3.2. The wave-drift damping coefficients B_{ij} are obtained by substituting equations (4.37) and (4.38) into equations (4.33) - (4.34) and using equation (A.13) to obtain the time-average. Including terms proportional to U only, the wave-drift damping due to the slow-drift surge motion is given by,

$$\begin{aligned} B_{11} &= \tfrac{1}{2}\rho \iint_{\bar{S}_\infty} [\varphi_x \psi_n^{U*} + \varphi_n \psi_x^{U*} - \nabla\varphi \cdot \nabla\psi^{U*} n_1]\, \mathrm{d}S + \\ &\quad \tfrac{1}{2}\rho \int_{c_\infty} \varphi \left(\nu\psi^{U*} n_1 - \kappa \frac{\omega_0}{g} \cos\beta \varphi^* n_1 \right) \mathrm{d}l, \end{aligned} \tag{4.41}$$

$$\begin{aligned} B_{21} &= \tfrac{1}{2}\rho \iint_{\bar{S}_\infty} \left[\varphi_y \psi_n^{U*} + \varphi_n \psi_y^{U*} - \nabla\varphi \cdot \nabla\psi^{U*} n_2 - \frac{1}{R} \frac{\partial \bar{\phi}_{20}}{\partial \Theta} \right] \mathrm{d}S + \\ &\quad \tfrac{1}{2}\rho \int_{c_\infty} \varphi \left(\nu\psi^{U*} n_2 - \kappa \frac{\omega_0}{g} \cos\beta \varphi^* n_2 + \frac{\mathrm{i}\omega_0}{gR} \varphi_\Theta^* \right) \mathrm{d}l, \end{aligned} \tag{4.42}$$

$$\begin{aligned} B_{61} &= \tfrac{1}{2}\rho \iint_{\bar{S}_\infty} \left[\varphi_\Theta \psi_n^{U*} + \varphi_n \psi_\Theta^{U*} - 2n_1 \frac{\partial \bar{\phi}_{20}}{\partial \Theta} + 2y \frac{\partial \bar{\phi}_{20}}{\partial n} \right] \mathrm{d}S + \\ &\quad \tfrac{1}{2} \frac{\rho \mathrm{i}\omega_0}{g} \int_{c_\infty} \varphi \left(-\varphi_\Theta^* n_1 + \varphi_n^* y \right) \mathrm{d}l. \end{aligned} \tag{4.43}$$

The expressions for B_{ij} could alternatively have been derived from equation (4.26) employing the expansion (2.11) instead of the separate expansions presented in this Section by equations (4.31), (4.37) and (4.38).

4.3.1 Conservation law for the slow-drift damping coefficients

Expressions (4.41) and (4.42), excluding the potential $\bar{\phi}_{20}$, will be shown to be in conservation form, i.e. its value does not depend on the position of the control surface S_∞. This will be shown to be the case for two arbitrary velocity potentials φ and ψ^U subject to the free-surface conditions

$$-\nu\varphi + \varphi_z = 0, \tag{4.44}$$

$$-\nu\psi^U + \psi^U_z = 2\mathrm{i}\frac{\omega_0}{g}\varphi_x - 2\kappa\frac{\omega_0}{g}\cos\beta\,\varphi. \tag{4.45}$$

Here it is important to note that all three wavelike components of ψ^U, described in Section 3.2.2, satisfy equation (4.45), when written in terms of the slow-drift coordinates. In particular, Ψ_1^j is subject to (4.45), while Ψ_2^j and Ψ_3^j satisfy the homogeneous form of (4.45).

We will use the following identity, valid for an arbitrary velocity potential ϕ over a closed surface S:

$$\boldsymbol{I}(\phi) = \mathrm{Re}\iint_S(\phi_n\nabla_{2D}\phi - \tfrac{1}{2}\nabla\phi\cdot\nabla\phi\;\boldsymbol{n}_{2D})\mathrm{d}S = 0, \tag{4.46}$$

where $\boldsymbol{n}_{2D} = (n_1, n_2)$ is the horizontal component of the unit normal vector on S pointing out of the enclosed domain and ∇_{2D} is the horizontal component of the gradient.

Apply now (4.46) to the potential $\phi = \varphi + \psi^{U*}$ over the surface $S = S_{c_1} + S_{c_2} + S_F$, where S_{c_1} and S_{c_2} are two vertical, neighboring surfaces and S_F is the annular strip on $z = 0$ between the intersecting contours c_1 and c_2 as indicated in Figure 4-1. The vertical surfaces S_{c_1} and S_{c_2} do not have to be circular. Assuming that the flow velocity vanishes at $z = -h$, equation (4.46) may be rewritten in the form

$$\mathrm{Re}\iint_{S_{c_1}+S_{c_2}+S_F}(\psi_n^{U*}\nabla_{2D}\varphi + \varphi_n\nabla_{2D}\psi^{U*} - \nabla\varphi\cdot\nabla\psi^{U*}\,\boldsymbol{n}_{2D})\mathrm{d}S = 0. \tag{4.47}$$

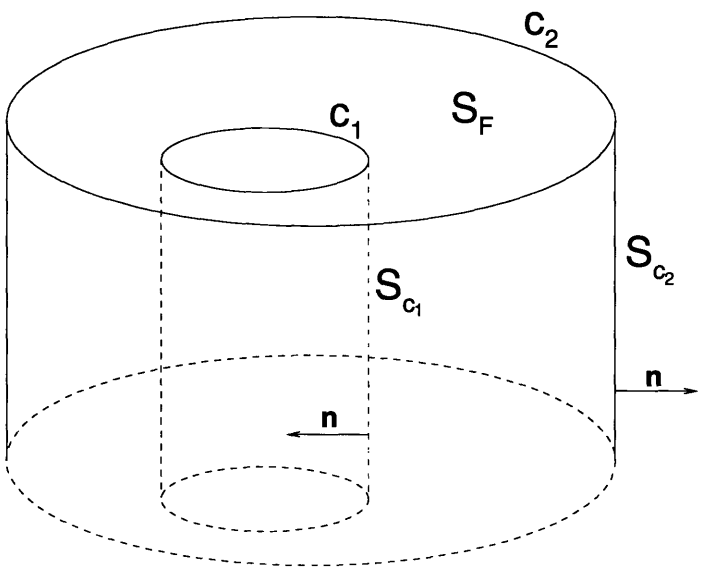

Figure 4-1: The vertical control-surfaces S_{c_1} and S_{c_2} and their intersections c_1 and c_2, respectively, with $z = 0$.

The integral over S_F, where $\boldsymbol{n}_{2D} = 0$, can be simplified using the free surface conditions (4.44) and (4.45). The integrand on this surface may be reduced to the form

$$\psi_z^{U*}\nabla_{2D}\varphi + \varphi_z\nabla_{2D}\psi^{U*} = (\nu\psi^{U*} - 2\mathrm{i}\frac{\omega_0}{g}\varphi_x^* - 2\kappa\frac{\omega_0}{g}\cos\beta\varphi^*)\nabla_{2D}\varphi + \nu\varphi\nabla_{2D}\psi^{U*}. \quad (4.48)$$

The x- and y-components of equation (4.48) are now treated separately in proving the conservation law for the wave-drift damping coefficients B_{11} and B_{21}, respectively. The x-component is simplified by employing the identities Re $(2\varphi_x\varphi^*) =$ Re $(\varphi_x\varphi^* + \varphi_x^*\varphi)$ and Re $(2\mathrm{i}\varphi_x\varphi_x^*) = 0$. It follows that

$$\begin{aligned}\mathrm{Re}\iint_{S_F}(\varphi_x\psi_z^{U*} + \varphi_z\psi_x^{U*})\mathrm{d}S &= \mathrm{Re}\iint_{S_F}\frac{\partial}{\partial x}(\nu\varphi\psi^{U*} - \kappa\frac{\omega_0}{g}\cos\beta\,\varphi\varphi^*)\mathrm{d}S \\ &= \mathrm{Re}\oint_{c_1+c_2}(\nu\varphi\psi^{U*} - \kappa\frac{\omega_0}{g}\cos\beta\,\varphi\varphi^*)\,n_1\mathrm{d}l, \quad (4.49)\end{aligned}$$

where Stokes' theorem has been used. Combining equations (4.49) and the x-component of equation (4.47), gives the following equation for the potentials φ and ψ^{U*}:

$$\mathrm{Re}\iint_{S_{c_1}+S_{c_2}}(\varphi_x\psi_n^{U*} + \varphi_n\psi_x^{U*} - \nabla\varphi\cdot\nabla\psi^{U*}\,n_1)\mathrm{d}S +$$

$$\mathrm{Re} \oint_{c_1+c_2} (\nu\varphi\psi^{U*} - \kappa\frac{\omega_0}{g}\cos\beta\,\varphi\varphi^*)\,n_1 \mathrm{d}l \;=\; 0. \qquad (4.50)$$

Comparing equations (4.41) and (4.50), noting that the unit normal vector $\boldsymbol{n}$ points inward on the inner surface S_{c_1}, it is found that expression (4.41) is independent of the position of S_∞, which proves the conservation law for the wave-drift damping coefficient B_{11}.

The proof of the conservation law for the coefficient B_{21} is similar to the above analysis. The y-component of equation (4.48) is first simplified using the identity

$$\mathrm{Re}\,[-2\mathrm{i}\varphi_y\varphi_x^*] \;=\; \mathrm{Re}\,\left[\mathrm{i}\frac{\partial}{\partial x}(\varphi\varphi_y^*) - \mathrm{i}\frac{\partial}{\partial y}(\varphi\varphi_x^*)\right]. \qquad (4.51)$$

The integral on S_F of the y-component in equation (4.48) can then be written

$$\begin{aligned}\mathrm{Re}\iint_{S_F}(\varphi_y\psi_z^* + \varphi_z\psi_y^*)\mathrm{d}S \;&=\; \mathrm{Re}\iint_{S_F}\frac{\partial}{\partial y}(\nu\varphi\psi^* - \omega_0\kappa\cos\beta\,\varphi\varphi^*)\mathrm{d}S + \\ &\quad \mathrm{Re}\,\mathrm{i}\frac{\omega_0}{g}\kappa\iint_{S_F}\left[\frac{\partial}{\partial x}(\varphi\varphi_y^*) - \frac{\partial}{\partial y}(\varphi\varphi_x^*)\right]\mathrm{d}S \\ &=\; \mathrm{Re}\oint_{c_1+c_2}\varphi(\nu\psi^* n_2 - \kappa\frac{\omega_0}{g}\cos\beta\,\varphi^* n_2 + \mathrm{i}\frac{\omega_0}{g}\varphi_l^*)\mathrm{d}l,\end{aligned} \qquad (4.52)$$

where φ_l^* is the derivative of φ^* along the positive tangential direction of the curves. For cylindrical coordinates it is given by $\varphi_l^* = \pm\frac{1}{R}\varphi_\circ^*$ for the outer/inner curves. Combining equations (4.49) and the y-component of equation (4.47), and comparing with (4.42) proves the conservation law for the damping coefficient B_{21} in equation (4.42), excluding the potential $\bar{\phi}_{20}$.

The position of the control surface S_∞ in (4.41) and (4.42) may therefore be selected arbitrarily. It may for example be taken to coincide with the body surface, as long as only the wavelike components are included in the definition of the velocity potential Ψ_2^j. The non-wavelike part of Ψ_2^j does not satisfy equation (4.45) and must therefore be omitted. All integrations suggested by expression (4.41) and (4.42) are carried out over the surface of each cylinder j by employing the explicit local wavelike solutions derived in Section 3.2.

Chapter 5

Results - frequency domain

This chapter presents plots of the hydrodynamic forces and motions of Chapter 4 for arrays of cylinders and real platforms. The results from the time-simulations are presented in Chapter 7.

The computations of the motions and forces were performed by the computer program SWIM (Slow Wave Induced Motions), which is an implementation of the theory in Chapters 3 and 4. The code is part of a joint industrial project that was started for the purpose of studying the slow-drift motions of real offshore structures.

The theory in Chapter 3 was derived for arrays of vertical cylinders with draft equal to the water-depth. Most real offshore structures, however, consists of an array of truncated cylinders attached to a set of pontoons. The theory in the previous chapters was therefore extended to account for the truncated cylinders and pontoons in an approximate manner. This is discussed later in this section.

In order to verify the results computed by SWIM, comparison has been made with other computer codes. Zero-speed quantities were provided by the radiation/diffraction panel program WAMIT (Korsmeyer, et. al., 1988). WAMIT is a mature 3-dimensional frequency domain program for the analysis of interactions of surface waves with offshore structures. Quantities associated with the effects of forward-speed were provided by a panel program of the University of Oslo (Nossen, 1991 and Grue, 1993).

5.1 Array of cylinders with draft equal to water-depth

First an array of vertical cylinders with draft equal to the water-depth was studied. This geometry may not be of great practical interest by itself, but provides a good basis for comparison of the hydrodynamic forces and motions. It is also shown later in the section that this geometry is useful for the study of more complex geometries.

The array of cylinders, referred to as platform I, consists of four equal cylinders with radii $a = 10[m]$ and draft equal to $3a$. Each cylinder is centered on the corners of a square with sides $7a$. The configuration of the cylinders and the sea bottom are shown in Figure 5-1. The linear forces, the zero-speed drift-forces and the wave-

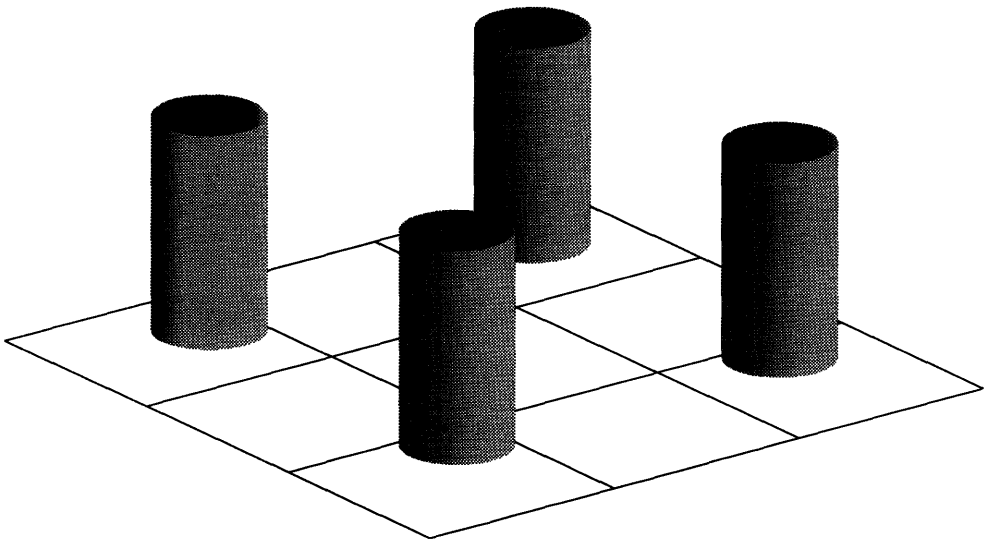

Figure 5-1: Platform I. The cylinder radii=10[m] and the cylinders are centered on the corners of a square with sides=70[m]. The draft of the cylinders and the water depth=30[m].

drift damping due to slow yaw rotations were computed by pressure integration, as described in Section 4.1. The wave-drift damping forces B_{11} and B_{21} were computed by the momentum conservation, described in Section 4.3.

The comparison with WAMIT and Nossen et. al. are excellent for both linear motions and the mean forces.

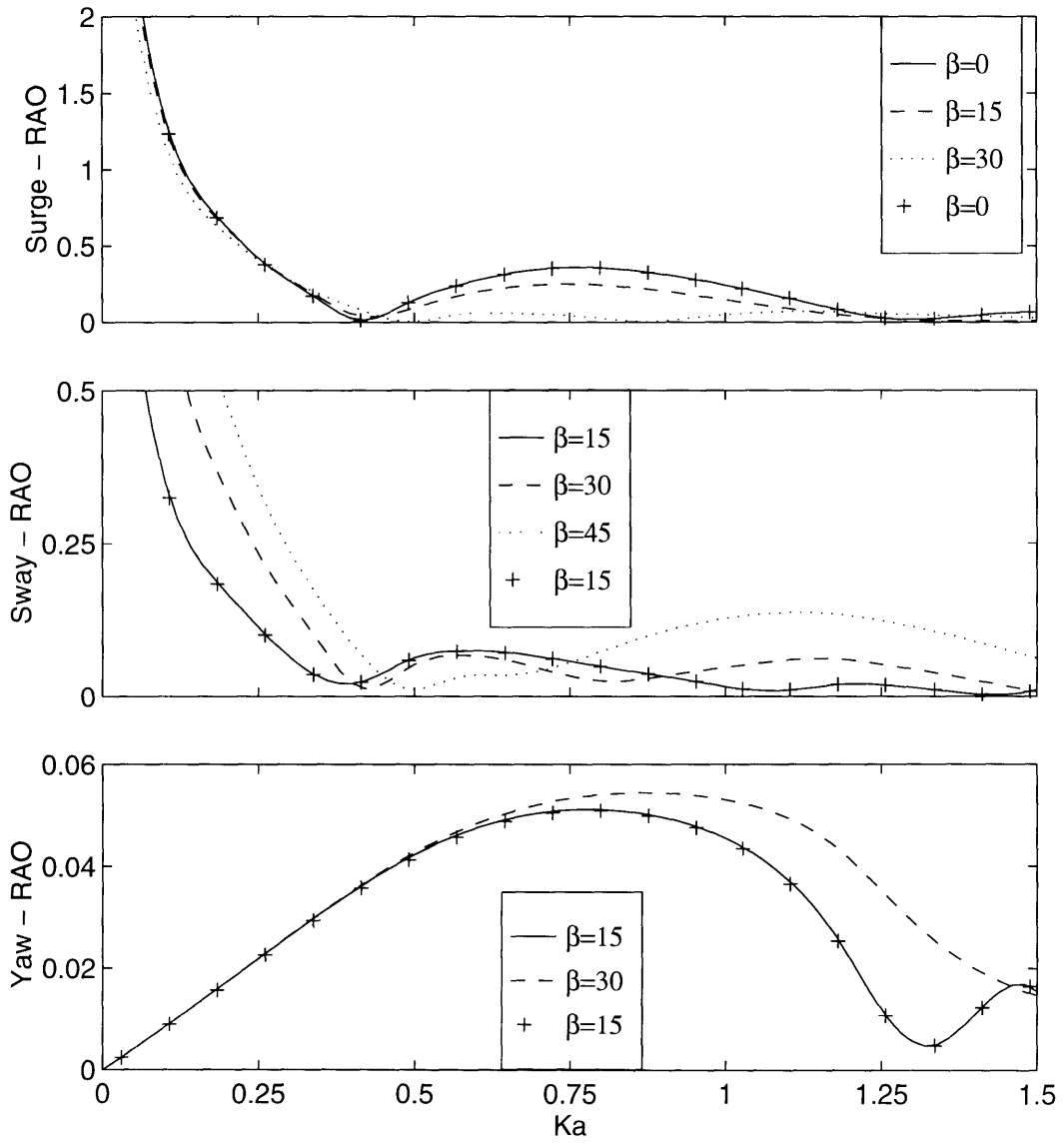

Figure 5-2: RAO of platform I for different wave-headings. The lines were computed by SWIM and the +'s by WAMIT. *Top*: $|\hat{\xi}_1^{(0)}/A|$. *Center*: $|\hat{\xi}_2^{(0)}/A|$. *Bottom*: $|\hat{\xi}_6^{(0)}/(A/a)|$.

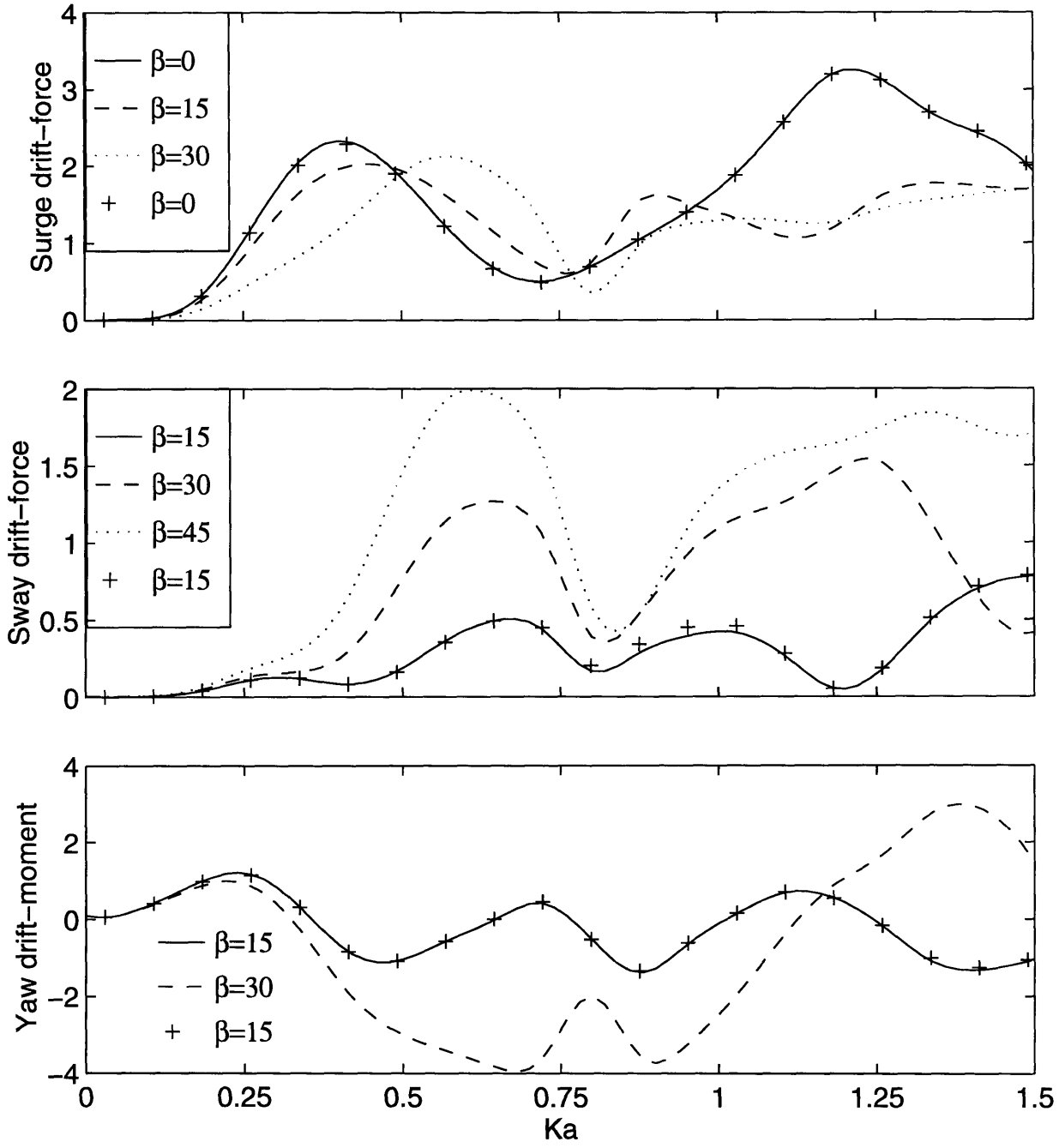

Figure 5-3: Drift-forces and drift moment of platform I for different wave-headings. The lines were computed by SWIM and the +'s by WAMIT. *Top*: $D_1/(\rho g A^2 a)$. *Center*: $D_2/(\rho g A^2 a)$. *Bottom*: $D_6/(\rho g A^2 a^2)$.

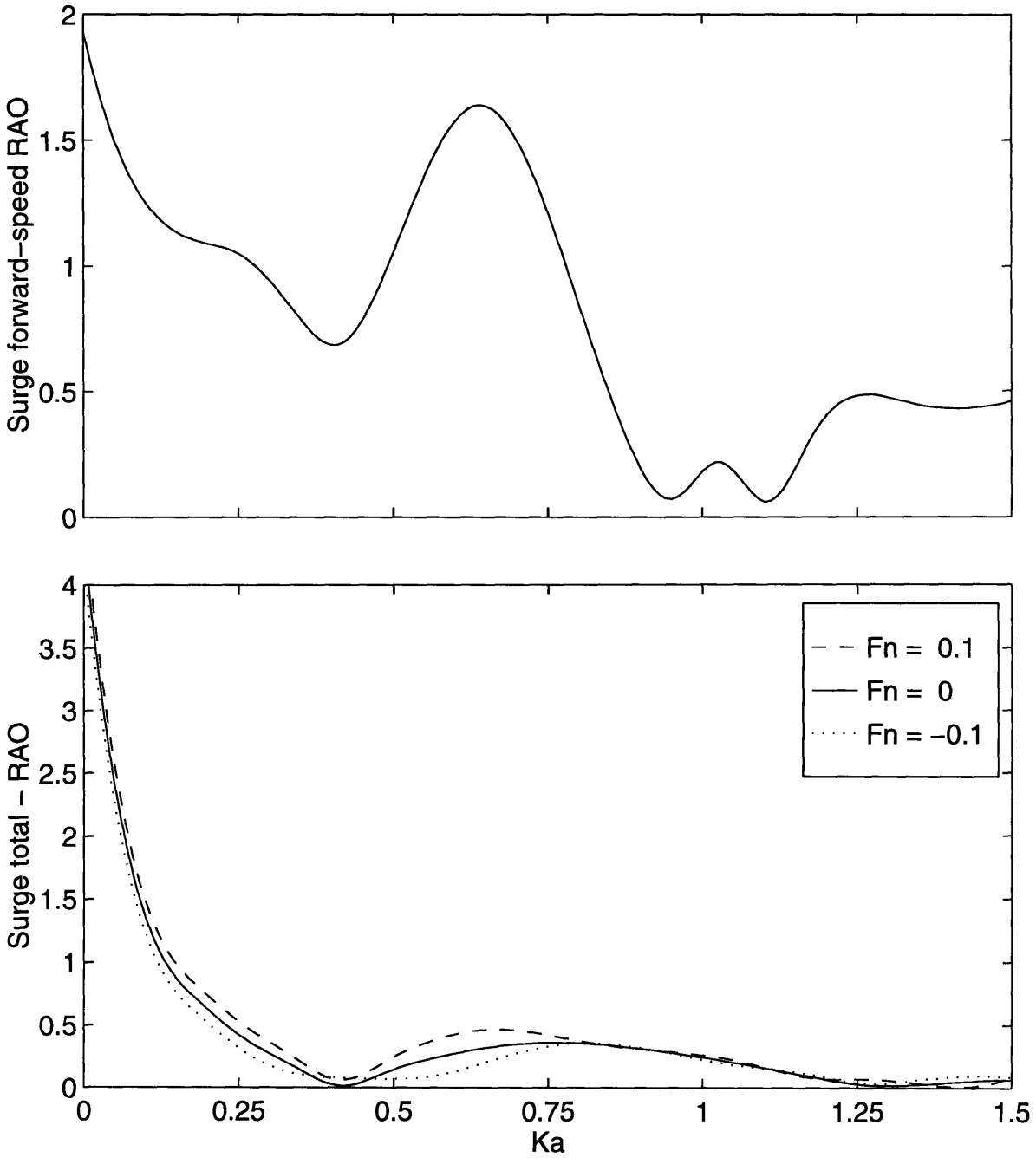

Figure 5-4: Surge RAO with and without slow-drift velocity U. *Top*: $\hat{\xi}_1^{(1)}/(AF_n)$. *Bottom*: $\hat{\xi}_1^{(0)}/A + \hat{\xi}_1^{(1)}/A)$) for $F_n = -0.1$, 0 and 0.1

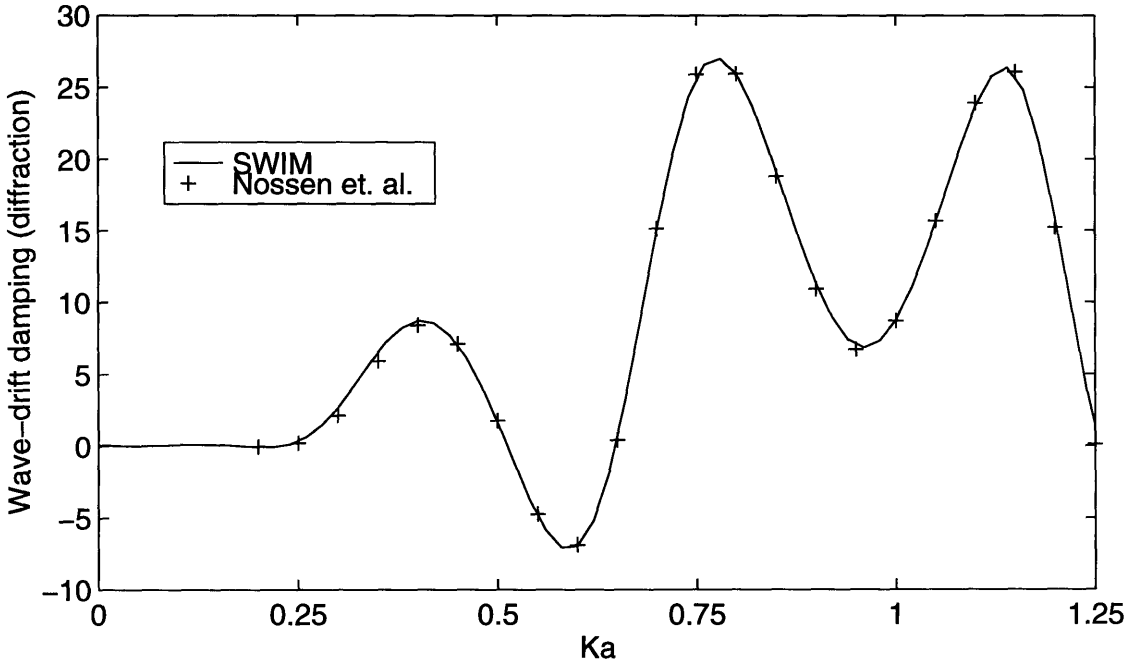

Figure 5-5: Wave-drift damping $(B_{11}/\rho(ga)^{1/2}A^2)$ for a restrained body. Wave-heading: $\beta = 0^o$. Comparison between SWIM and Nossen, Grue & Palm (1991).

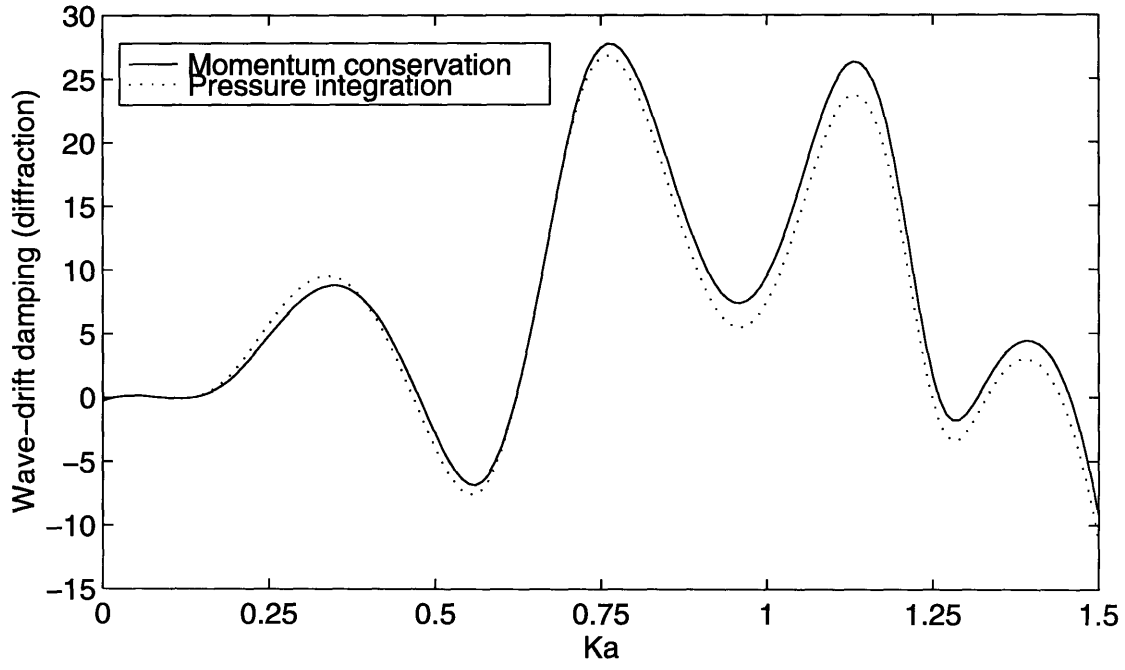

Figure 5-6: Wave-drift damping $B_{11}/(\rho(ga)^{1/2}A^2)$ of platform I, restrained, with $\beta = 0^o$. Comparison between pressure integration and the momentum conservation. In the pressure integration, only wave-like terms are included in the forward-speed potential.

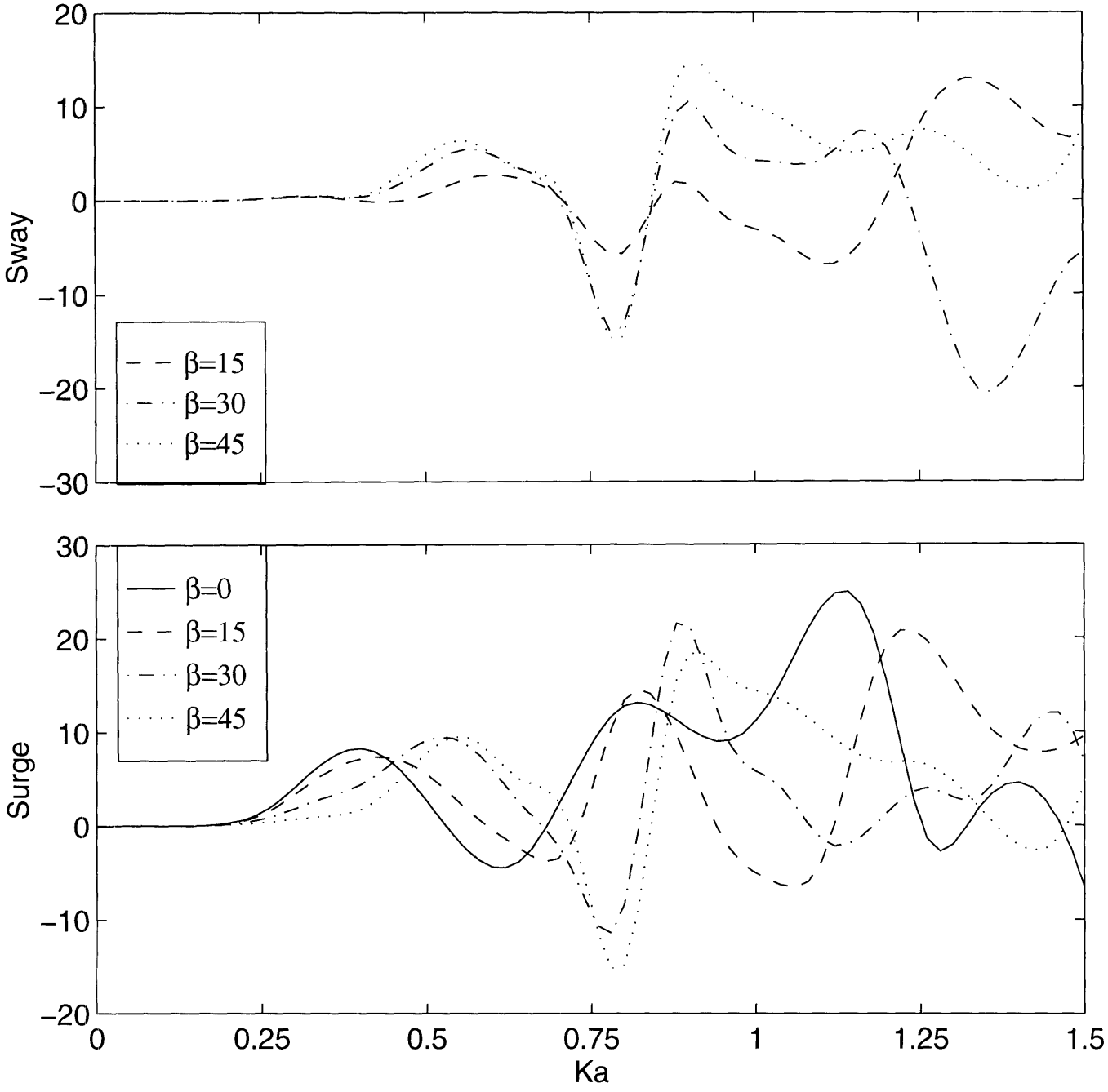

Figure 5-7: Wave-drift damping due to slow-drift surge motion of platform I, free to surge, sway and yaw in linear motions. *Top*: Sway force $(B_{21}/\rho(ga)^{1/2}A^2)$. *Bottom*: Surge force $(B_{11}/\rho(ga)^{1/2}A^2)$.

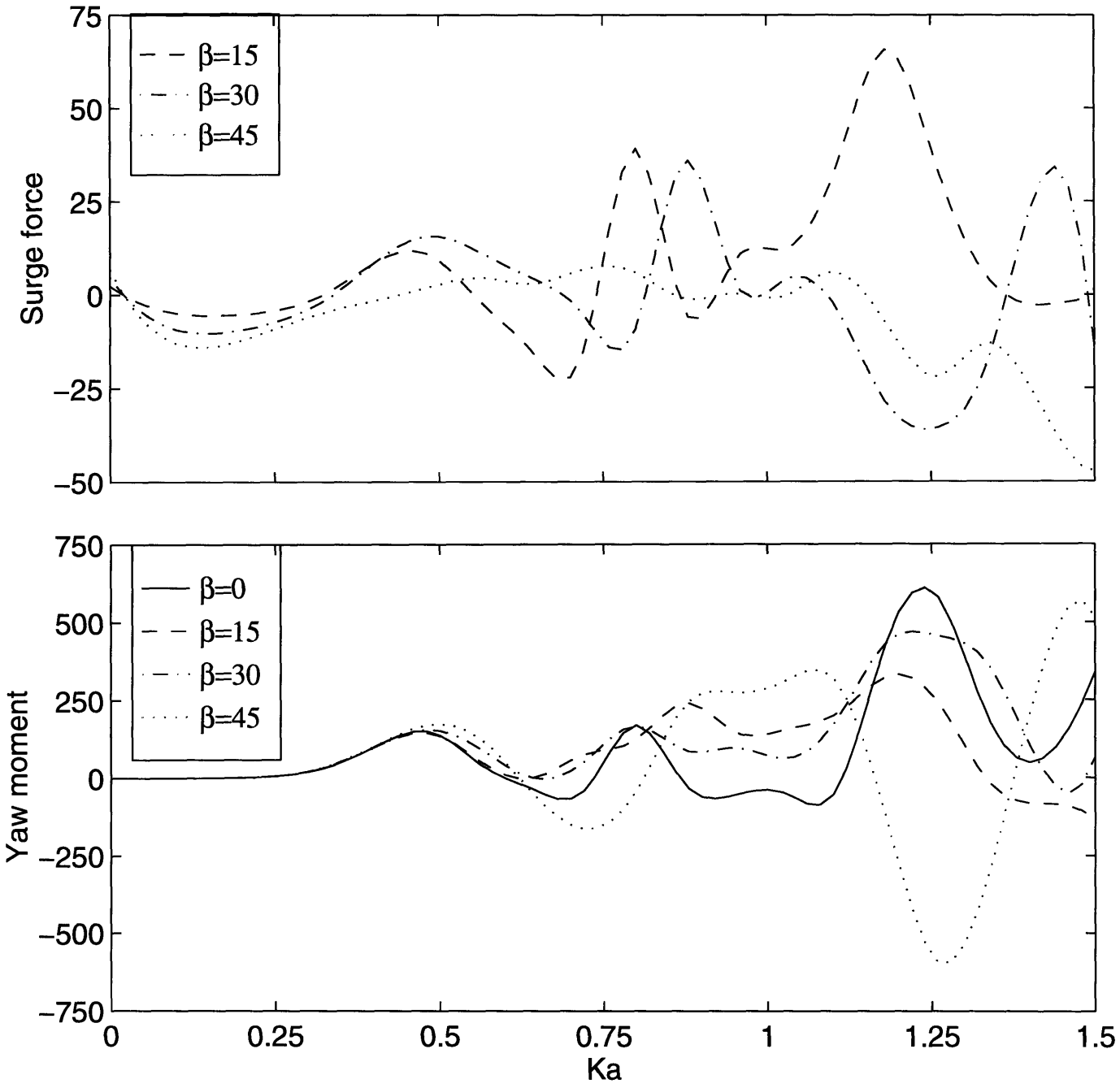

Figure 5-8: Wave-drift damping due to slow-drift yaw motion of platform I, free to surge, sway and yaw in linear motions. *Top*: Surge force $(B_{16}/\rho g A^2 a(a/g)^{1/2})$. *Bottom*: Yaw moment $(B_{66})/\rho g A^2 a^2 (a/g)^{1/2}$.

5.2 Truncated cylinders

The array of cylinders from the previous section is here studied in deep water, and is referred to as platform II. The truncation of the cylinders have been accounted for in an approximate manner in SWIM. The fluid-flow is solved for as if the cylinders were extended down to the bottom. The forces, however, are integrated only over the actual surface of the body.

For waves with wave-length less than twice the draft of the body, the truncation error is not expected to contribute significantly to the forces, since most of the wave-action occurs above the draft of the cylinders. This can be seen from Figures 5-10 and 5-11, where the corresponding region is for $Ka > 1$. For longer waves, however, the fluid-flow near the bottom of the truncated cylinder is not expected to be correctly modelled by SWIM. These are 3-dimensional effects that in general tend to reduce the force on the body. For long waves, the drift-forces are therefore generally overestimated by SWIM.

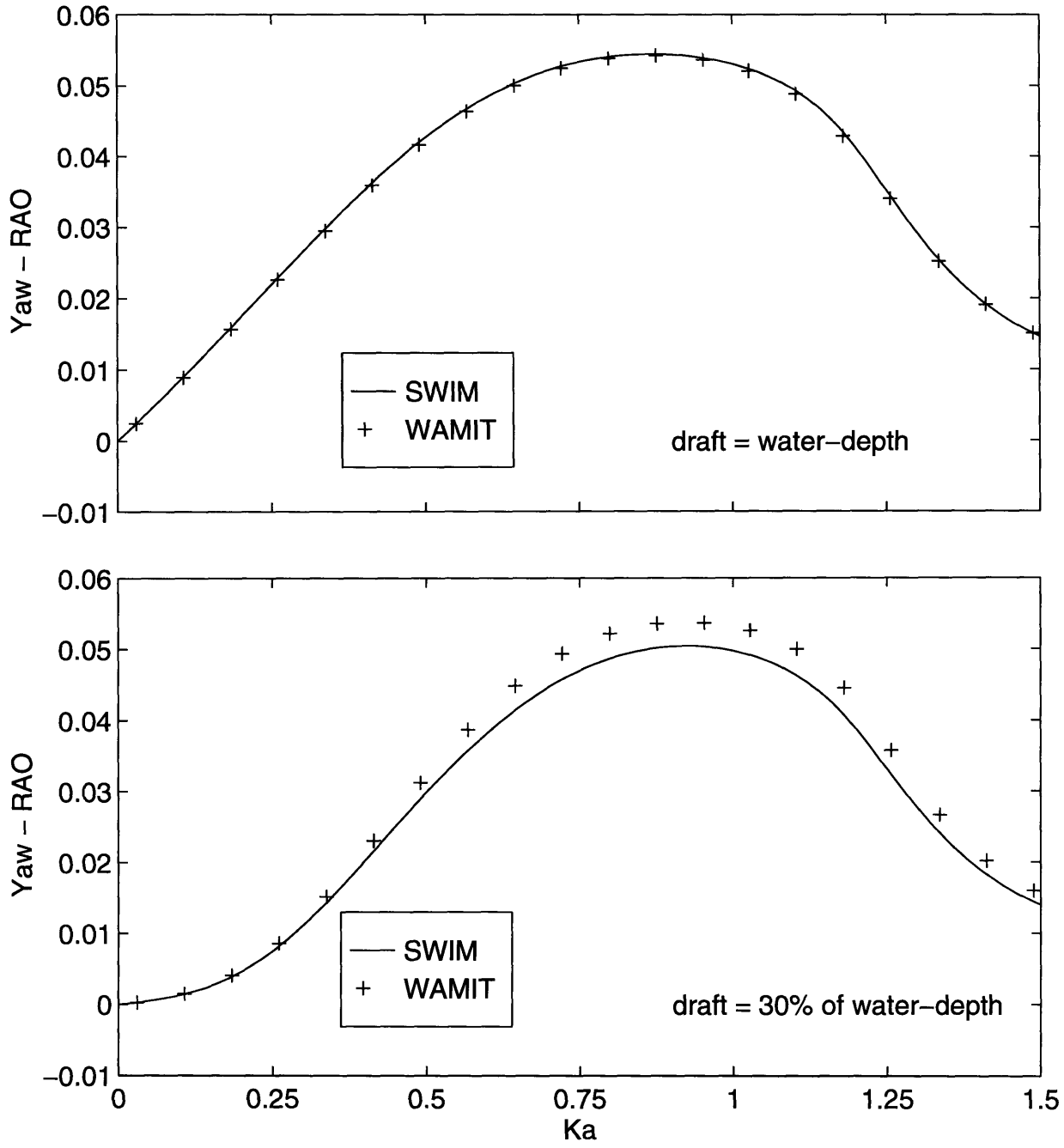

Figure 5-9: Yaw RAO ($|\alpha_3|$) of platform I, computed by SWIM and WAMIT for $\beta = 30^o$. *Top*: Draft of cylinders = water-depth. *Bottom*: Draft of cylinders = 30% of water-depth.

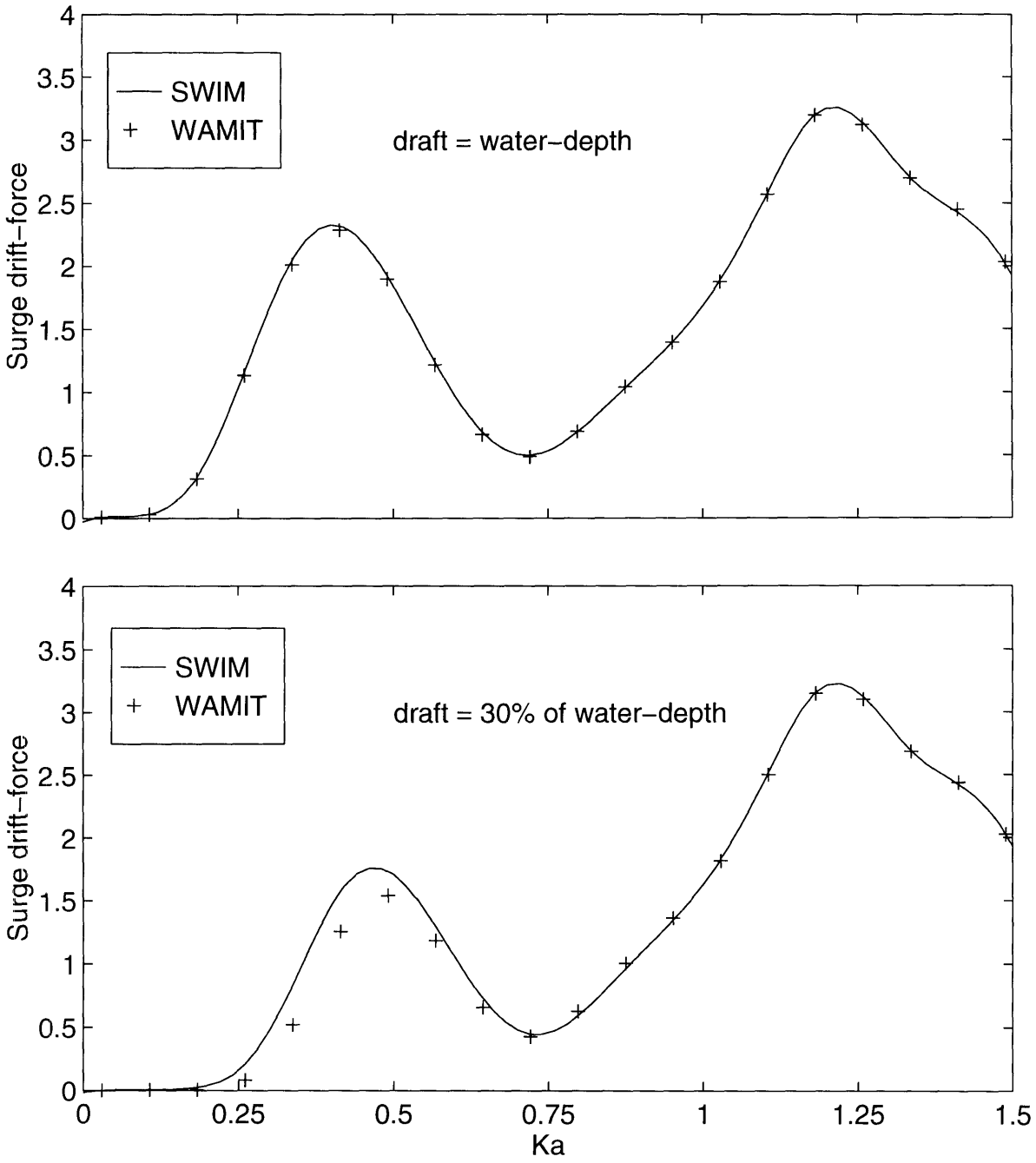

Figure 5-10: Surge drift force ($D_1/\rho g A^2 a$) of platform I, computed by SWIM and WAMIT for $\beta = 0^o$. *Top*: Draft of cylinders = water-depth. *Bottom*: Draft of cylinders = 30% of water-depth.

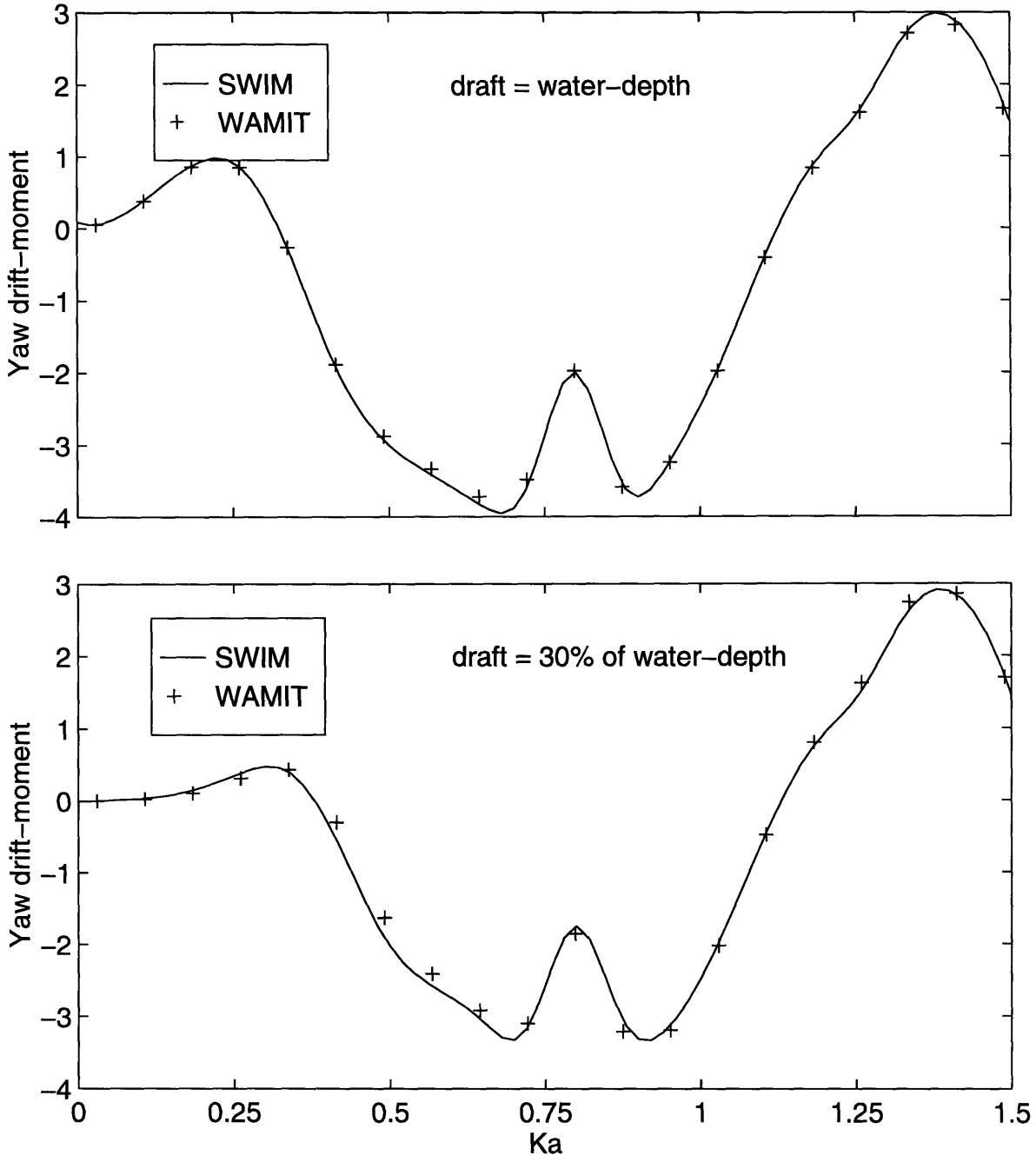

Figure 5-11: Yaw drift moment ($D_6/\rho g A^2 a^2$) of platform I, computed by SWIM and WAMIT for $\beta = 30^o$. *Top*: Draft of cylinders = water-depth. *Bottom*: Draft of cylinders = 30% of water-depth.

5.3 Truncated cylinders with rectangular pontoons

The hydrodynamic forces on a realistic platform are studied. The cylinder configuration and draft are identical to the cylinder array of Section 5.1. The rectangular pontoons are modelled as illustrated in Figure 5-12. The pontoons have width equal to the diameter of the cylinders and height=14$[m]$. The draft of the pontoons equals 44$[m]$. The platform is referred to as platform III.

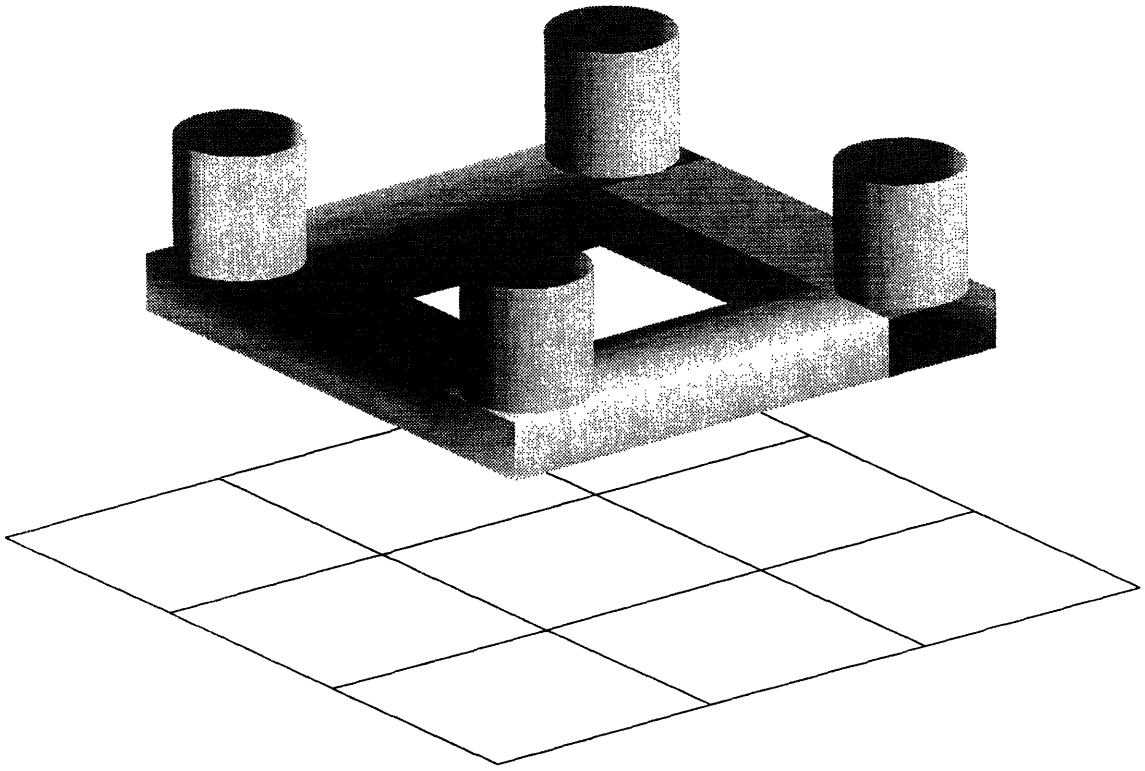

Figure 5-12: A realistic offshore platform, with the same cylinder configuration as in the previous section, and pontoons with dimensions: width= , height= and length= .

The effects of rectangular pontoons are accounted for in the computations of the linear motions and the zero-speed forces. The linear forces on the pontoons are computed using a long wave approximation to relate the diffraction forces to the added-mass and damping coefficients. The Froude-Krilov force is computed with no approximation. The added-mass of the pontoons are obtained from the 2-dimensional values of the cross-section. Consistently with the long wave approximation, the damping-

coefficients of the pontoons are neglected. For the zero-speed forces, a long wave approximation by Nielsen (1987) was employed.

The flow interaction between the cylinders and the pontoons was not accounted for, nor was the interaction between pontoons considered. These effects are expected to become important at resonance of the waves between the cylinders and for very long waves.

As can be seen from Figure 5-13, the linear motions are well predicted by SWIM.

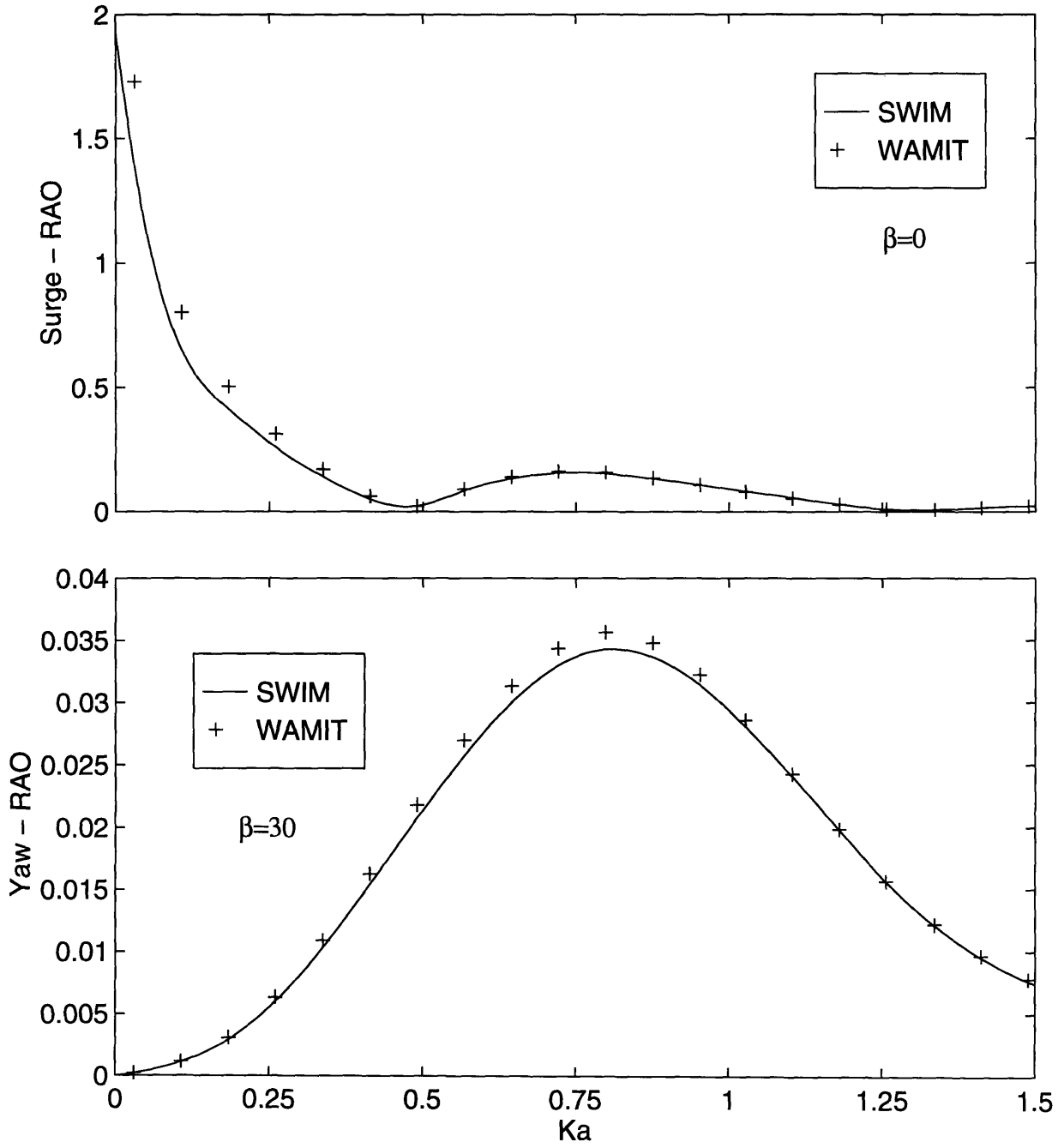

Figure 5-13: Surge and yaw RAO of platform III, computed by SWIM and WAMIT. *Top*: Surge ($\hat{\xi}_1^{(0)}/A$) for $\beta = 0^o$. *Bottom*: Yaw ($\hat{\xi}_6^{(0)}/(A/a)$) for $\beta = 30^o$.

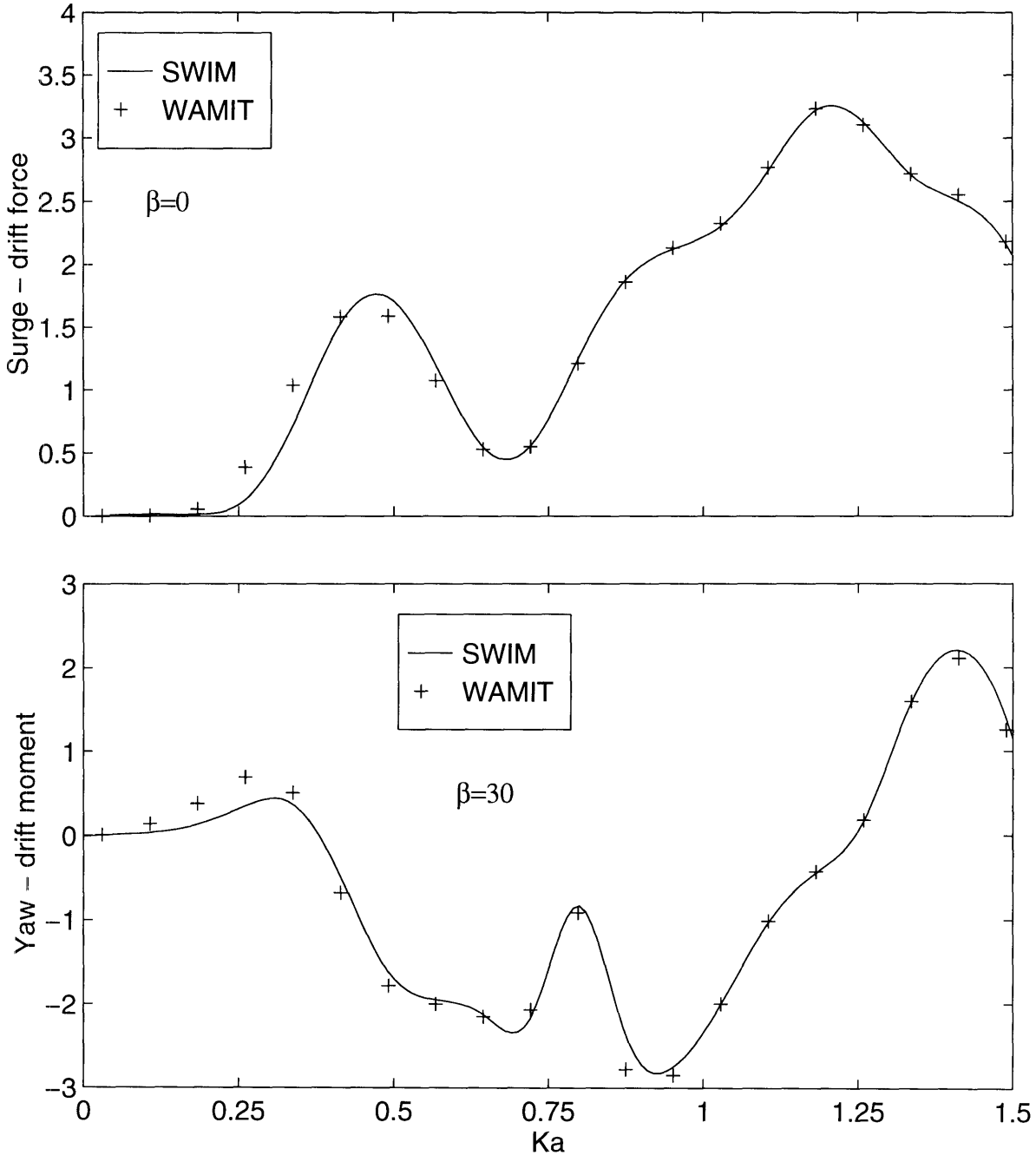

Figure 5-14: Surge drift force and yaw drift moment of platform III, computed by SWIM and WAMIT. *Top*: Surge ($D_1/\rho g A^2 a$) for $\beta = 0^o$. *Bottom*: Yaw ($D_6/\rho g A^2 a^2$) for $\beta = 30^o$.

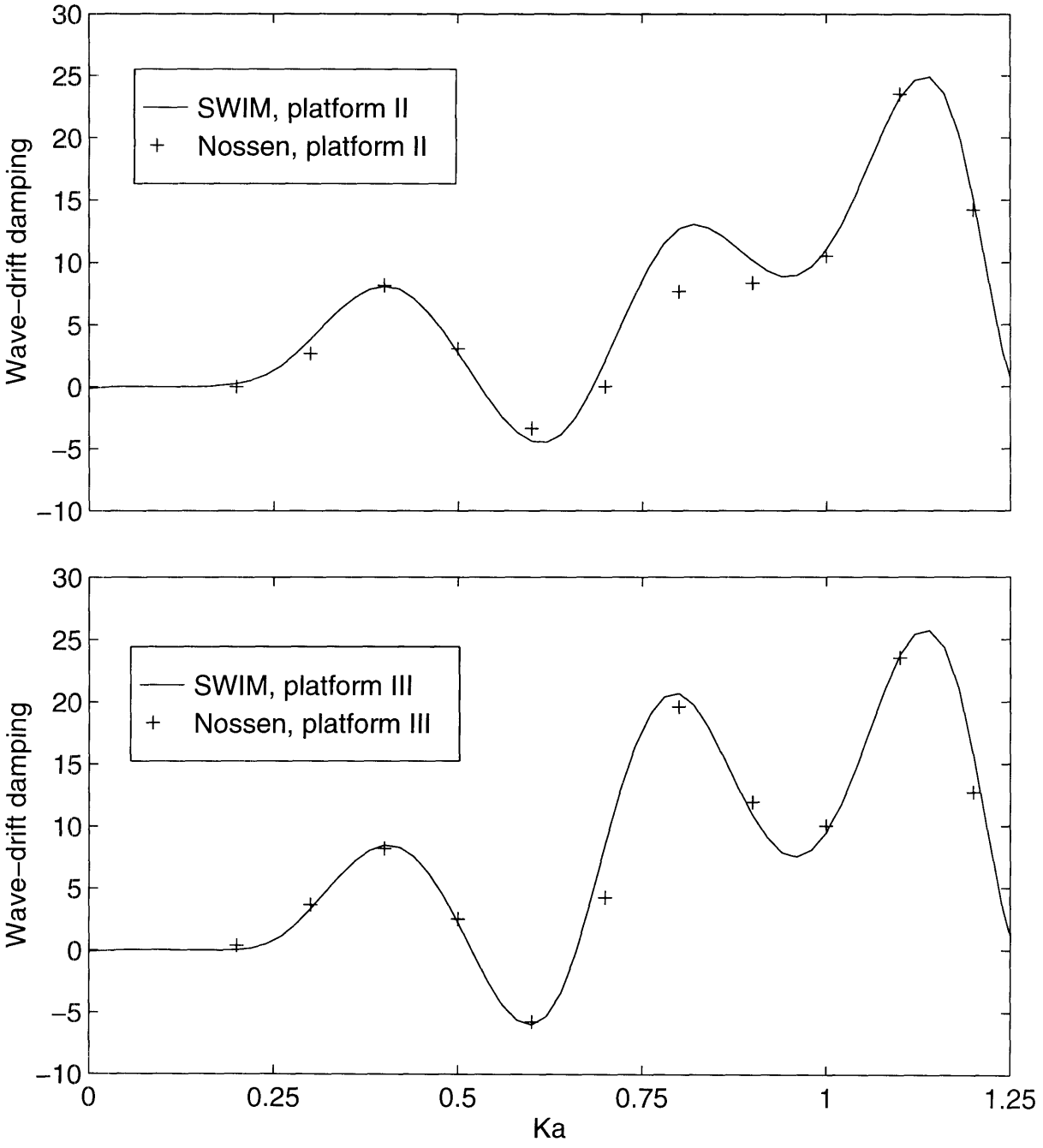

Figure 5-15: Wave-drift damping $B_{11}/(\rho(ga)^{1/2}A^2)$ of platform I with and without pontoons in deep water. Wave-heading: $\beta = 0^o$. Comparison between SWIM and Nossen, Grue & Palm (1991).

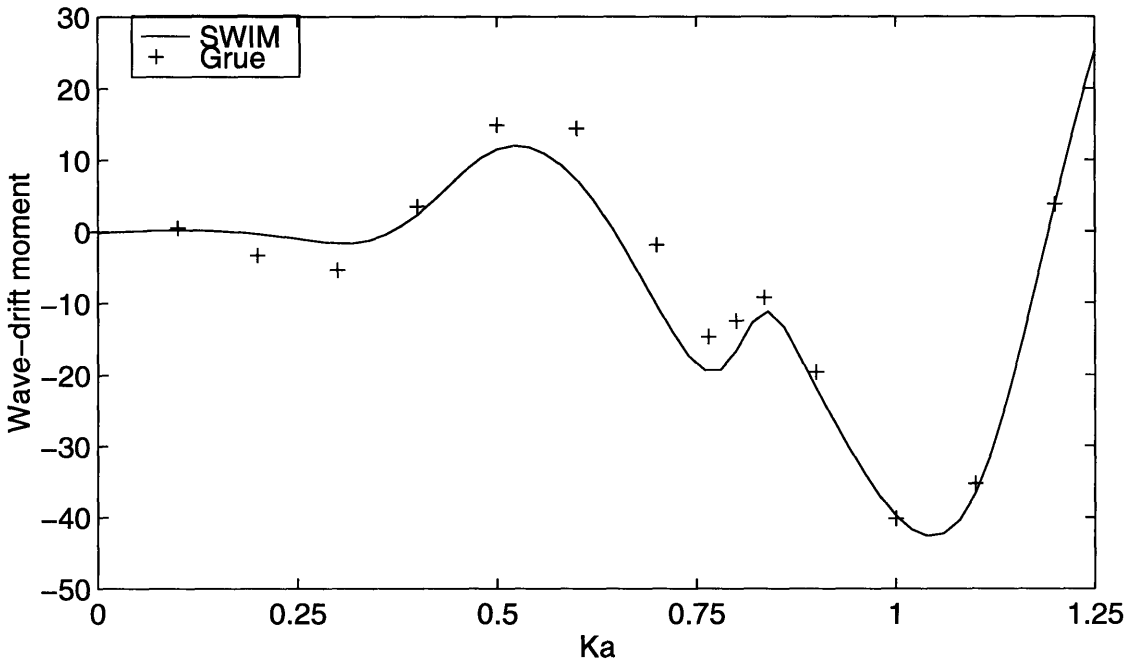

Figure 5-16: Wave-drift damping moment ($B_{31}/\rho(ga)^{1/2}A^2a$) of platform I with the same pontoons as described in the previous figure. Deep water with wave-heading $\beta = 0^o$. The platform is free to surge in linear motions. Comparison between SWIM and Grue & Palm (1992).

Chapter 6

Time-simulation of slow-drift motions

The chapter presents a method of simulating the slow-drift motions in time, using the hydrodynamic forces obtained in the previous sections. A model slow-drift equation for the surge-sway-yaw modes of motion, based on Sclavounos (1994), is employed. Realizations of the random second-order forces in a sea-state are computed by the filtering of white Gaussian noise and the double summation of time series. The equations of the slow-drift motions are solved numerically by a Runge-Kutta scheme. The numerical scheme allows for non-linear damping and restoring forces, and the former has been included in the simulations.

6.1 A model slow-drift equation of motion

Using Newton's second law and a multiple time-scales analysis to separate the fast-scales from the slow-scales, the slow-drift equations of motions can be derived. In Sclavounos (1994), a model based on potential flow theory and small slow-drift velocities was used in deriving the slow-drift surge-sway-yaw equations of motion. This

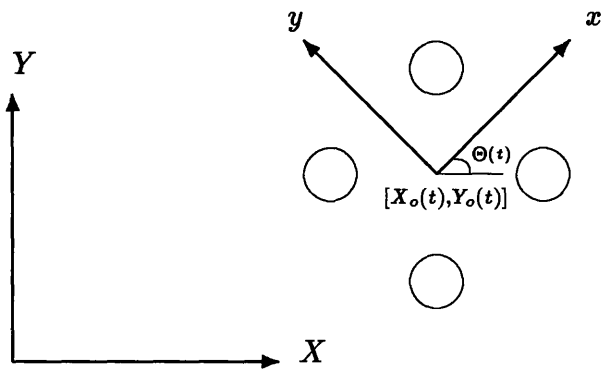

Figure 6-1: The inertial frame (X, Y, Z) and the slow-drift frame (x, y, z). The position of the body (here illustrated by four vertical cylinders), is determined by the coordinates $X_o(t)$, $Y_o(t)$ and the yaw-angle of rotation $\Theta(t)$, relative to the inertial frame.

model will be used in the following analysis with some minor modifications. The potential flow forces of second-order in the slow-drift velocities are here neglected. However, viscous damping is present via a Morison type force.

Denote by $\boldsymbol{\mathcal{X}}_0(t) = (X_o(t), Y_o(t), \Theta(t))^T$ the surge-sway-yaw slow-drift vector, where $X_o(t)$, $Y_o(t)$ and $\Theta(t)$ are the respective coordinates of the slow-drift frame, which is following the slow-drift motion of the structure, see Figure 6.1. The magnitude of the slow-drift velocities $\dot{X}_o(t)$, $\dot{Y}_o(t)$ and $\dot{\Theta}(t)$ are here assumed small. However, no assumptions are made with respect to $X_o(t)$, $Y_o(t)$ and $\Theta(t)$. The slow-drift equations will be given with respect to the inertial frame (X, Y, Z). The hydrodynamic forces, which are given with respect to the slow-drift frame, are therefore transformed via the transformation matrix $[S]$, defined below. Based on Sclavounos (1994) and the above discussion, the surge-sway-yaw slow-drift equation matrix is thus written,

$$[S]\left([M]+[A]\right)[S]^T\ddot{\boldsymbol{\mathcal{X}}}_0 + [S][B(t)][S]^T\dot{\boldsymbol{\mathcal{X}}}_0 + \boldsymbol{\mathcal{F}}_v(\dot{\boldsymbol{\mathcal{X}}}_0) + [C]\boldsymbol{\mathcal{X}}_0 \;=\; [S]\boldsymbol{\mathcal{F}}(t), \quad (6.1)$$

where $[M]$ is the inertia matrix, $[A]$ is the added-mass matrix, $[C]$ is the linear restoring coefficient matrix, $B(t)$ is the wave-drift damping matrix and $\mathcal{F}(t)$ is the zero-speed drift force vector. $\mathcal{F}_v(\dot{\mathcal{X}}_0)$ is the viscous damping force of $O(\dot{\mathcal{X}}_0^{\,2})$, as described in Appendix D. The transformation matrix $[S]$ is defined by equation (2.4). The quantities $[M]$, $[A]$, $[B(t)]$ and $\mathcal{F}(t)$ are given with respect to the slow-drift frame, while $[C]$ is given with respect to the inertial frame. They are defined as follows,

$$[M] = \begin{bmatrix} I_{11} & 0 & 0 \\ 0 & I_{22} & 0 \\ 0 & 0 & I_{66} \end{bmatrix}, \quad [A] = \begin{bmatrix} A_{11} & A_{12} & A_{16} \\ A_{21} & A_{22} & A_{26} \\ A_{61} & A_{62} & A_{66} \end{bmatrix}, \quad \mathcal{F}(t) = \begin{pmatrix} D_1(t) \\ D_2(t) \\ D_6(t) \end{pmatrix}, \tag{6.2}$$

$$[B(t)] = \begin{bmatrix} B_{11}(t) & B_{12}(t) & B_{16}(t) \\ B_{21}(t) & B_{22}(t) & B_{26}(t) \\ B_{61}(t) & B_{62}(t) & B_{66}(t) \end{bmatrix}, \quad [C] = \begin{bmatrix} C_{XX} & C_{XY} & C_{X\Theta} \\ C_{YX} & C_{YY} & C_{Y\Theta} \\ C_{\Theta X} & C_{\Theta Y} & C_{\Theta\Theta} \end{bmatrix}. \tag{6.3}$$

The subscripts 1, 2, 6 and X, Y, Θ here refer to surge, sway, yaw, in the slow-drift frame and the inertial frame, respectively. $I_{11} = I_{22}$ is the mass of the structure and I_{66} the moment of inertia about the z-axis. The center of gravity and the origin of the slow-drift frame are assumed to be along the same vertical line, such that $I_{ij} = 0$ for $i = 1, 2$, $j = 6$ and $i = 6$, $j = 1, 2$.

In order to make the equation of motions more suitable for a numerical solution-scheme, equation (6.1) is written,

$$\ddot{\mathcal{X}}_0 \;=\; [a]^{-1}\left(\boldsymbol{f} - [b]\dot{\mathcal{X}}_0 - \mathcal{F}_v(\dot{\mathcal{X}}_0) - [C]\mathcal{X}_0\right), \tag{6.4}$$

where $[a] = [M] + [S][A][S]^T$, $[b] = [S][B(t)][S]^T$ and $\boldsymbol{f} = [S]\mathcal{F}(t)$. $[a]^{-1}$ is the inverse matrix of $[a]$. The second-order differential equation (6.4) can now be written as two first-order differential equations. Introduce the vector $\mathcal{X}_1 = \dot{\mathcal{X}}_0$. Replacing $\dot{\mathcal{X}}_0$ and $\ddot{\mathcal{X}}_0$ in equation (6.4) by $\mathcal{X}_1$ and $\dot{\mathcal{X}}_1$, respectively, leads to the following two first-order

differential equations for $\boldsymbol{\mathcal{X}}_0$ and $\boldsymbol{\mathcal{X}}_1$,

$$\dot{\boldsymbol{\mathcal{X}}}_0 = \boldsymbol{\mathcal{X}}_1, \tag{6.5}$$

$$\dot{\boldsymbol{\mathcal{X}}}_1 = [a]^{-1}\left(\boldsymbol{f} - [b]\boldsymbol{\mathcal{X}}_1 - \boldsymbol{\mathcal{F}}_v(\boldsymbol{\mathcal{X}}_1) - [C]\boldsymbol{\mathcal{X}}_0\right). \tag{6.6}$$

6.2 White Gaussian noise

This section gives a brief presentation of the white Gaussian noise (WGN) process $w(t)$ and some related quantities that will be used as a basis for the study of the slow-drift motions in a random sea-state.

The process $w(t)$ which will be used throughout this analysis is stationary white Gaussian noise with zero mean, unit variance and unit spectral density. The Fourier transform of $w(t)$ is defined $W(\omega)$, and the Fourier transform pair is written,

$$w(t) = \frac{1}{2\pi}\int_{-\infty}^{+\infty} W(\omega)\,\mathrm{e}^{-\mathrm{i}\omega t}\mathrm{d}\omega, \tag{6.7}$$

$$W(\omega) = \int_{-\infty}^{+\infty} w(t)\,\mathrm{e}^{\mathrm{i}\omega t}\mathrm{d}t, \tag{6.8}$$

where $W(\omega)$ is a stochastic process in the variable ω. Since $w(t)$ is a real process, the Fourier transform satisfies the condition,

$$W(-\omega) = W^*(\omega), \tag{6.9}$$

where the $*$ denotes complex conjugate. By the statistical properties of $w(t)$ and equations (6.7) - (6.8) it can be shown that $W(\omega)$ is stationary with zero mean and auto-correlation,

$$E\left[W(\omega_1)W^*(\omega_2)\right] = 2\pi\delta(\omega_1 - \omega_2), \tag{6.10}$$

where the notation $E[\cdot]$ denotes the mean of the quantities inside the brackets. $\delta(t)$ is the Dirac delta function. It can be inferred from equations (6.8) and (6.10) that $W(\omega)$ is a WGN process. $W(\omega)$ is in general a complex process, and will here be written,

$$W(\omega) = W_R(\omega) + \mathrm{i}W_I(\omega), \tag{6.11}$$

where $W_R(\omega)$ and $W_I(\omega)$ are real stochastic processes. In Papoulis, pp. 306-308, it is shown that $W_R(\omega)$ and $W_I(\omega)$ are jointly normal with zero mean, and from equation (6.10) and equation (10-158) in Papoulis, it can further be shown that the processes are uncorrelated. From the above discussion, it can therefore be concluded that $W_R(\omega)$ and $W_I(\omega)$ are independent zero mean WGN processes with variance, $\mathrm{Var}[W_R(\omega)] = \mathrm{Var}[W_I(\omega)] = \pi$.

6.3 Wave-elevation

The linear wave-elevation $\zeta(t)$ in a given sea-state is assumed to be a stationary, Gaussian, random process. Due to the linearity, $\zeta(t)$ can therefore be obtained by linear filtering of the WGN process $w(t)$, described in Section 6.2. The wave-elevation $\zeta(t)$ and its Fourier transform $Z(\omega)$ are defined as follows,

$$\zeta(t) = \int_{-\infty}^{+\infty} w(\tau)h(t-\tau)\mathrm{d}\tau, \tag{6.12}$$

$$Z(\omega) = W(\omega)H(\omega), \tag{6.13}$$

where $h(t)$ is the linear filter and $H(\omega)$ its Fourier transform. Given the spectral density $S_\zeta(\omega)$ of the wave-elevation, the transfer function $H(\omega)$ is determined by the

relation, $S_\zeta(\omega) = |H(\omega)|^2 S_w(\omega)$, which defines $H(\omega)$ as,

$$H(\omega) \;=\; [S_\zeta(\omega)]^{1/2}, \tag{6.14}$$

since the spectral density of $w(t)$ is $S_w(\omega) = 1$. A realization of the wave-signal $\zeta(t)$ can now be obtained from the expression (6.12), by first computing the Fourier transform of $H(\omega)$ and a realization of $w(t)$. This approach requires the computation of one Fourier transform and one convolution integral in addition to the generation of $w(t)$. An alternative approach, which only requires the computation of one Fourier transform and the realization of a WGN process, is obtained by computing the quantities listed below:

1. A realization of the process $W(\omega)$, which is a WGN process.
2. The 'wave-amplitudes' $Z(\omega) = W(\omega)\,[S_\zeta(\omega)]^{1/2}$.
3. The Fourier transform of $Z(\omega)$:

$$\zeta(t) \;=\; \frac{1}{2\pi}\int_{-\infty}^{+\infty} Z(\omega)\,\mathrm{e}^{-\mathrm{i}\omega t}\mathrm{d}\omega. \tag{6.15}$$

Note that the wave-elevation in equation (6.15) is evaluated at $X = Y = 0$. In order to evaluate $\zeta(t)$ at (X_o, Yo), the factor $\mathrm{e}^{\mathrm{i}\kappa(X_o\cos\beta_0 + Y_o\sin\beta_0)}$ must be multiplied $\mathrm{e}^{-\mathrm{i}\omega t}$ in equation (6.15). β_0 is the angle between the inertial X-axis and the direction of wave-propagation. By virtue of equation (6.9) and the identity $S_\zeta(-\omega) = S_\zeta(\omega)$, the realization of $\zeta(t)$ is a purely real signal. Also notice that the spectral density $S_\zeta(\omega)$ as presented here, is multiplied a factor of 2π compared to wave-spectra most commonly used in ocean engineering. The variance of the process $\zeta(t)$ is therefore found to be,

$$E\,[\zeta^2(t)] \;=\; \frac{1}{2\pi}\int_{-\infty}^{+\infty} S_\zeta(\omega)\mathrm{d}\omega. \tag{6.16}$$

6.4 Second-order forces

The leading-order slowly-varying forces in an irregular sea-state are proportional to the wave-amplitude squared. Denote by $D(t)$ the second-order force acting on the body. $D(t)$ here represents any of the second-order forces described in Section 4. A realization of $D(t)$ is obtained by a proper filtering of the wave-elevation ζ, given the the second-order filter $h(t_1, t_2)$. The second-order force is thus written,

$$\begin{aligned} D(t) &= \int_{-\infty}^{+\infty}\int_{-\infty}^{+\infty} \zeta(t_1)\zeta(t_2)h(t-t_1, t-t_2)\mathrm{d}t_1\mathrm{d}t_2 \\ &= (2\pi)^{-2}\int_{-\infty}^{+\infty}\int_{-\infty}^{+\infty} Z(\omega_1)Z(\omega_2)H(\omega_1,\omega_2)\,\mathrm{e}^{-\mathrm{i}(\omega_1+\omega_2)t}\mathrm{d}\omega_1\mathrm{d}\omega_2, \end{aligned} \tag{6.17}$$

where $h(t_1, t_2)$ and $H(\omega_1, \omega_2)$ are the double Fourier transform pair defined by,

$$h(t_1,t_2) = (2\pi)^{-2}\int_{-\infty}^{+\infty}\int_{-\infty}^{+\infty} H(\omega_1,\omega_2)\,\mathrm{e}^{-\mathrm{i}(\omega_1 t_1+\omega_2 t_2)}\mathrm{d}\omega_1\mathrm{d}\omega_2, \tag{6.18}$$

$$H(\omega_1,\omega_2) = \int_{-\infty}^{+\infty}\int_{-\infty}^{+\infty} h(t_1,t_2)\,\mathrm{e}^{\mathrm{i}(\omega_1 t_1+\omega_2 t_2)}\mathrm{d}t_1\mathrm{d}t_2. \tag{6.19}$$

$H(\omega_1, \omega_2)$ is the transfer function of the second-order force on the body. The expression (6.17) contains both sum-frequency components ($\omega_1\omega_2 > 0$) and difference-frequency components ($\omega_1\omega_2 < 0$) of $D(t)$. The former are acting over a time-scale which is much shorter than the time-scale of the slow-drift motions, and are therefore not considered in the following analysis. In order to remove the sum-frequency components from $D(t)$, the second-order difference-frequency force $D^-(t)$ is defined,

$$D^-(t) = (2\pi)^{-2}\int_{-\infty}^{+\infty}\int_{-\infty}^{+\infty} \epsilon(\omega_1,\omega_2)Z(\omega_1)Z(\omega_2)H(\omega_1,\omega_2)\,\mathrm{e}^{-\mathrm{i}(\omega_1+\omega_2)t}\mathrm{d}\omega_1\mathrm{d}\omega_2, \tag{6.20}$$

where $\epsilon(\omega_1, \omega_2) = \frac{1}{2}\left[1 - \mathrm{sgn}(\omega_1)\mathrm{sgn}(\omega_2)\right]$ and $\mathrm{sgn}(\omega) = \pm 1$ for $\omega \gtrless 0$. The expression for $D^-(t)$ can be significantly simplified by employing the assumption of a narrow-banded wave spectrum, which will be considered next.

6.4.1 Narrow-banded wave-spectrum

In a sea-state with a narrow-banded wave-spectrum, a major part of the energy is concentrated around a particular frequency. This is often the case for severe sea-states, which are used in designing offshore structures. In this case, the Newman's approximation can be applied to the difference-frequency transfer function as follows,

$$H(\omega_i,\omega_j) \;=\; \tfrac{1}{2}\left[H(\omega_i,-\omega_i)+H(\omega_j,-\omega_j)\right], \qquad \omega_i\omega_j<0. \tag{6.21}$$

It is here assumed that $H(\omega_i,\omega_j)$ does not vary appreciably near the diagonal $\omega_i=\omega_j$. The approximation (6.21) reduces the computation of the full matrix $H(\omega_i,\omega_j)$ to only the diagonal terms $H(\omega_i,\omega_i)$, which represents the mean force acting on the body. The computation of the off-diagonal terms generally requires an order of magnitude more effort than the diagonal terms. Introduce the second-order mean force $\bar{D}(\omega)$,

$$\bar{D}(\omega) \;=\; \mathrm{Re}\left[\mathcal{D}(\omega)\right], \tag{6.22}$$

which represents any of the forces of $O(\delta^2)$ and $O(\delta^2\tau_j)$ obtained in Section 4.3 and Appendix A.2, A.3. The complex force $D(\omega)$ satisfies the identity $\mathcal{D}(-\omega)=\mathcal{D}^*(\omega)$, where $*$ denotes complex conjugate. The relation between $\mathcal{D}(\omega)$ and $H(\omega,-\omega)$ is given by,

$$H(\omega,-\omega) \;=\; 2\mathcal{D}(\omega), \tag{6.23}$$

The double integral in equation (6.20) can be reduced to a single integral by substituting the expression (6.21) for $H(\omega_1,\omega_2)$. After some algebra and using equations (6.22) - (6.23), the second-order force $D^-(t)$ is written,

$$\begin{aligned} D^-(t) \;=\; \frac{1}{4\pi^2}\mathrm{Re}\Big[&\int_{-\infty}^{+\infty} Z(\omega_1)\mathcal{D}(\omega_1)\,\mathrm{e}^{-\mathrm{i}\omega_1 t}\mathrm{d}\omega_1 \int_{-\infty}^{+\infty} Z(\omega_2)\,\mathrm{e}^{-\mathrm{i}\omega_2 t}\mathrm{d}\omega_2 - \\ &\int_{-\infty}^{+\infty} \mathrm{sgn}(\omega_1)Z(\omega_1)\mathcal{D}(\omega_1)\,\mathrm{e}^{-\mathrm{i}\omega_1 t}\mathrm{d}\omega_1 \int_{-\infty}^{+\infty} \mathrm{sgn}(\omega_2)Z(\omega_2)\,\mathrm{e}^{-\mathrm{i}\omega_2 t}\mathrm{d}\omega_2\Big]. \end{aligned} \tag{6.24}$$

Expression (6.24) applies to the forces $D_i(t)$ and $B_{ij}(t)$ of equations (6.2)-(6.3), for $i,j = 1,2,6$, given the appropriate expressions for $\mathcal{D}(\omega)$. In particular, the realization of the surge wave-drift damping coefficient $B_{11}^{-}(t)$, is thus written,

$$B_{11}^{-}(t) = \frac{1}{4\pi^2}\mathrm{Re}\left[\int_{-\infty}^{+\infty} Z(\omega_1)\mathcal{B}_{11}(\omega_1)\,\mathrm{e}^{-\mathrm{i}\omega_1 t}\mathrm{d}\omega_1 \int_{-\infty}^{+\infty} Z(\omega_2)\,\mathrm{e}^{-\mathrm{i}\omega_2 t}\mathrm{d}\omega_2 - \int_{-\infty}^{+\infty} \mathrm{sgn}(\omega_1)Z(\omega_1)\mathcal{D}_{11}(\omega_1)\,\mathrm{e}^{-\mathrm{i}\omega_1 t}\mathrm{d}\omega_1 \int_{-\infty}^{+\infty} \mathrm{sgn}(\omega_2)Z(\omega_2)\,\mathrm{e}^{-\mathrm{i}\omega_2 t}\mathrm{d}\omega_2\right], \tag{6.25}$$

where $\mathcal{B}_{11}(\omega)$ is obtained from equation (4.41), which is written,

$$\mathcal{B}_{11}(\omega) = \tfrac{1}{2}\rho\iint_{\bar{S}_\infty}\left[\varphi_x\psi_n^{U^*} + \varphi_n\psi_x^{U^*} - \nabla\varphi\cdot\nabla\psi^{U^*}n_1\right]\mathrm{d}S + \tfrac{1}{2}\rho\int_{c_\infty}\varphi\left(\nu\psi^{U^*}n_1 - \kappa\frac{\omega_0}{g}\cos\beta\varphi^* n_1\right)\mathrm{d}l. \tag{6.26}$$

The mean value of $D^{-}(t)$ in an irregular sea-state is obtained by averaging (6.24) over time and is given by,

$$E\left[D^{-}(t)\right] = \frac{1}{2\pi}\int_{-\infty}^{+\infty} 2S_\zeta(\omega)\bar{D}(\omega)\mathrm{d}\omega. \tag{6.27}$$

6.5 Numerical implementation

The expressions for the wave-elevation and the hydrodynamic forces in Sections 6.3 and 6.4 were discretized in time with constant time-step, Δt, at the discrete times, t_i, $i = 1,...,N$. The frequency-axis was similarly discretized at the discrete frequencies ω_i, $i = 1,...,N$, with spacing $\Delta\omega$. Due to its computational advantages, the Fast Fourier Transform (FFT) was used in calculating the Fourier integrals, which restricts the number of time-steps to be a multiplier of 2. Realizations of the stochastic processes $W(\omega)$ and hence the wave-amplitude $Z(\omega)$, were therefore evaluated at

the frequencies ω_i for $i = 1, ..., N$. A sequence of independent Gaussian numbers was generated by first using a random number generator of equally distributed numbers between 0 and 1, and then employing a transformation to obtain the Gaussian distribution. The particular random number generator, *RAN1* from the Numerical Recipes library, is able to generate a sequence of 2^{32} independent numbers without repeating itself, which enables the simulation of very long records of the slow-drift motions.

An approximation has been made with respect to the wave-drift damping matrix $[B(t)]$ and the drift force $\boldsymbol{\mathcal{F}}(t)$ in the equation of motions (6.1), in order to calculate the hydro-dynamic forces by the FFT. The simulations in Section 7, were performed by evaluating all forces at the position $X_o(t) = Y_o(t) = 0$ and constant yaw-rotation $\Theta(t)$. This allows the computation of the forces prior to the simulations of the motions. The errors introduced by the approximation are insignificant when the surge-sway translations are small relative to the dominant wave-lengths, which is the case in most real sea-states. The approximation may be less good for finite values of the yaw-rotation, since the hydro-dynamic yaw moment and the force perpendicular to the wave-heading, in general are very sensitive to a change in the wave-heading.

The dependence upon the slow-drift coordinates can alternatively be accounted for by computing the time-history of the forces for an array of constant values of $X_o(t)$, $Y_o(t)$ and $\Theta(t)$. During the simulation of the slow-drift motions, the forces at the exact slow-drift position can thus be interpolated from the array of data. This approach allows for the use of FFT, since the slow-drift coordinates appear as constant parameters in $[B(t)]$ and $\boldsymbol{\mathcal{F}}(t)$.

The solution of the slow-drift equations were performed by a fourth-order Runge-Kutta scheme, which evaluates the forces at half time-steps. In order to use the time-step Δt for the forces, the motions are therefore calculated at t_{2i}, with time-step $2\Delta t$. The Runge-Kutta scheme is robust in all practical cases.

Chapter 7

Results - time domain simulations

This chapter presents the results of the time-simulations that were described in Chapter 6. A sensitivity study of relevant parameters of the slow-drift motions has been performed and are presented.

The time-simulations were carried out by the module *motion*, which is a part of the SWIM program. The module *motion* is an implementation of the theory of Chapter 6. The hydrodynamic input to *motion* is provided by the *swim* module, described in Chapter 5.

The time-simulation of the slow-drift motions for a given structure, depend upon a number of parameters. Some of these parameters are related to the physical environments, such as the wave-spectrum, the directional spreading of the waves, statistical properties of the sea-state and the current. Other parameters are related to the modelling of the forces on the structure, *e. g.* the drag-coefficient. A third group of parameters is related to the time-simulation scheme. This includes the size of the time-steps and the length of the simulations. This section gives a brief description of the parameters with plots of their dependence upon simple statistical properties of the slow-drift motions, such as the mean deflection and the standard deviation.

Unless otherwise stated, the results of this chapter were obtained using a JONSWAP spectrum for the waves, with significant height $H_s = 13$ [m], peak period $T_p = 14$ [sec] and gamma parameter $\gamma = 3.3$.

7.1 Wave-elevation and linear motions

The wave-elevation in a long-crested sea-state is given by equation (6.15). This section presents simulated time history of $\zeta(t)$ along with the corresponding linear motions of a platform, computed by FFT. As a verification of the statistical properties of $\zeta(t)$, comparison is made between the probability density function (pdf) of the simulated signal and the Gaussian distribution. The energy contents of the different spectral components in the signal are compared with the input spectrum. The convergence of the pdf and the spectrum are demonstrated by increasing the length of the simulations.

Figure 7-1 shows the simulated wave-elevation and the corresponding motions of platform III, with wave-heading $\beta = 30^o$.

In Figure 7-2, the pdf of a simulated record of length $T = 2^{\mathrm{KN}}$ [sec] is compared with the Gaussian distribution. The pdf of a the shortest record does not look like the Gaussian distribution, but the computed pdf approaches the Gaussian as KN increases. It is here worth noting that the signal $\zeta(t)$ follows a Gaussian distribution for any number of discrete frequencies ω, since the complex wave-amplitudes $Z(\omega)$ are Gaussian.

Figure 7-3 shows the spectrum of wave-elevation records of length $T = 2^{\mathrm{KN}}$ [sec] in comparison with the input spectrum (JONSWAP). The spectrum of the signal was computed using a maximum entropy method. The comparison is good for a record of length $T = 2^{17}$ [sec]. Some of the discrepancy for shorter records may be due to difficulties in calculating the spectrum. Besides, the magnitude of the wave-amplitudes are random variables (following a Rayleigh distribution), and the spectrum of a single record can therefore not be expected to be equal to the input spectrum.

The boxplots in Figure 7-4 display the spread of the mean value $\bar{\zeta}$ and the rms σ_ζ for a number (100) of records with length $T = 2^{\mathrm{KN}}$ [sec]. Each box represents the range of 50% of the data. All data were inside the range of the whiskers. In the

bottom plot, the spread of $\bar{\zeta}$ and σ_ζ are quantified by their rms values.

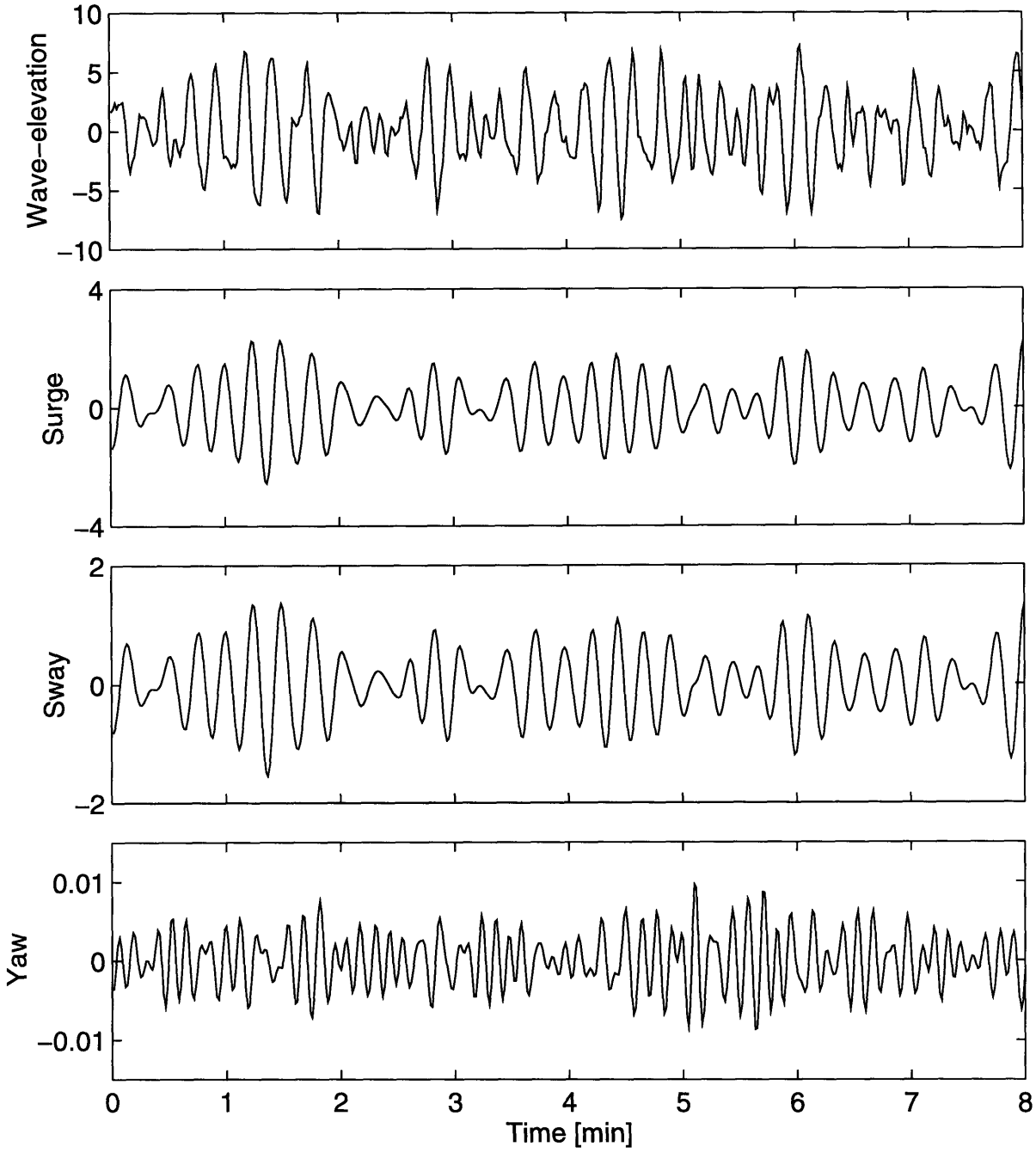

Figure 7-1: The four plots show simulations of the wave-elevation and the corresponding linear surge-sway-yaw motions of platform III, for $\beta = 30^o$. The three first plots are given in [meters] and the last in [DEG].

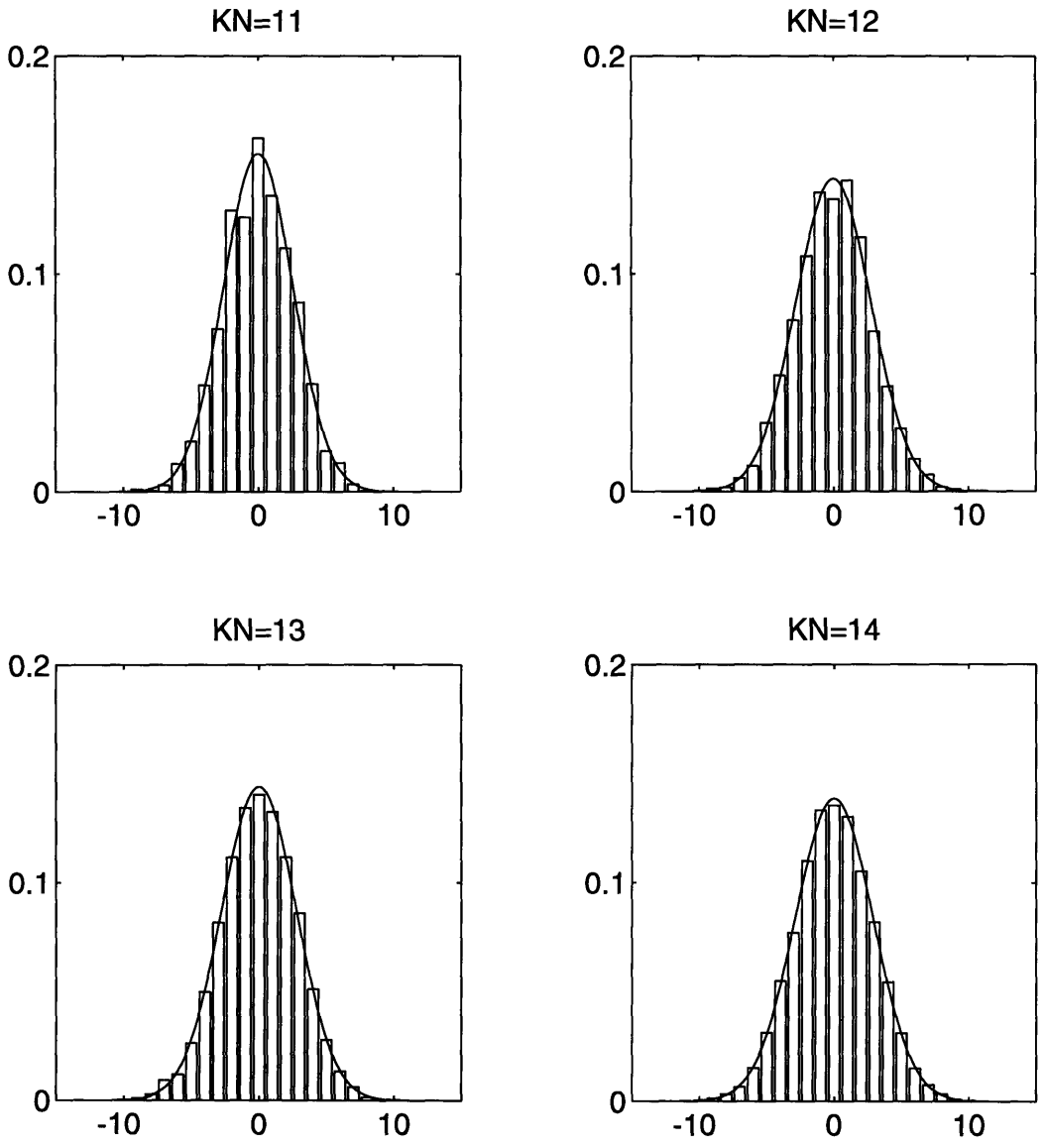

Figure 7-2: Computed probability density functions for the wave-elevation (bars) compared with the Gaussian distribution (solid line), for different lengths of simulation.

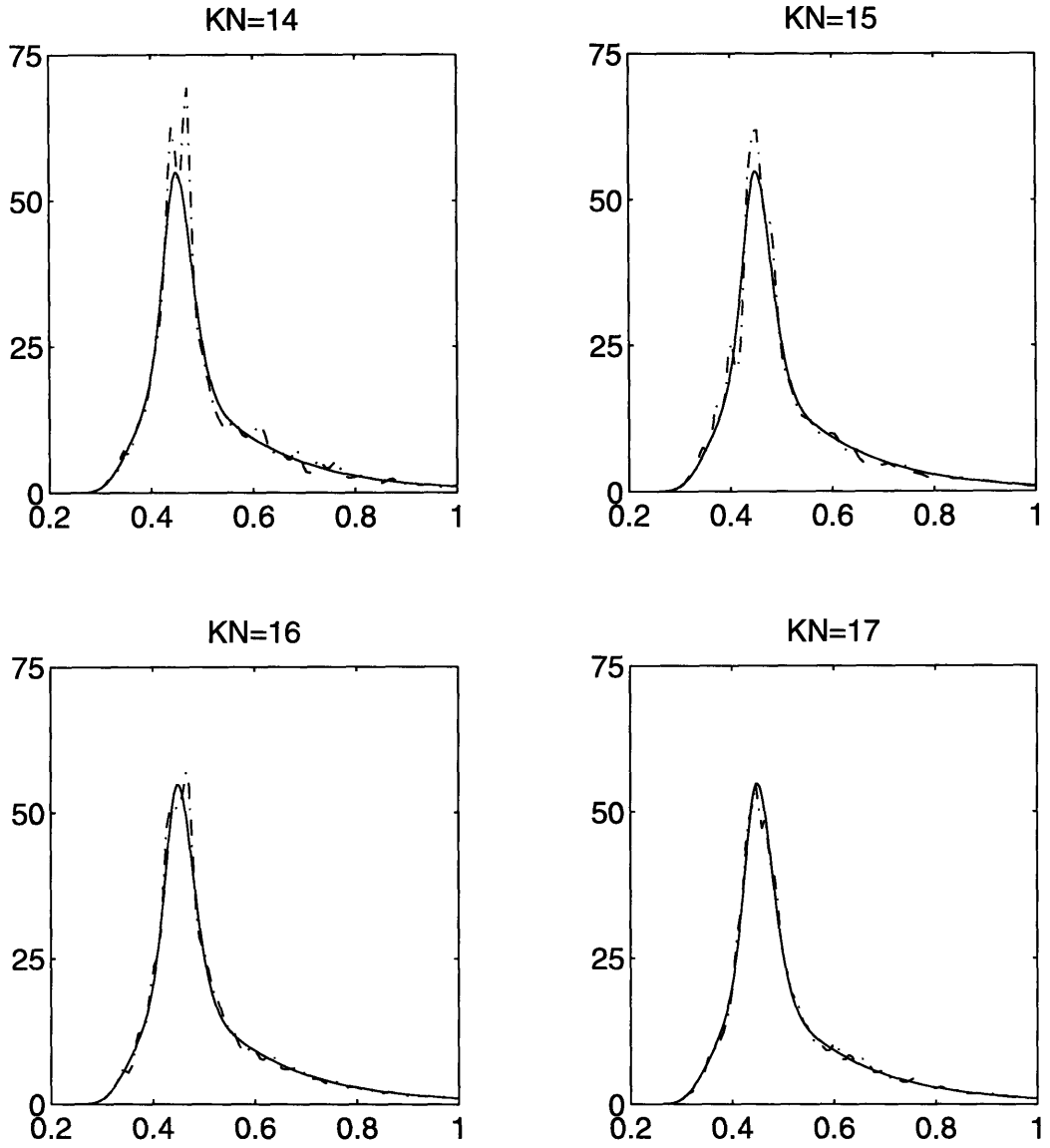

Figure 7-3: Computed spectral density of the wave-elevation (dashed-line) compared with the input spectrum (solid line), for different lengths of simulation.

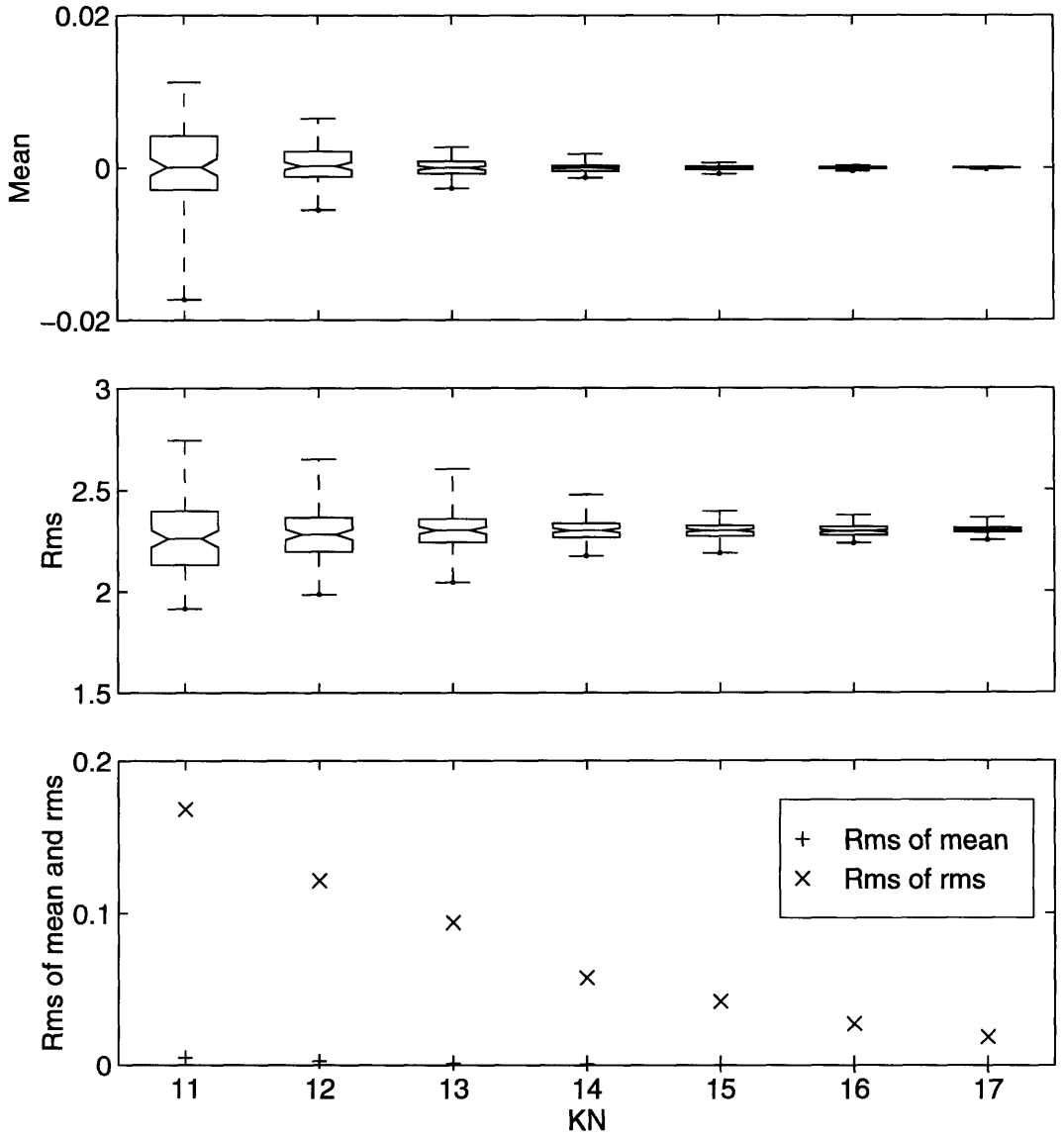

Figure 7-4: *Top and center plots*: Boxplots of the mean ($\bar{\zeta}$) and rms (σ_ζ) values, respectively, of the wave-elevation, based on 100 samples, each of duration $t = 2^{KN}$ [seconds]. 50 % of the data are within the upper and lower edges of the box and all data are within the whiskers. The horizontal line inside the box marks the average of the data. *Bottom:* Rms values of $\bar{\zeta}$ and σ_ζ.

7.2 Slow-drift motions

Results from simulations of the slow-drift motions are here presented. The equations of motions, given by equations (6.5) and (6.6) were solved by a Runge-Kutta scheme. The mean deflection and the rms of the simulated slow-drift motions were computed and plotted against several parameters; the length of the record, transients, drag-coefficient, current velocity and directional spreading of the sea-state.

In Figure 7-5 the difference between the time-scales of the linear motions (fast-scale) and the slow-drift motions (slow-scale) are emphasized. A comparison of the slow-drift spectral components in Figure 7-6 and the wave spectral components in Figure 7-3 illustrates the difference in the frequency domain. A third scale, the slow slow-scale is introduced by the envelope of the slow-drift motions.

Examples of the surge-sway-yaw slow-drift motions are displayed in Figure 7-7. Notice the different amplitudes of the slow-drift motions and the linear motions in Figure 7-1, which were calculated for the same sea-state.

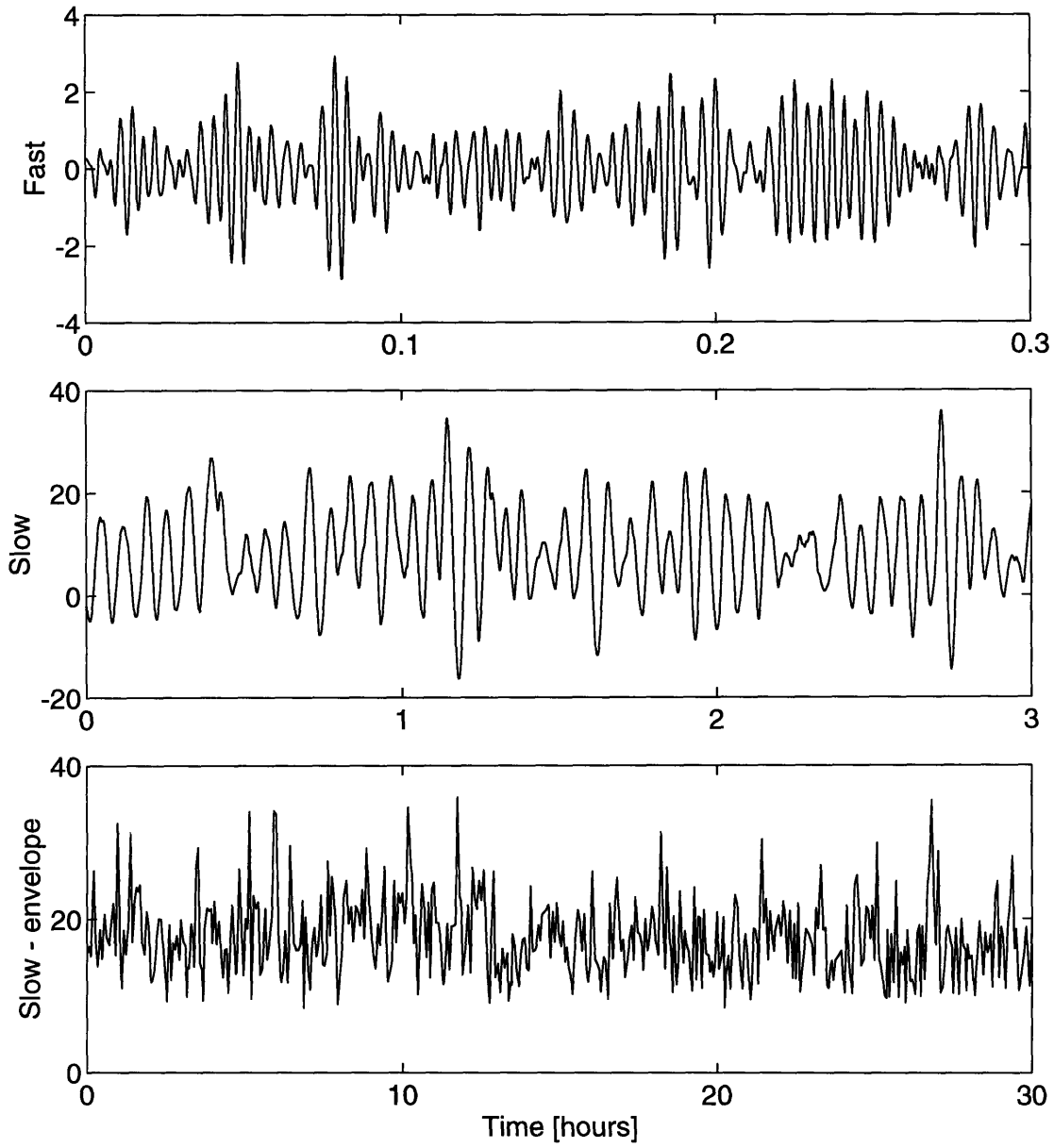

Figure 7-5: Surge motions of platform I. *Top*: Linear motions ($\xi_1(t)$). *Center*: Slow-drift motions ($X_o(t)$). *Bottom*: Envelope of slow-drift motions. Notice the different time-scales between the plots.

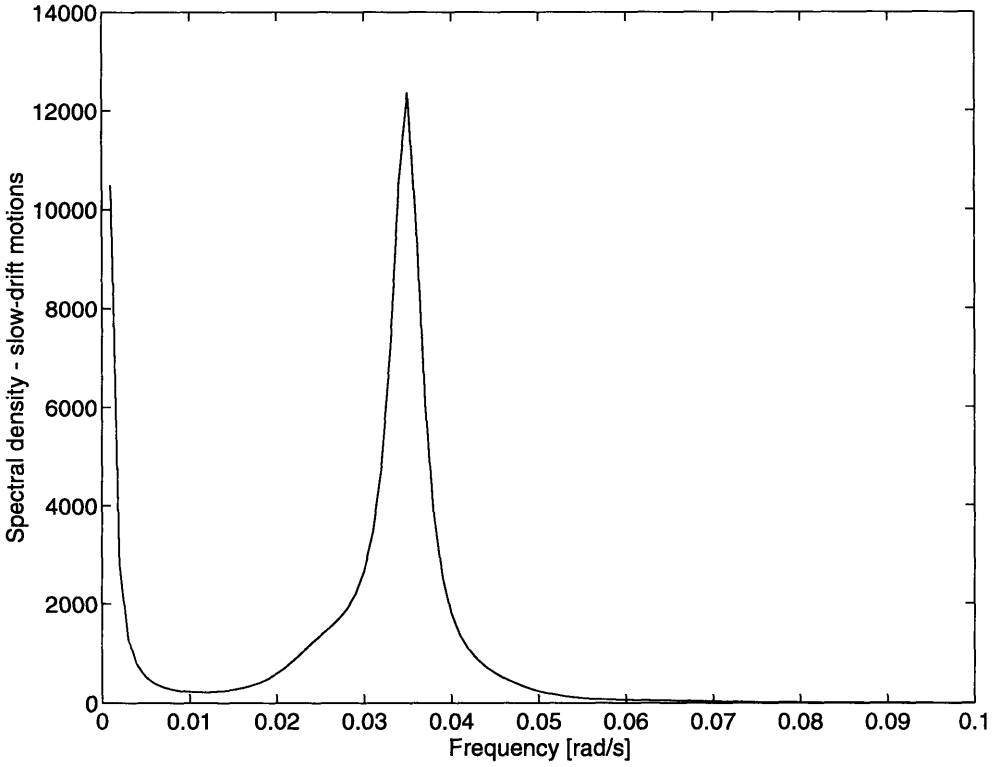

Figure 7-6: Spectral density of the slow-drift motion (surge) of platform III. The natural period of the system is 180 [sec].

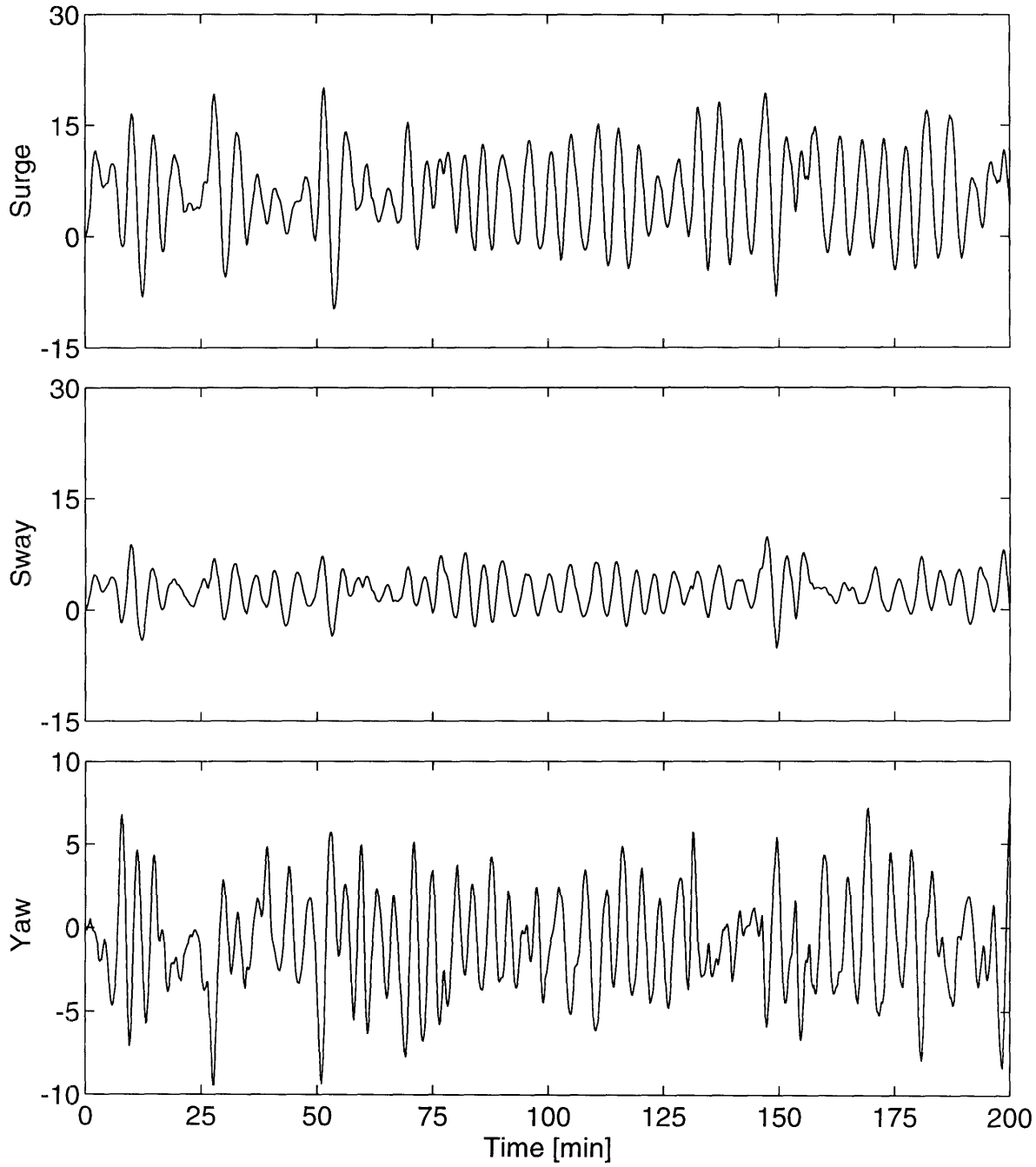

Figure 7-7: The slow-drift motions in surge, sway and yaw, respectively, of platform III for $\beta = 30°$. The two first plots are given in [meters] and the last in [DEG].

7.2.1 Length of simulations

Estimates of the mean deflection and rms of the slow-drift motions were calculated for different lengths of the simulations. The mean and rms values for 1000 simulated records are shown in the boxplots in Figure 7-8. 50% of the data are contained within the edges of the boxes and all data are within the whiskers. The bottom plot shows quantitatively how spread the estimates of the mean and the rms of the slow-drift motions were.

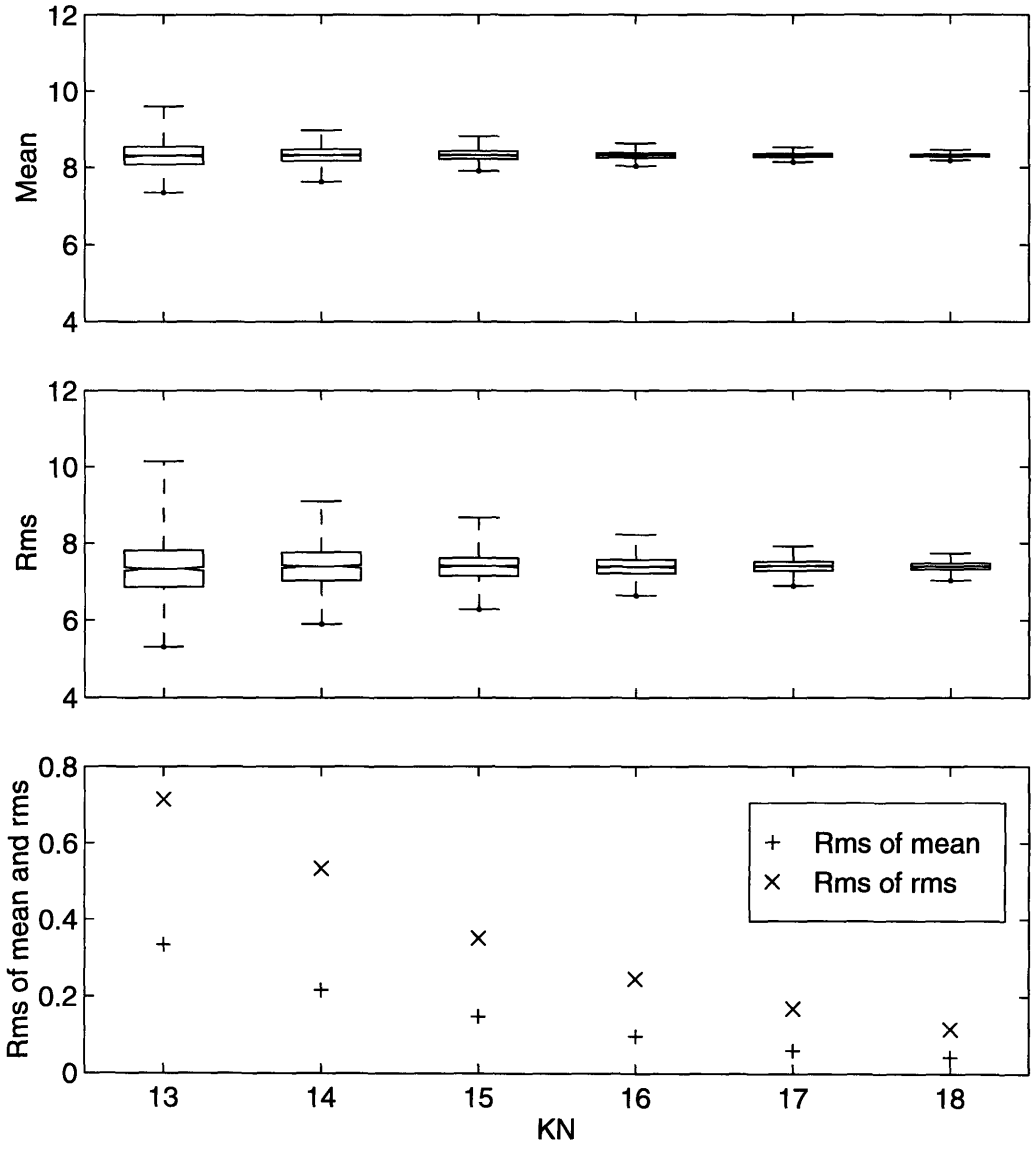

Figure 7-8: *Top and center plots*: Boxplots of the mean ($\bar{X}_o$) and rms (σ_X) values, respectively, of the surge slow-drift motions, based on 1000 samples, each of duration $t = 2^{KN}$ [seconds]. 50 % of the data are within the upper and lower edges of the box and all data are within the whiskers. The horizontal line inside the box marks the average of the data. *Bottom:* Rms values of $\bar{X}_o$ and σ_x.

7.2.2 Drag-coefficient

The derivations in Chapters 2 - 4 were based on ideal flow. It has been found, however, that viscous flows play an important part in the slow-drift motions. It is very difficult to include viscous flows in the calculations at a level of the derivations of the wave-drift damping. The effects of the viscosity in the fluid were therefore accounted for by a drag-force of the Morison type. This model requires a drag-coefficient, which depends on both the Reynolds number and the Strouhal number. Aside from the determination of the drag-coefficient, one must also consider whether the linear motions are to be included in the expressions for the drag-force. The fast-scale and the slow-scale equations of motions are in this study separated, and the linear motions were therefore not included in the drag-forces.

The dependence of the drag-coefficient on the rms of the slow-drift motions is illustrated in Figure 7-9. The linear motions were not included in the relative velocity term of the drag-force.

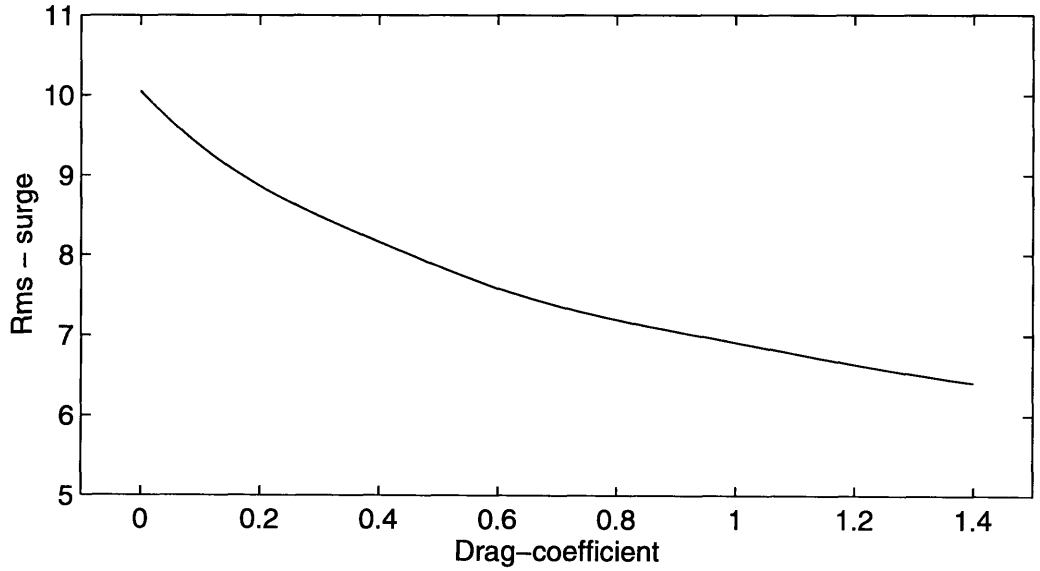

Figure 7-9: Rms value of slow-drift motions in surge as a function of the drag-coefficient C_D.

7.2.3 Current

From the boundary conditions in Chapter 2 it is found that a small current along the negative x-direction is identical to a slow-drift velocity of the body in the positive x-direction. The effects of a small, steady current can therefore be accounted for by adding the current velocity vector to the slow-drift velocities in the equations of motions. One must remember, however, that it now is the sum of the slow-drift velocity and the current that must be small in order for the expansion in the slow-drift velocities to be valid. If this sum is large, effects due to higher order terms and viscous forces will become important.

Figure 7-10 shows the dependence of the current on the mean deflection and the rms of the slow-drift motions. A drag-coefficient of $C_D = 0.7$ was used in the calculations. The large increase in the mean deflection is mainly due to the drag-force.

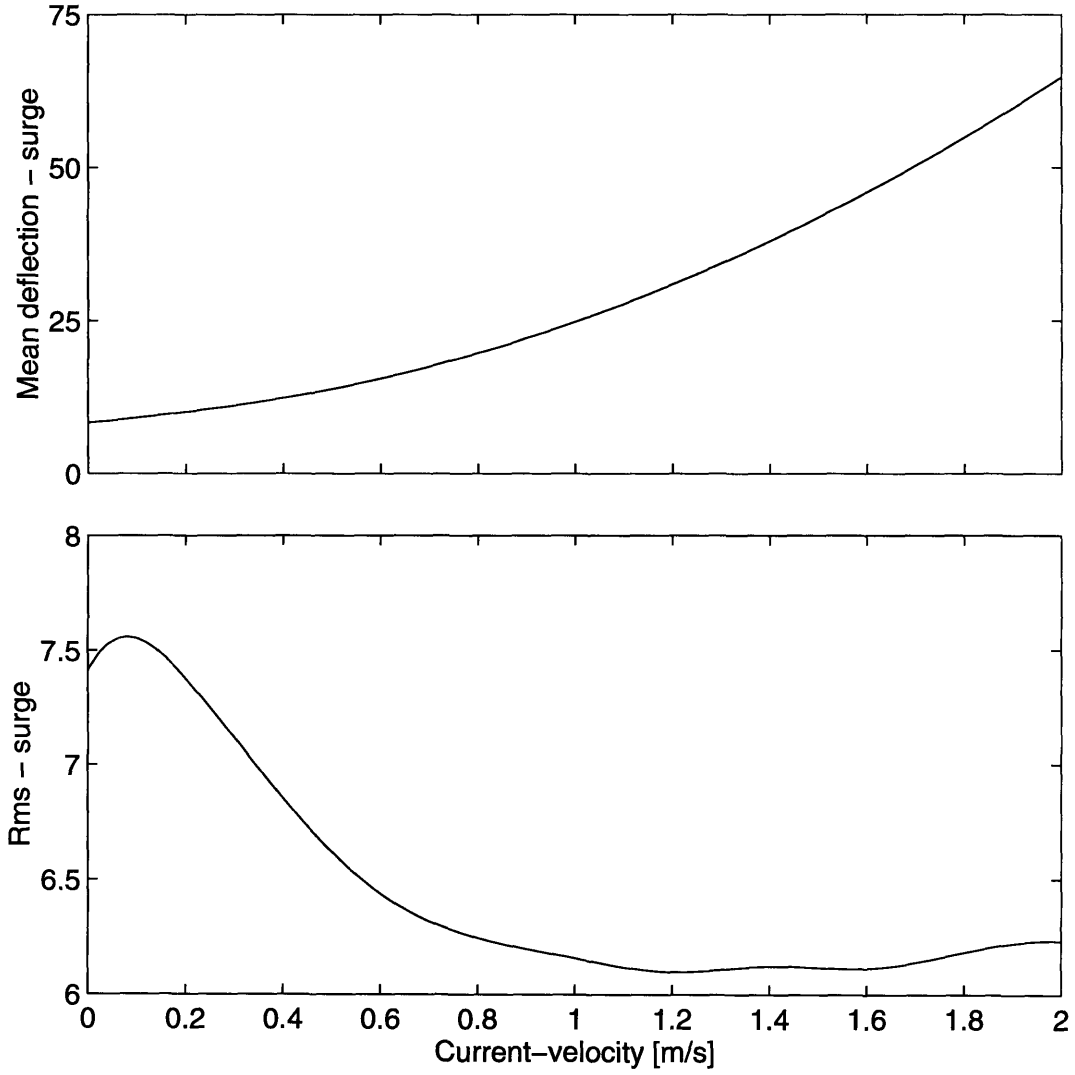

Figure 7-10: Mean deflection and rms value of slow-drift motions in surge as a function of the current-velocity U.

7.2.4 Transient

The simulations of the slow-drift motions are started up with specified position and velocity of the body at $t = 0$. These specified initial conditions are most likely different from what would have been the case if the simulations had started at some time before $t = 0$. The start-up of the simulations are therefore usually associated with a transient period, before the motions have reached a 'steady-state'.

Figure 7-11 displays the change of the calculated rms of the slow-drift motions as a function of time. The rms was calculated for consecutive segments, each of 10 slow-drift cycles. 25000 simulations were performed and the mean value of the rms is shown in the upper plot. The lower plot shows the rms of the rms. The values are clearly different for the first 10 cycles. The initial position of the body was selected at the mean position and the initial velocity an average velocity (based on the average of the slow-drift amplitudes). A longer transient period was found if the initial position and velocity were just set equal to zero (not shown in the figure).

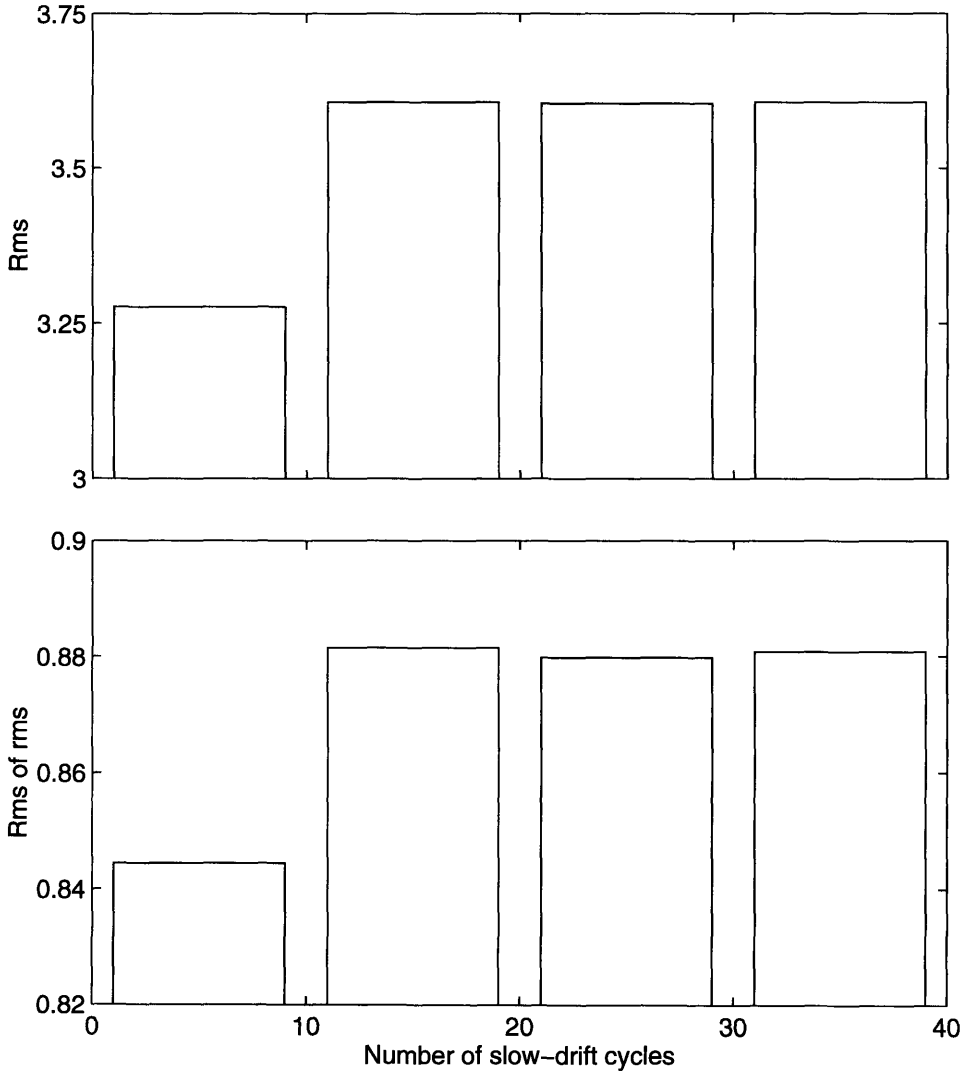

Figure 7-11: Rms of surge slow-drift motion (top) and rms of rms of surge slow-drift motion (bottom). Each bar represents the rms of approximately 10 slow-drift cycles. 25000 runs were used to obtain the data.

7.2.5 Directional spreading

The slow-drift motions are often studied in long-crested waves, with response in only one horizontal mode of motion. In real sea-states, however, the waves are short-crested and the structure will respond in all horizontal modes of motion. One is often interested in knowing the difference between the surge motions in long-crested and short-crested sea-states.

The short-crested simulations were performed in a sea-state defined by the following wave-spectrum,

$$S_w(\omega,\theta) \;=\; S_w(\omega)\cos^{\mathrm{NCOS}}\theta, \tag{7.1}$$

where $S(\omega)$ is the JONSWAP spectrum and θ is angle of the wave-direction. NCOS is usually an even integer between 2 and ∞, where the latter limit defines a long-crested sea-state. Figure 7-12 shows the spreading function for different values of NCOS. The sensitivity of NCOS upon the surge and sway slow-drift motions are demonstrated in Figure 7-13. The short-crested waves were approximated by a summation of waves along the 7 discrete directions, $\theta = -45°, -30°, -15°, 0°, 15°, 30°, 45°$. A closer spacing between the different θ's is recommended in the study of short-crested seas.

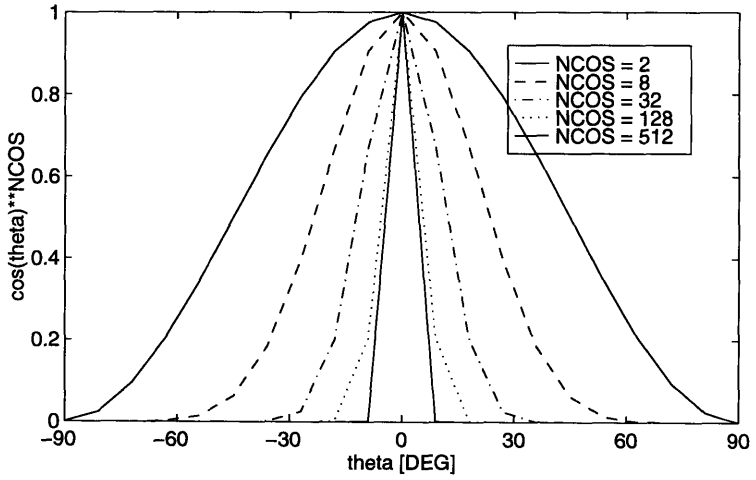

Figure 7-12: The spreading functions that were used in obtaining the mean and rms values of the slow-drift motions in the following figure.

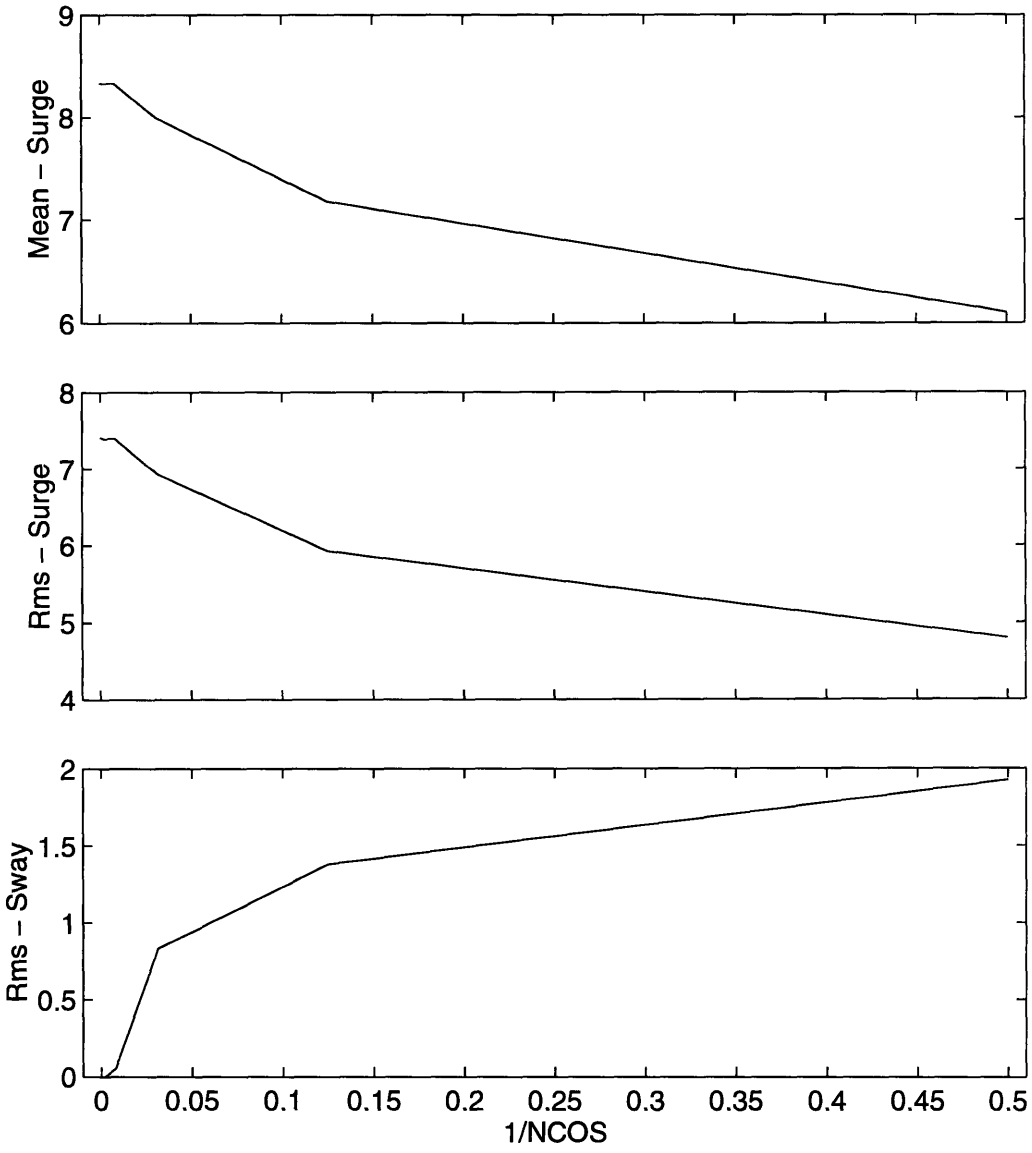

Figure 7-13: The mean and rms of the slow-drift motions in a short-crested sea-state. The peak of the directional spectrum was along $\theta = 0^o$, which defines the x-axis. *Top*: Mean deflection of the surge slow-drift motions. *Center*: Rms of the surge slow-drift motions. *Bottom:* Rms of the sway slow-drift motions.

Chapter 8

Discussion

The thesis studies the large amplitude surge-sway-yaw slow-drift motions of floating bodies constrained by weak restoring forces in random waves. The study divides into two tasks: 1) The computation of linear motions and forces, the mean drift force and the wave-drift damping in the frequency domain. 2) The simulation of the slow-drift motions in irregular short-crested seas. The two tasks are described in the following paragraphs, respectively.

The boundary value problem in the fluid around a floating body with a small horizontal translation and rotation about the vertical axis are derived. The velocity potential expands in the small wave-amplitude A and the small slow-drift velocities U, V and Ω. Explicit solution for the linear zero-speed and forward-speed potentials for arrays of vertical cylinder in regular waves are obtained using the theory of Linton and Evans (1990). Expressions for the zero-speed drift forces are provided both by pressure integration over the body and by momentum conservation principles. The wave-drift damping, which is proportional to the wave-amplitude squared and linear in the slow-drift velocities, is given by the two methods above. The momentum conservation principle is used in computing the wave-drift damping due to horizontal translation, where the far-field formula was reduced to an integral over the body surface. The wave-drift damping due to the rotation about the vertical axis is computed by direct pressure integration. The interactions of waves from different directions are accounted for in the expressions for the mean forces. The linear motions, the drift forces and

the wave-drift damping of an array of cylinders are compared with other methods, and the agreement is very satisfactory.

The second task consists of the simulation of the surge-sway-yaw forces and motions in the time-domain. The slow-drift motions are decoupled from the fast (linear) motions by a multiple scale analysis, which allows the equations of motions to be written in terms of the slowly varying forces only. The latter are computed by the summation of time-series using the results for the mean forces of the frequency domain and the Newman approximation. The expressions for the slowly varying forces generally contain double time series, but were here reduced to products of single series, which reduces the computational time by several orders of magnitude. The time series are evaluated by Fast Fourier Transform. Samples of the random, short crested waves are generated by filtering of white Gaussian noise, and allows for the simulation of very long records without repeating itself. The differential equation of the slow-drift motions is solved numerically by the robust Runge-Kutta scheme. The simulations of surge-sway-yaw slow-drift motions in a long-crested sea-state of 6 hour duration, takes about 15 seconds on a DEC alpha station.

The sensitivity of the mean and the rms of the surge-sway-yaw slow-drift motions of an offshore platform upon certain parameters are presented. The convergence of the mean and rms are illustrated for increasing length of the simulations. The transients associated with the start-up were found to last for a few cycles of the slow-drift motions. The dependence upon the drag-coefficient, a steady current and directional spreading of the waves are also demonstrated.

The hydrodynamic problem of a floating structure moving with a small slow-drift velocity in regular waves has been subject to several studies. The wave-drift damping coefficient due to a slow surge translation was studied by Zhao & Faltinsen (1988), Nossen, Grue & Palm (1991), Emmerhoff & Sclavounos (1992) and Newman (1993). The wave-drift damping due to a slow yaw rotation was studied by Emmerhoff & Sclavounos (1993), Newman (1993) and Palm & Grue (1994). Except for Newman (1993), these studies assume the slow-drift velocity constant. This assumption is consistent with neglegting wave-effects of $O(U)^2$. However, terms of $O(U)^2$ that are

not due to wave-effects, for example the added-mass due to the slow-drift motions, can not be omitted. The dependence on both the wave-amplitude and the slow-drift velocities must be considered in order to consistently include the leading order terms. In Newman (1993) the oscillations of the slow-drift motions are considered, however, the amplitudes of the slow-drift motions are assumed small. The comparison with the current method gives identical expressions for the wave-drift damping. In the studies by Zhao & Faltinsen (1988) and Nossen, Grue & Palm (1991), the hydrodynamic flow was solved by 3-dimensional panel programs. With apropriate discretizations of the floating body, these programs give reliable results for the wave-drift damping coefficients for a large number of geometries. The current method applies strictly only to an array of vertical cylinders with draft equal to the water depth, but the results for the wave-drift damping are derived by analytic methods. These analytic results serve as bench-mark tests, and are valuable for the comparison of different methods. The comparison with the method of Nossen, Grue & Palm (1991) for truncated cylinders with pontoons in Chapter 5, shows good agreement, and indicates a wider applicability of the method.

This study considers the horizontal modes surge, sway and yaw of the slow-drift motions, which are of most importance for structures with stiff, vertical mooring lines (TLPs). Floating structures with large draft and catenary mooring lines may experience significant slow-drift motions in the vertical modes heave, roll and pitch as well. Slow-drift motions in the vertical modes can be accounted for in a similar manner to the derivations of the horizontal modes. An array of cylinders which expands the depth of the fluid, models a real structure with truncated cylinders poorly when it comes to the heave mode, since major contributions to the forces are due to the bottom of the cylinders. The method of Linton and Evans (1991) can therefore be supplemented by approximate methods to account for the bottom effects of the cylinders.

The slowly varying forces that enter into the equations were obtained from the mean forces, by virtue of the Newman approximation. This approximation, however, is less applicable in wide-banded sea-states or for the vertical modes, where the

natural period is not much larger than the dominant wave-period. In this case, the potentials ϕ_{20} and ϕ_{21} must be calculated. Their boundary conditions can be obtained by extending the derivation of Chapter 2.

The overall intention of the thesis was to develop a tool for studying the slow-drift motions of floating offshore structures. This goal has been reached through an efficient program which calculates the hydrodynamic coefficients of an array of cylinders with a small slow-drift velocity, and performes the time simulations of the surge-sway-yaw slow-drift motions in random, short-crested waves. The slow-drift equations accept non-linear terms, which allow for Morison type drag and non-linear restoring forces. The efficiency of the method enables the simulation of very long records. This opens up for more accurate studies of the extremes, and contributes to advance the field of slow-drift motions.

Appendix A

Forces (pressure integration)

The forces and moments in this section are obtained by the pressure-integration, as presented in Section 4.1, for regular waves with frequency ω_0 and direction β relative to the slow-drift x-axis.

A.1 Linear forces

The linear forces acting on the body in direction i for small slow-drift velocities are obtained from equation (4.12), and are here written,

$$[\boldsymbol{F}_{10}(t)]_i = \text{Re}\left[F_i^{(0)}\,\mathrm{e}^{\mathrm{i}\omega t}\right], \tag{A.1}$$

$$[\boldsymbol{F}_{11}(t)]_i = \text{Re}\left[F_i^{(1)}\,\mathrm{e}^{\mathrm{i}\omega t}\right]. \tag{A.2}$$

The decomposition of the potentials ϕ_{10} and ϕ_{11} into diffraction and radiation potentials, cf equations (3.2) and (3.41), leads to an equivalent decomposition of the hydrodynamic forces $F_i^{(0)}$ and $F_i^{(1)}$. Consider first the zero-speed quantities with the super-script (0). Denote by $X_i^{(0)}$ the exciting force in direction i and $A_{ij}^{(0)}$, $B_{ij}^{(0)}$ the added-mass and damping-coefficients, respectively in direction i due to the motion

$\hat{\xi}_j^{(0)}$ in direction j, cf equations (4.20) and (4.21). The linear force of $O(\delta)$ acting on the body is then written

$$F_i^{(0)} = X_i^{(0)} - \hat{\xi}_j^{(0)} \left(-\omega_0^2 A_{ij}^{(0)} + \mathrm{i}\omega_0 B_{ij}^{(0)}\right), \tag{A.3}$$

where $X_i^{(0)}$, $A_{ij}^{(0)}$, and $B_{ij}^{(0)}$ are given by

$$X_i^{(0)} = \rho g A \iint_{\bar{S}_B} \varphi_D n_i \,\mathrm{d}S, \tag{A.4}$$

$$A_{ij}^{(0)} = \rho \mathrm{Re} \iint_{\bar{S}_B} \varphi_R^j n_i \,\mathrm{d}S, \tag{A.5}$$

$$B_{ij}^{(0)} = -\rho\omega_0 \mathrm{Im} \iint_{\bar{S}_B} \varphi_R^j n_i \,\mathrm{d}S. \tag{A.6}$$

In order to obtain an expression for the linear forward-speed force $F_i^{(1)}$ in the form of equation (A.3), the pressure p_{11} in equation (4.3) is substituted into equation (4.12), using the expressions for ϕ_{10} and ϕ_{11} in equations (3.2), (3.41). The time-derivative of ϕ_{11} is given by equation (3.42). $F_i^{(1)}$ can then be written,

$$\begin{aligned} F_i^{(1)} = {} & X_i^{(1)} - \hat{\xi}_j^{(0)} \left(-\omega_0^2 A_{ij}^{(1)} + \mathrm{i}\omega_0 B_{ij}^{(1)}\right) - \\ & \frac{\partial \hat{\xi}_j^{(0)}}{\partial \beta} \left(-\omega_0^2 A_{ij}^{\beta} + \mathrm{i}\omega_0 B_{ij}^{\beta}\right) - \hat{\xi}_j^{(1)} \left(-\omega_0^2 A_{ij}^{(0)} + \mathrm{i}\omega_0 B_{ij}^{(0)}\right), \end{aligned} \tag{A.7}$$

where $X_i^{(1)}$, $A_{ij}^{(1)}$, $B_{ij}^{(1)}$, A_{ij}^{β} and B_{ij}^{β} are defined as follows,

$$\begin{aligned} X_i^{(1)} = {} & \rho g A \iint_{\bar{S}_B} \left[\psi_D + \frac{\mathrm{i}}{\omega_0}(\boldsymbol{f}\cdot\Delta\varphi_D - \nabla\phi_{01}\cdot\nabla\varphi_D)\right] n_i \,\mathrm{d}S - \\ & \frac{\kappa}{\omega_0}(U\cos\beta + V\sin\beta) X_i^{(0)} + \frac{\mathrm{i}\Omega}{\omega_0}\frac{\partial X_i^{(0)}}{\partial\beta}, \end{aligned} \tag{A.8}$$

$$\begin{aligned} A_{ij}^{(1)} = {} & \rho \mathrm{Re} \iint_{\bar{S}_B} \left[\psi_R^j - \frac{1}{\mathrm{i}\omega_0}(\boldsymbol{f}\cdot\Delta\varphi_R^j - \nabla\phi_{01}\cdot\nabla\varphi_R^j)\right] n_i \,\mathrm{d}S - \\ & \frac{\kappa}{\omega_0}(U\cos\beta + V\sin\beta) A_{ij}^{(0)}, \end{aligned} \tag{A.9}$$

$$B_{ij}^{(1)} = -\rho\omega_0 \mathrm{Im} \iint_{\bar{S}_B} \left[\psi_R^j - \frac{1}{\mathrm{i}\omega_0}(\boldsymbol{f}\cdot\Delta\varphi_R^j - \nabla\phi_{01}\cdot\nabla\varphi_R^j)\right] n_i \,\mathrm{d}S -$$

$$\frac{\kappa}{\omega_0}(U\cos\beta + V\sin\beta)B_{ij}^{(0)}, \tag{A.10}$$

$$A_{ij}^{\beta} = \rho\mathrm{Re}\iint_{\bar{S}_B}\psi_R^{\beta i}n_i\,\mathrm{d}S + \frac{\Omega}{\omega_0^2}B_{ij}^{(0)}, \tag{A.11}$$

$$B_{ij}^{\beta} = -\rho\omega_0\mathrm{Im}\iint_{\bar{S}_B}\psi_R^{\beta i}n_i\,\mathrm{d}S - \Omega A_{ij}^{(0)}. \tag{A.12}$$

A.2 Zero-speed drift forces

The mean drift-force $\boldsymbol{F}_{20}$ and moment $\boldsymbol{M}_{20}$ of $O(\delta^2)$ in regular waves are derived next. The potential ϕ_{10} is given by equation (3.2) and the following identity is used in taking the time-average of the expressions (4.14) and (4.15),

$$\overline{\mathrm{Re}\left[\mathcal{A}\,\mathrm{e}^{\mathrm{i}\omega t}\right]\mathrm{Re}\left[\mathcal{B}\,\mathrm{e}^{\mathrm{i}\omega t}\right]} = \tfrac{1}{2}\mathrm{Re}\left[\mathcal{A}\mathcal{B}^*\right], \tag{A.13}$$

where the $*$ denotes complex conjugate. Substituting for the pressures p_{10} and p_{20} in (4.14)-(4.15), leads to the following expressions for the mean forces and moments,

$$\begin{aligned}\bar{\boldsymbol{F}}_{20} &= -\rho\int_{\bar{S}_B}\left[\overline{\left(\tfrac{1}{2}\nabla\phi_{10}\cdot\nabla\phi_{10} + (\boldsymbol{\xi}^{(0)} + \boldsymbol{\alpha}^{(0)}\times\boldsymbol{x}')\cdot\nabla\frac{\partial\phi_{10}}{\partial t}\right)\boldsymbol{n} + \frac{\partial\phi_{10}}{\partial t}\boldsymbol{\alpha}\times\boldsymbol{n}}\right]\mathrm{d}S \\ &\quad + \frac{\rho}{2g}\oint_{C_w}\overline{\frac{\partial\phi_{10}}{\partial t}\frac{\partial\phi_{10}}{\partial t}}\,\boldsymbol{n}\,\mathrm{d}l \\ &= -\frac{\rho}{2}\mathrm{Re}\int_{\bar{S}_B}\left[\tfrac{1}{2}\nabla\varphi\cdot\nabla\varphi^* + \mathrm{i}\omega_0\left(\hat{\boldsymbol{\xi}}^{(0)} + \hat{\boldsymbol{\alpha}}^{(0)}\times\boldsymbol{x}'\right)\cdot\nabla\varphi^*\right]\boldsymbol{n}\,\mathrm{d}S \\ &\quad + \frac{\rho\nu}{4}\mathrm{Re}\oint_{c_w}\varphi\,\varphi^*\,\boldsymbol{n}\,\mathrm{d}l + \tfrac{1}{2}\mathrm{Re}\left(\hat{\boldsymbol{\alpha}}^{(0)}\times\hat{\boldsymbol{F}}_{10}^*\right),\end{aligned} \tag{A.14}$$

$$
\begin{aligned}
\bar{\boldsymbol{M}}_{20} &= -\rho \int_{\bar{S}_B} \overline{\left(\tfrac{1}{2} \nabla\phi_{10} \cdot \nabla\phi_{10} + (\boldsymbol{\xi}^{(0)} + \boldsymbol{\alpha}^{(0)} \times \boldsymbol{x}') \cdot \nabla \frac{\partial \phi_{10}}{\partial t} \right)} \, \boldsymbol{x}' \times \boldsymbol{n} \, \mathrm{d}S \\
&\quad -\rho \int_{\bar{S}_B} \overline{\frac{\partial \phi_{10}}{\partial t} \left(\boldsymbol{\xi}^{(0)} \times \boldsymbol{n} + \boldsymbol{\alpha}^{(0)} \times (\boldsymbol{x}' \times \boldsymbol{n}) \right)} \, \mathrm{d}S + \frac{\rho}{2g} \oint_{c_w} \overline{\frac{\partial \phi_{10}}{\partial t} \frac{\partial \phi_{10}}{\partial t}} \, \boldsymbol{x}' \times \boldsymbol{n} \, \mathrm{d}l \\
&= -\frac{\rho}{2} \mathrm{Re} \int_{S_B} \left[\tfrac{1}{2} \nabla\varphi \cdot \nabla\varphi^* + \mathrm{i}\omega_0 \left(\hat{\boldsymbol{\xi}}^{(0)} + \hat{\boldsymbol{\alpha}}^{(0)} \times \boldsymbol{x}' \right) \cdot \nabla\varphi^* \right] (\boldsymbol{x}' \times \boldsymbol{n}) \, \mathrm{d}S \\
&\quad + \frac{\rho\nu}{4} \mathrm{Re} \oint_{c_w} \varphi\, \varphi^* \, (\boldsymbol{x}' \times \boldsymbol{n}) \, \mathrm{d}l + \tfrac{1}{2} \mathrm{Re} \left(\hat{\boldsymbol{\alpha}}^{(0)} \times \hat{\boldsymbol{M}}^*_{10} + \hat{\boldsymbol{\xi}}^{(0)} \times \hat{\boldsymbol{F}}^*_{10} \right). \qquad \text{(A.15)}
\end{aligned}
$$

A.3 Wave-drift damping

The derivation of the wave-drift damping force of $O(\delta^2 \tau_j)$ is derived along the lines of the derivation in the previous section. The potential ϕ_{11} and its time-derivative is provided by equations (3.41) and (3.42). The term $\partial\phi_{21}/\partial t$ contributes the term $-\Omega \partial \bar{\phi}_{20}/\partial\beta$, which follows from the analysis that lead to equation (3.42). The drift-damping force and moment are written,

$$
\begin{aligned}
\bar{\boldsymbol{F}}_{21} &= -\rho \int_{\bar{S}_B} \overline{\left(\frac{\partial \phi_{21}}{\partial t} - \boldsymbol{f} \cdot \Delta\phi_{20} + \nabla\phi_{01} \cdot \nabla\phi_{20} + \nabla\phi_{10} \cdot \nabla\phi_{11} \right)} \, \boldsymbol{n} \, \mathrm{d}S \\
&\quad -\rho \int_{\bar{S}_B} \overline{(\boldsymbol{\xi}^{(0)} + \boldsymbol{\alpha}^{(0)} \times \boldsymbol{x}') \cdot \nabla \left(\frac{\partial \phi_{11}}{\partial t} - \boldsymbol{f} \cdot \Delta\phi_{10} + \nabla\phi_{01} \cdot \nabla\phi_{10} \right)} \, \boldsymbol{n} \, \mathrm{d}S \\
&\quad -\rho \int_{\bar{S}_B} \overline{(\boldsymbol{\xi}^{(1)} + \boldsymbol{\alpha}^{(1)} \times \boldsymbol{x}') \cdot \nabla \frac{\partial \phi_{10}}{\partial t}} \boldsymbol{n} \, \mathrm{d}S \\
&\quad + \boldsymbol{\alpha}^{(0)} \times \int_{\bar{S}_B} \overline{p_{11}} \boldsymbol{n} \mathrm{d}S + \boldsymbol{\alpha}^{(1)} \times \int_{\bar{S}_B} \overline{p_{10}} \boldsymbol{n} \mathrm{d}S \\
&\quad + \frac{\rho}{g} \oint_{c_w} \overline{\frac{\partial \phi_{10}}{\partial t} \left(\frac{\partial \phi_{11}}{\partial t} - \boldsymbol{f} \cdot \Delta\phi_{10} + \nabla\phi_{01} \cdot \nabla\phi_{10} \right)} \, \boldsymbol{n} \, \mathrm{d}l \\
&= -\rho \mathrm{Re} \int_{\bar{S}_B} \left(-\Omega \frac{\partial \bar{\phi}_{20}}{\partial\beta} - \boldsymbol{f} \cdot \Delta\bar{\phi}_{20} + \nabla\phi_{01} \cdot \nabla\bar{\phi}_{20} + \tfrac{1}{2} \nabla\varphi \cdot \nabla\psi^* \right) \boldsymbol{n} \, \mathrm{d}S
\end{aligned}
$$

$$
\begin{aligned}
&-\frac{\rho}{2}\mathrm{Re}\int_{\bar{S}_B}\left(\hat{\boldsymbol{\xi}}^{(0)}+\hat{\boldsymbol{\alpha}}^{(0)}\times\boldsymbol{x}'\right)\cdot\nabla[\mathrm{i}\omega_0\psi^*-\mathrm{i}\kappa(U\cos\beta+V\sin\beta)\varphi^*\\
&\qquad\qquad -\Omega\frac{\partial\varphi^*}{\partial\beta}-\boldsymbol{f}\cdot\Delta\varphi^*+\nabla\phi_{01}\cdot\nabla\varphi^*]\boldsymbol{n}\,\mathrm{d}S\\
&-\frac{\rho}{2}\mathrm{Re}\int_{\bar{S}_B}\mathrm{i}\omega_0\left(\hat{\boldsymbol{\xi}}^{(1)}+\hat{\boldsymbol{\alpha}}^{(1)}\times\boldsymbol{x}'\right)\cdot\nabla\varphi^*\boldsymbol{n}\,\mathrm{d}S\\
&+\tfrac{1}{2}\,\mathrm{Re}\left(\hat{\boldsymbol{\alpha}}^{(0)}\times\hat{\boldsymbol{F}}^*_{11}+\hat{\boldsymbol{\alpha}}^{(1)}\times\hat{\boldsymbol{F}}^*_{10}\right)\\
&+\frac{\rho}{2g}\oint_{c_w}[\omega_0^2\varphi\psi^*-\omega_0\kappa(U\cos\beta+V\sin\beta)\varphi\varphi^*-\mathrm{i}\omega_0\Omega\varphi\frac{\partial\varphi^*}{\partial\beta}\\
&\qquad -\mathrm{i}\omega_0\varphi\boldsymbol{f}\cdot\Delta\varphi^*+\mathrm{i}\omega_0\varphi\nabla\phi_{01}\cdot\nabla\varphi^*]\boldsymbol{n}\,\mathrm{d}l, \qquad (A.16)
\end{aligned}
$$

$$
\begin{aligned}
\bar{\boldsymbol{M}}_{21} &= -\rho\int_{\bar{S}_B}\overline{\left(\frac{\partial\phi_{21}}{\partial t}-\boldsymbol{f}\cdot\Delta\phi_{20}+\nabla\phi_{01}\cdot\nabla\phi_{20}+\nabla\phi_{10}\cdot\nabla\phi_{11}\right)}(\boldsymbol{x}'\times\boldsymbol{n})\,\mathrm{d}S\\
&\quad -\rho\int_{\bar{S}_B}\overline{(\boldsymbol{\xi}^{(0)}+\boldsymbol{\alpha}^{(0)}\times\boldsymbol{x}')\cdot\nabla\left(\frac{\partial\phi_{11}}{\partial t}-\boldsymbol{f}\cdot\Delta\phi_{10}+\nabla\phi_{01}\cdot\nabla\phi_{10}\right)}(\boldsymbol{x}'\times\boldsymbol{n})\,\mathrm{d}S\\
&\quad -\rho\int_{\bar{S}_B}\overline{(\boldsymbol{\xi}^{(1)}+\boldsymbol{\alpha}^{(1)}\times\boldsymbol{x}')\cdot\nabla\frac{\partial\phi_{10}}{\partial t}}(\boldsymbol{x}'\times\boldsymbol{n})\,\mathrm{d}S\\
&\quad +\int_{\bar{S}_B}\overline{p_{11}\left(\boldsymbol{\xi}^{(0)}\times\boldsymbol{n}+\boldsymbol{\alpha}^{(0)}\times(\boldsymbol{x}'\times\boldsymbol{n})\right)}\mathrm{d}S\\
&\quad +\int_{\bar{S}_B}\overline{p_{10}\left(\boldsymbol{\xi}^{(1)}\times\boldsymbol{n}+\boldsymbol{\alpha}^{(1)}\times(\boldsymbol{x}'\times\boldsymbol{n})\right)}\mathrm{d}S\\
&\quad -\rho\int_{\bar{S}_B}\overline{\frac{\partial\phi_{10}}{\partial t}\left(\boldsymbol{\alpha}^{(1)}\times(\boldsymbol{x}'\times\boldsymbol{n})+\boldsymbol{\xi}^{(1)}\times\boldsymbol{n}\right)}\mathrm{d}S\\
&\quad +\frac{\rho}{g}\oint_{c_w}\overline{\frac{\partial\phi_{10}}{\partial t}\left(\frac{\partial\phi_{11}}{\partial t}-\boldsymbol{f}\cdot\Delta\phi_{10}+\nabla\phi_{01}\cdot\nabla\phi_{10}\right)}(\boldsymbol{x}'\times\boldsymbol{n})\,\mathrm{d}l
\end{aligned}
$$

$$
\begin{aligned}
&= -\rho\mathrm{Re}\int_{\bar{S}_B}\left(-\Omega\frac{\partial\bar{\phi}_{20}}{\partial\beta}-\boldsymbol{f}\cdot\Delta\bar{\phi}_{20}+\nabla\phi_{01}\cdot\nabla\bar{\phi}_{20}+\tfrac{1}{2}\nabla\varphi\cdot\nabla\psi^*\right)(\boldsymbol{x}'\times\boldsymbol{n})\,\mathrm{d}S\\
&\quad -\frac{\rho}{2}\mathrm{Re}\int_{\bar{S}_B}\left(\hat{\boldsymbol{\xi}}^{(0)}+\hat{\boldsymbol{\alpha}}^{(0)}\times\boldsymbol{x}'\right)\cdot\nabla[\mathrm{i}\omega_0\psi^*-\mathrm{i}\kappa(U\cos\beta+V\sin\beta)\varphi^*\\
&\qquad\qquad -\Omega\frac{\partial\varphi^*}{\partial\beta}-\boldsymbol{f}\cdot\Delta\varphi^*+\nabla\phi_{01}\cdot\nabla\varphi^*](\boldsymbol{x}'\times\boldsymbol{n})\,\mathrm{d}S\\
&\quad -\frac{\rho}{2}\mathrm{Re}\int_{\bar{S}_B}\mathrm{i}\omega_0\left(\hat{\boldsymbol{\xi}}^{(1)}+\hat{\boldsymbol{\alpha}}^{(1)}\times\boldsymbol{x}'\right)\cdot\nabla\varphi^*(\boldsymbol{x}'\times\boldsymbol{n})\,\mathrm{d}S\\
&\quad +\tfrac{1}{2}\,\mathrm{Re}\left(\hat{\boldsymbol{\alpha}}^{(0)}\times\hat{\boldsymbol{M}}^*_{11}+\hat{\boldsymbol{\alpha}}^{(1)}\times\hat{\boldsymbol{M}}^*_{10}+\hat{\boldsymbol{\xi}}^{(0)}\times\hat{\boldsymbol{F}}^*_{11}+\hat{\boldsymbol{\xi}}^{(1)}\times\hat{\boldsymbol{F}}^*_{10}\right)\\
&\quad +\frac{\rho}{2g}\oint_{c_w}[\omega_0^2\varphi\psi^*-\omega_0\kappa(U\cos\beta+V\sin\beta)\varphi\varphi^*-\mathrm{i}\omega_0\Omega\varphi\frac{\partial\varphi^*}{\partial\beta}\\
&\qquad -\mathrm{i}\omega_0\varphi\boldsymbol{f}\cdot\Delta\varphi^*+\mathrm{i}\omega_0\varphi\nabla\phi_{01}\cdot\nabla\varphi^*](\boldsymbol{x}'\times\boldsymbol{n})\,\mathrm{d}l. \qquad (A.17)
\end{aligned}
$$

Appendix B

The m-terms

The *m-terms* of equation (2.29), defined by (2.30)-(2.31), were obtained as follows: Four vector identities will be used,

$$\boldsymbol{n}\cdot(\boldsymbol{\xi}^{(0)}\cdot\nabla)\nabla\phi_{01} = \boldsymbol{\xi}^{(0)}\cdot(\boldsymbol{n}\cdot\nabla)\nabla\phi_{01}, \tag{B.1}$$

$$(\boldsymbol{n}\cdot\nabla)(\boldsymbol{x}\times\nabla\phi_{01}) = \boldsymbol{n}\times\nabla\phi_{01}+\boldsymbol{x}\times[(\boldsymbol{n}\cdot\nabla)\nabla\phi_{01}], \tag{B.2}$$

$$\boldsymbol{n}\cdot[(\boldsymbol{\alpha}^{(0)}\times\boldsymbol{x})\cdot\nabla]\nabla\phi_{01} = \boldsymbol{\alpha}^{(0)}\cdot(\boldsymbol{x}\times[(\boldsymbol{n}\cdot\nabla)\nabla\phi_{01}]), \tag{B.3}$$

$$(\boldsymbol{\alpha}^{(0)}\times\boldsymbol{n})\cdot\nabla\phi_{01} = \boldsymbol{\alpha}^{(0)}\cdot(\boldsymbol{n}\times\nabla\phi_{01}),. \tag{B.4}$$

The equation (2.30) was obtained by collecting terms proportional to $\boldsymbol{\xi}^{(0)}$ in (2.29) and using equation (B.1). In order to show how the expression for (m_4, m_5, m_6) in (2.31) was obtained, the first term on the right hand side of equation (2.31) is expanded according to (B.2). Equation (B.3) is further used to rewrite the last term in (B.2). Using equation (B.4) and the expanded form of (2.31), it is thus seen how the (m_4, m_5, m_6) term is obtained from (2.29).

The expressions for the m_1, m_2, m_6 terms for a vertical cylinder are shown next. The steady potential ϕ_{01} and its derivatives with respect to the body coordinates x_j and y_j for a single cylinder are given by,

$$\phi_{01} = -\frac{a_j^2}{r_j}\left[(U-\Omega\bar{y}_j)\cos\theta_j+(V+\Omega\bar{x}_j)\sin\theta_j\right] \tag{B.5}$$

$$\frac{\partial \phi_{01}}{\partial x_j} = \frac{a_j^2}{r_j^2}\left[(U-\Omega\bar{y}_j)\cos 2\theta_j + (V+\Omega\bar{x}_j)\sin 2\theta_j\right] \tag{B.6}$$

$$\frac{\partial \phi_{01}}{\partial y_j} = \frac{a_j^2}{r_j^2}\left[(U-\Omega\bar{y}_j)\sin 2\theta_j - (V+\Omega\bar{x}_j)\cos 2\theta_j\right], \tag{B.7}$$

where the notation from Chapter 3 has been used. m_1, m_2 and m_6 are then obtained from equations (2.30)-(2.31),

$$\begin{aligned} m_1 &= \frac{\partial^2 \phi_{01}}{\partial r_j \partial x_j} \\ &= -\frac{2}{a_j}\left[(U-\Omega\bar{y}_j)\cos 2\theta_j + (V+\Omega\bar{x}_j)\sin 2\theta_j\right], \end{aligned} \tag{B.8}$$

$$\begin{aligned} m_2 &= \frac{\partial^2 \phi_{01}}{\partial r_j \partial y_j} \\ &= -\frac{2}{a_j}\left[(U-\Omega\bar{y}_j)\sin 2\theta_j - (V+\Omega\bar{x}_j)\cos 2\theta_j\right], \end{aligned} \tag{B.9}$$

$$\begin{aligned} m_6 &= \frac{\partial}{\partial r_j}\left[(\bar{x}_j + x_j)\frac{\partial \phi_{01}}{\partial y_j} - (\bar{y}_j + y_j)\frac{\partial \phi_{01}}{\partial x_j}\right] + \cos\theta_j(U-\Omega\bar{y}_j) - \sin\theta_j(V+\Omega\bar{x}_j) \\ &= (\bar{x}_j + x_j)m_2 - (\bar{y}_j + y_j)m_1 + \cos\theta_j\frac{\partial \phi_{01}}{\partial y_j} - \sin\theta_j\frac{\partial \phi_{01}}{\partial x_j} + \\ &\quad \cos\theta_j(U-\Omega\bar{y}_j) - \sin\theta_j(V+\Omega\bar{x}_j) \\ &= \bar{x}_j m_2 - \bar{y}_j m_1. \end{aligned} \tag{B.10}$$

Appendix C

The evaluation of Ψ_1^j and Ψ_{2m}^j

The evaluation of Ψ_1^j requires the ν- and β-derivative of the influence coefficients A_{Dm}^j and A_{Rm}^{ij}, where $\nu = \omega^2/g$ is the deep-water wave number and β is the wave-heading. The respective derivatives are obtained by differentiation of equations (3.21) and (3.34). It was found more convenient to evaluate the κ-derivative rather than the ν-derivative, which are related by,

$$\begin{aligned} \frac{\partial}{\partial \nu} &= \frac{\mathrm{d}\kappa}{\mathrm{d}\nu}\frac{\partial}{\partial \kappa} \\ &= \frac{1}{\kappa h/\cosh^2(\kappa h) + \nu/\kappa}\,\frac{\partial}{\partial \kappa} \end{aligned} \tag{C.1}$$

where the dispersion relation was used. Define,

$$\begin{aligned} &B_{Dm}^j \equiv \kappa\frac{\partial A_{Dm}^j}{\partial \kappa}, \quad C_{Dm}^j \equiv \frac{\partial A_{Dm}^j}{\partial \beta}, \quad D_{Dm}^j \equiv \kappa\frac{\partial^2 A_{Dm}^j}{\partial \kappa \partial \beta}, \\ &B_{Rm}^{ij} \equiv \kappa\frac{\partial A_{Rm}^{ij}}{\partial \kappa}. \end{aligned} \tag{C.2}$$

The radiation coefficients do not depend upon the wave-heading β, and the respective derivatives are therefore equal to zero. The κ- and β-derivatives of the influence

coefficients are then written,

$$B^k_{Dm} + \underbrace{\sum_{j=1}^{N}}_{\neq k} \sum_{n=-\infty}^{\infty} B^j_{Dn} Z^j_n \mathrm{e}^{\mathrm{i}(n-m)\alpha_{jk}} H^{(2)}_{n-m}(\kappa R_{jk}) = -I'_k \mathrm{e}^{-\mathrm{i}m(\pi/2+\beta)}$$

$$- \underbrace{\sum_{j=1}^{N}}_{\neq k} \sum_{n=-\infty}^{\infty} A^j_{Dn} \left[\kappa a_j Z^{j\prime}_n H^{(2)}_{n-m}(\kappa R_{jk}) + \kappa R_{jk} Z^j_n H^{(2)\prime}_{n-m}(\kappa R_{jk})\right] \mathrm{e}^{\mathrm{i}(n-m)\alpha_{jk}}, \qquad \text{(C.3)}$$

$$C^k_{Dm} + \underbrace{\sum_{j=1}^{N}}_{\neq k} \sum_{n=-\infty}^{\infty} C^j_{Dn} Z^j_n \mathrm{e}^{\mathrm{i}(n-m)\alpha_{jk}} H^{(2)}_{n-m}(\kappa R_{jk}) = -I^m_k e^{-im(\pi/2+\beta)}, \qquad \text{(C.4)}$$

$$D^k_{Dm} + \underbrace{\sum_{j=1}^{N}}_{\neq k} \sum_{n=-\infty}^{\infty} D^j_{Dn} Z^j_n \mathrm{e}^{\mathrm{i}(n-m)\alpha_{jk}} H^{(2)}_{n-m}(\kappa R_{jk}) = -I^{m\prime}_k \mathrm{e}^{-\mathrm{i}m(\pi/2+\beta)}$$

$$- \underbrace{\sum_{j=1}^{N}}_{\neq k} \sum_{n=-\infty}^{\infty} C^j_{Dn} \left[\kappa a_j Z^{j\prime}_n H^{(2)}_{n-m}(\kappa R_{jk}) + \kappa R_{jk} Z^j_n H^{(2)\prime}_{n-m}(\kappa R_{jk})\right] \mathrm{e}^{\mathrm{i}(n-m)\alpha_{jk}}, \qquad \text{(C.5)}$$

$$B^{ik}_{Rm} + \underbrace{\sum_{j=1}^{N}}_{\neq k} \sum_{n=-\infty}^{\infty} B^{ij}_{Rn} Z^j_n \mathrm{e}^{\mathrm{i}(n-m)\alpha_{jk}} H^{(2)}_{n-m}(\kappa R_{jk}) =$$

$$- \underbrace{\sum_{j=1}^{N}}_{\neq k} \sum_{n=-\infty}^{\infty} \left(\gamma^{ij}_{m0} H^{(2)}_{n-m}(\kappa R_{jk}) + \kappa R_{jk} \beta^{ij}_{m0} H^{(2)\prime}_{n-m}(\kappa R_{jk})\right) \mathrm{e}^{\mathrm{i}(n-m)\alpha_{jk}}$$

$$- \underbrace{\sum_{j=1}^{N}}_{\neq k} \sum_{n=-\infty}^{\infty} A^{ij}_{Rn} \left(\kappa a_j Z^{j\prime}_n H^{(2)}_{n-m}(\kappa R_{jk}) + \kappa R_{jk} Z^j_n H^{(2)\prime}_{n-m}(\kappa R_{jk})\right) \mathrm{e}^{\mathrm{i}(n-m)\alpha_{jk}}, \qquad \text{(C.6)}$$

where the indices k, m in equations (C.3)-(C.6) run over the values $k = 1, \ldots, N$ and $m = -\infty, \ldots, \infty$. The following notation has been used,

$$I'_k = \left[C' - i\,C\kappa\left(\bar{x}_j \cos\beta + \bar{y}_j \sin\beta\right)\right] \mathrm{e}^{-\mathrm{i}\kappa(\bar{x}_j \cos\beta + \bar{y}_j \sin\beta)} \qquad \text{(C.7)}$$

$$C = \sqrt{\frac{\kappa h/\cosh^2 \kappa h + \nu/\kappa}{2\kappa}} \tag{C.8}$$

$$C' = -\frac{1}{2\kappa C}\frac{\nu}{\kappa}\left[(\kappa h/\cosh \kappa h)^2 + 1 - \frac{1}{2\sigma}\right] \tag{C.9}$$

$$\sigma = \frac{\nu}{\kappa}\frac{\mathrm{d}\kappa}{\mathrm{d}\nu} \tag{C.10}$$

$$Z_n^{j\prime} = \frac{J_n''(\kappa a_j)H_n^{(2)\prime}(\kappa a_j) - J_n'(\kappa a_j)H_n^{(2)\prime\prime}(\kappa a_j)}{H_n^{(2)\prime 2}(\kappa a_j)}. \tag{C.11}$$

$$I_k^m = -\mathrm{i}I_k\left(m - \kappa\bar{x}_j \sin\beta + \kappa\bar{y}_j \cos\beta\right), \tag{C.12}$$

$$I_k^{m\prime} = -\mathrm{i}I_k'\left(m - \kappa\bar{x}_j \sin\beta + \kappa\bar{y}_j \cos\beta\right) - \mathrm{i}I_k\left(-\kappa\bar{x}_j \sin\beta + \kappa\bar{y}_j \cos\beta\right), \tag{C.13}$$

$$\gamma_{m0}^j = \beta_{m0}^j\left(\frac{1}{\sigma} - \frac{5}{2} - \kappa a_j \frac{H_m^{(2)\prime\prime}(\kappa a_j)}{H_m^{(2)\prime}(\kappa a_j)} - \frac{1}{S}S'\right), \tag{C.14}$$

$$S = \sqrt{\frac{\kappa h}{\cosh^2 \kappa h} + \frac{\nu}{\kappa}} \tag{C.15}$$

$$S' = \frac{1}{S}\frac{\kappa h}{\cosh^2 \kappa h}(1 - \nu h). \tag{C.16}$$

The Weber transform pair for Ψ_{2m}^j is given by equations (3.71) - (3.73). The Weber transform of the Laplace equation in equation (3.74), is obtained by the following analysis.

The Laplace equation $\nabla^2\Psi_2^j$ in the cylindrical coordinates (r_j, θ_j, z_j) is given by

$$\begin{aligned} \frac{1}{r_j}\frac{\partial}{\partial r_j}\left(r_j\frac{\partial\Psi_2^j}{\partial r_j}\right) + \frac{1}{r_j^2}\frac{\partial^2\Psi_2^j}{\partial\theta_j^2} + \frac{\partial^2\Psi_2^j}{\partial z_j^2} &= 0 \\ \Updownarrow & \\ \frac{1}{r_j}\frac{\partial}{\partial r_j}\left(r_j\frac{\partial\Psi_{2m}^j}{\partial r_j}\right) - \frac{m^2}{r_j^2}\Psi_2^j + \frac{\partial^2\Psi_{2m}^j}{\partial z_j^2} &= 0. \end{aligned} \tag{C.17}$$

The quantity $f_0(z_j)W_m(kr_j)\mathrm{e}^{\mathrm{i}m\theta_j}$ satisfies Laplace equation, which leads to the follow-

ing identity for $W_m(kr_j)$:

$$\frac{m^2}{r_j^2}W_m = k^2 W_m + \frac{1}{r_j}\frac{\partial}{\partial r_j}\left(r_j \frac{\partial W_m}{\partial r_j}\right). \tag{C.18}$$

The Weber transform is now applied to the Laplace equation (C.17), using the identity for $W_m(kr_j)$ and integration by parts, leading to the result in equation (3.74).

$$\begin{aligned} -\frac{\partial^2 \tilde{\Psi}^j_{2m}}{\partial z_j^2} &= \int_{a_j}^{\infty} r_j \mathrm{d}r_j \left[\frac{1}{r_j}\frac{\partial}{\partial r_j}\left(r_j \frac{\partial \Psi^j_{2m}}{\partial r_j}\right) - \frac{m^2}{r_j^2}\Psi^j_2\right] W_m \\ &= \int_{a_j}^{\infty} r_j \mathrm{d}r_j \left[\frac{1}{r_j}\frac{\partial}{\partial r_j}\left(r_j \frac{\partial \Psi^j_{2m}}{\partial r_j}\right) W_m - k^2 \Psi^j_{2m} W_m - \frac{1}{r_j}\frac{\partial}{\partial r_j}\left(r_j \frac{\partial W_m}{\partial r_j}\right)\Psi^j_{2m}\right] \\ &= \left[r_j \frac{\partial \Psi^j_{2m}}{\partial r_j} W_m - r_j \frac{\partial W_m}{\partial r_j}\Psi^j_{2m}\right]_{a_j}^{\infty} - k^2 \tilde{\Psi}^j_{2m}. \end{aligned} \tag{C.19}$$

The quantity in brackets on the last line in equation (C.19) vanishes at $r_j = \infty$ since the radiation conditions can be applied for Ψ^j_{2m} and asymptotic expressions for $W_m(kr_j)$ as $r_j \to \infty$ and vanishes at $r_j = a_j$ since the r_j-derivative of both Ψ^j_{2m} and $W_m(kr_j)$ vanishes at $r_j = a_j$, cf equations (3.72) and (3.73).

Appendix D

Viscous force

The expressions for the Morison type viscous forces on each cylinder are presented. Other non axis-symmetric geometries, such as pontoons, are not considered. Interactions of the flow between cylinders are neglected.

The magnitude of the slow-drift velocity of cylinder j can be written,

$$|U_j| = \sqrt{(X_o - \bar{y}_j\dot{\Theta})^2 + (Y_o + \bar{x}_j\dot{\Theta})^2}, \tag{D.1}$$

where $(\bar{x}_j, \bar{y}_j)$ is the horizontal location of cylinder j with respect to the slow-drift frame (see Figure 3-2). The viscous forces on cylinder j in the global X- and Y-directions are then written,

$$\mathcal{F}^j_{v1} = \tfrac{1}{2}\rho C_D A_j |U_j| \dot{X}_o, \tag{D.2}$$

$$\mathcal{F}^j_{v2} = \tfrac{1}{2}\rho C_D A_j |U_j| \dot{Y}_o, \tag{D.3}$$

$$\mathcal{F}^j_{v6} = \left(-\mathcal{F}^j_{v1}\sin\Theta + \mathcal{F}^j_{v2}\cos\Theta\right)\bar{x}_j - \left(\mathcal{F}^j_{v1}\cos\Theta + \mathcal{F}^j_{v2}\sin\Theta\right)\bar{y}_j. \tag{D.4}$$

where C_D is the drag-coefficient and A_j is the projected area of cylinder j onto a vertical plane. The total viscous force, $\boldsymbol{\mathcal{F}}_v(\dot{\boldsymbol{\mathcal{X}}}_0) = (\mathcal{F}_{v1}, \mathcal{F}_{v2}, \mathcal{F}_{v6})^T$ on the platform is obtained by the summation over all N_c cylinders,

$$\mathcal{F}_{vi} = \sum_{j=1}^{N_c} \mathcal{F}^j_{vi}, \qquad i = 1, 2, 6. \tag{D.5}$$

Appendix E

Short-crested seas

E.1 Mean-forces

The expressions (4.41) - (4.43) and (A.14) - (A.17) for the mean forces in long-crested waves propagating in direction β relative to the slow-drift x-axis, are here extended to short-crested waves. Denote by $\bar{F}$ the second-order mean-force in the above-mentioned equations. $\bar{F}$ consists of products of the linear quantities φ, ψ, $\boldsymbol{\xi}$, $\boldsymbol{\alpha}$ as well as the second-order potential $\bar{\phi}_{20}$. In short-crested seas, pairs of waves from different directions must be considered in order to account for the interactions between waves. The linear quantities in bi-directional waves are simply the sum of the respective quantities in one-directional waves, given by

$$\varphi = \varphi_i + \varphi_j, \tag{E.1}$$

$$\psi = \psi_i + \psi_j, \tag{E.2}$$

$$\hat{\boldsymbol{\xi}} = \hat{\boldsymbol{\xi}}_i + \hat{\boldsymbol{\xi}}_j, \tag{E.3}$$

$$\hat{\boldsymbol{\alpha}} = \hat{\boldsymbol{\alpha}}_i + \hat{\boldsymbol{\alpha}}_j, \tag{E.4}$$

where the subscripts i and j refer to directions β_i and β_j, respectively. In order to obtain the second-order potential $\bar{\phi}_{20}$, which is a function of the linear quantities (E.1) - (E.4), $\bar{\phi}_{20}$ is decomposed into the components $\bar{\phi}_{20}^{ij}$ as follows,

$$\bar{\phi}_{20} = \sum_{i,j} \bar{\phi}_{20}^{ij}, \tag{E.5}$$

where the boundary conditions of the potentials $\bar{\phi}_{20}^{ij}$ may be inferred from equations (3.82) and (3.83),

$$\frac{\partial \bar{\phi}_{20}^{ij}}{\partial z} = -\frac{\omega_0}{2g} \mathrm{Im}\left(\varphi_i \frac{\partial^2 \varphi_j^*}{\partial z^2}\right), \tag{E.6}$$

$$\frac{\partial \bar{\phi}_{20}^{ij}}{\partial n} = \tfrac{1}{2}\mathrm{Re}\left(\hat{\boldsymbol{\alpha}}_j^* \times \boldsymbol{n} \cdot [\mathrm{i}\omega(\hat{\boldsymbol{\xi}}_i + \hat{\boldsymbol{\alpha}}_i \times \boldsymbol{x}) - \nabla\varphi_i] - \boldsymbol{n} \cdot [(\hat{\boldsymbol{\xi}}_i + \hat{\boldsymbol{\alpha}}_i \times \boldsymbol{x}) \cdot \nabla]\nabla\varphi_j^*\right). \tag{E.7}$$

The decomposition of the mean-force $\bar{F}$ into $\bar{F}_{ij}$ with waves coming from N_β different directions, now follows from the above analysis, and is given by,

$$\bar{F} = \sum_{i=1}^{N_\beta} \sum_{j=1}^{N_\beta} \bar{F}_{ij}, \tag{E.8}$$

where the components $\bar{F}_{ij}$ can be obtained from expressions (4.41) - (4.43) and (A.14) - (A.17) similarly to the derivation of equations (E.6) and (E.7). In the expressions for the forward-speed forces, however, the wave-heading β appears explicitly via the terms $\cos\beta$ and $\sin\beta$. These terms derives from the time-derivative of the potential ϕ_{11}. By introducing the decomposition of the linear quantities in equations (E.1) - (E.4) into the expressions of the mean-forces before the assumption of time-harmonic waves, e. g. equations (4.33) - (4.35), the correct index can be put on the wave-heading β. Applying this to the wave-drift damping of equations (4.41) - (4.43), the

$\bar{F}_{ij}$ components are written,

$$B_{11}^{ij} = \tfrac{1}{2}\rho \iint_{\bar{S}_\infty} \left[\varphi_{ix}\psi_{jn}^{U*} + \varphi_{in}\psi_{jx}^{U*} - \nabla\varphi_i \cdot \nabla\psi_j^{U*} n_1\right] \mathrm{d}S + \tfrac{1}{2}\rho \int_{c_\infty} \varphi_i \left(\nu\psi_j^{U*} n_1 - \kappa\frac{\omega_0}{g}\cos\beta_j \varphi_j^* n_1\right) \mathrm{d}l, \tag{E.9}$$

$$B_{21}^{ij} = \tfrac{1}{2}\rho \iint_{\bar{S}_\infty} \left[\varphi_{iy}\psi_{jn}^{U*} + \varphi_{in}\psi_{jy}^{U*} - \nabla\varphi_i \cdot \nabla\psi_j^{U*} n_2 - \frac{1}{R}\frac{\partial\bar{\phi}_{20}^{ij}}{\partial\Theta}\right] \mathrm{d}S + \tfrac{1}{2}\rho \int_{c_\infty} \varphi_i \left(\nu\psi_j^{U*} n_2 - \kappa\frac{\omega_0}{g}\cos\beta_j \varphi_j^* n_2 + \frac{\mathrm{i}\omega_0}{gR}\varphi_{j\Theta}^*\right) \mathrm{d}l, \tag{E.10}$$

$$B_{61}^{ij} = \tfrac{1}{2}\rho \iint_{\bar{S}_\infty} \left[\varphi_{i\Theta}\psi_{jn}^{U*} + \varphi_{in}\psi_{j\Theta}^{U*} - 2n_1\frac{\partial\bar{\phi}_{20}^{ij}}{\partial\Theta} + 2y\frac{\partial\bar{\phi}_{20}^{ij}}{\partial n}\right] \mathrm{d}S + \tfrac{1}{2}\frac{\rho\mathrm{i}\omega_0}{g} \int_{c_\infty} \varphi_i \left(-\varphi_{j\Theta}^* n_1 + \varphi_{jn}^* y\right) \mathrm{d}l. \tag{E.11}$$

The component $\bar{F}_{ii}$ denotes the mean-force due to waves along direction i only, while the components $\bar{F}_{ij}$ and $\bar{F}_{ji}$ account for interactions between directions i and j.

E.2 Wave-elevation

The extension of Section 6.3 to short-crested waves is here considered. In a short-crested sea-state, waves are generally propagating in all directions. The wave-elevation $\zeta(t)$ can in this case be constructed by a linear superposition of plane progressive waves from a number of directions. Denote by $\zeta(t,\beta_i)$ the wave-elevation of plane progressive waves in direction i, and β_i the corresponding angle between the inertial X-axis and the direction of wave-propagation. The total wave-elevation, which is the

sum of waves from all possible directions is thus written,

$$\zeta(t) = \sum_{i=1}^{N_\beta} \zeta(t, \beta_i), \tag{E.12}$$

where N_β is the number of wave-directions. N_β and β_i must be chosen such that directions with significant energy are well represented by the discrete summation. A realization of the wave-elevation $\zeta(t, \beta_i)$ can be obtained along the same lines as described in Section 6.3. $\zeta(t, \beta_i)$ and its Fourier transform $Z(\omega, \beta_i)$, cf equations (6.12) - (6.13), are given by,

$$\zeta(t, \beta_i) = \int_{-\infty}^{+\infty} w(\tau, \beta_i) h(t - \tau, \beta_i) \mathrm{d}\tau, \tag{E.13}$$

$$Z(\omega, \beta_i) = W(\omega, \beta_i) H(\omega, \beta_i), \tag{E.14}$$

where $W(\omega, \beta_i)$ is a WGN process in the variables ω and β_i and the transfer function $H(\omega, \beta_i)$ is defined as follows,

$$H(\omega, \beta_i) = [S_\zeta(\omega, \beta_i) \Delta\beta_i]^{1/2}. \tag{E.15}$$

The quantity $S_\zeta(\omega, \beta_i)$ defines the spectral energy of the wave-components for a given direction β_i, and $\Delta\beta_i$ the directional increments associated with direction β_i. $S_\zeta(\omega, \beta_i)$ and $\Delta\beta_i$ must be defined such that,

$$S_\zeta(\omega) = \sum_{i=1}^{N_\beta} S_\zeta(\omega, \beta_i) \Delta\beta_i, \tag{E.16}$$

where $S_\zeta(\omega)$ is the spectral density of the total wave-elevation in the short-crested sea-state.

E.3 Second-order forces

Expression (6.24) is here extended to include combinations of incident waves from different directions. The total linear wave-elevation in a short-crested sea-state is given by equation (E.12) and the 'amplitudes' for each direction by (E.14). Denote by $H(\omega_1, \omega_2, \beta_i, \beta_j)$ the transfer function for the second order force due to incident waves from directions β_i and β_j. The second order force in a short-crested sea state can thus be written,

$$D(t) = (2\pi)^{-2} \sum_{i=1}^{N_\beta} \sum_{j=1}^{N_\beta} \int_{-\infty}^{+\infty} \int_{-\infty}^{+\infty} Z(\omega_1, \beta_i) Z(\omega_2, \beta_j) H(\omega_1, \omega_2, \beta_i, \beta_j) \, \mathrm{e}^{-\mathrm{i}(\omega_1 + \omega_2)t} \mathrm{d}\omega_1 \mathrm{d}\omega_2. \tag{E.17}$$

The narrow-band approximation in Section 6.4.1 will be applied to the transfer function $H(\omega_1, \omega_2, \beta_i, \beta_j)$, but no approximations with respect to the incident wave-headings β_i, β_j. The second-order mean force $\bar{D}(\omega, \beta_i, \beta_j)$ is introduced,

$$\bar{D}(\omega, \beta_i, \beta_j) = \mathrm{Re}\left[\mathcal{D}(\omega, \beta_i, \beta_j)\right], \tag{E.18}$$

which represents the forces of $O(\delta^2)$ and $O(\delta^2 \tau_j)$ obtained in this section. The relation between $\mathcal{D}(\omega, \beta_i, \beta_j)$ and $H(\omega, -\omega, \beta_i, \beta_j)$ is given by,

$$H(\omega, -\omega, \beta_i, \beta_j) = 2\mathcal{D}(\omega, \beta_i, \beta_j). \tag{E.19}$$

The second-order difference-frequency force in an irregular sea-state, cf equation (6.24), is then written,

$$\begin{aligned} D^-(t) = \frac{1}{8\pi^2} \mathrm{Re} \sum_{i=1}^{N_\beta} \sum_{j=1}^{N_\beta} \Bigg[& \int_{-\infty}^{+\infty} Z(\omega_1, \beta_i) [\mathcal{D}(\omega_1, \beta_i, \beta_j) + \mathcal{D}(\omega_1, \beta_j, \beta_i)] \, \mathrm{e}^{-\mathrm{i}\omega_1 t} \mathrm{d}\omega_1 \\ & \int_{-\infty}^{+\infty} Z(\omega_2, \beta_j) \, \mathrm{e}^{-\mathrm{i}\omega_2 t} \mathrm{d}\omega_2 - \\ & \int_{-\infty}^{+\infty} \mathrm{sgn}(\omega_1) Z(\omega_1, \beta_i) [\mathcal{D}(\omega_1, \beta_i, \beta_j) + \mathcal{D}(\omega_1, \beta_j, \beta_i)] \, \mathrm{e}^{-\mathrm{i}\omega_1 t} \mathrm{d}\omega_1 \end{aligned}$$

$$\int_{-\infty}^{+\infty} \operatorname{sgn}(\omega_2) Z(\omega_2, \beta_j)\, \mathrm{e}^{-\mathrm{i}\omega_2 t} \mathrm{d}\omega_2 \Big] . \qquad \text{(E.20)}$$

Bibliography

[1] Abramowitz, M. & Stegun, I. A. 1972 *Handbook of mathematical functions.* Dover.

[2] Agnon, Y. & Mei, C. C. 1985 Slow-drift motion of a two-dimensional block in beam seas. *J. Fluid Mech.* **151**, 279-294.

[3] Chau, F. P. 1989 The second-order velocity potential for diffraction waves by fixed offshore structures. PhD. Thesis, University College London.

[4] Davies, B. 1978 *Integral Transforms and their applications.* Dover.

[5] Eatock Taylor, R. & Hung, S. M. 1985 Second-order diffraction forces on a vertical cylinder in regular waves. *Applied Ocean Research* 6 (2), 19.

[6] Emmerhoff, O. J. & Sclavounos, P. D. 1991 Slow-drift simulations of a multi-leg structure in a short crested sea state. *Proc. 6th Intl Workshop on Water Waves and Floating Bodies, Woods Hole.*

[7] Emmerhoff, O. J. & Sclavounos, P. D. 1992 The slow-drift motion of arrays of vertical cylinders. *J. Fluid Mech.*, **242** 31-50.

[8] Emmerhoff, O. J. & Sclavounos, P. D. 1993 The slow yaw motion of offshore structures. *Proc. 8th Intl Workshop on Water Waves and Floating Bodies, St. John's.*

[9] Faltinsen, O. M. & Løken, A. E. 1978 Drift forces and slowly varying horizontal forces on a ship in waves. *Symposium on Applied Mathematics dedicated to the late Prof. Dr. R. Timman*, Delft, Netherlands.

[10] Faltinsen, O. M. 1990 *Sea loads on ships and offshore structures.* Cambridge University Press.

[11] Gradshteyn, I. S. & Ryzhik, I. M. 1980 Table of integrals, series and products. Academic Press.

[12] Greenberg, M. D. 1978 *Foundations of applied mathematics.* Prentice-Hall.

[13] Grue, J. & Palm, E. 1992 Mean yaw moment on floating bodies advancing with a forward speed in waves. Preprint Series, Institute of Mathematics, University of Oslo.

[14] Grue, J. & Palm, E. 1993 The mean drift force and yaw moment on marine structures in waves and current. *J. Fluid Mech.* **250**, 121-142.

[15] Johnsen, J. M. & Naess, A. 1991 Time variant wave drift damping and its effect on the response statistics of moored offshore structures. *Proc. First Intl Offshore and Polar Eng. Conference (ISOPE-92), Edinburgh.*

[16] Hildebrand, F. B. 1976 *Advanced calculus for application.* Second edition. Prentice-Hall.

[17] Kim, M.-H. & Yue, D. K. P. 1991 The complete second-order diffraction solution for an axisymmetric body. Part 2. Bichromatic incident waves and body motions. *J. Fluid Mech.* **211**, 557-593.

[18] Korsmeyer, F. T., Lee, C.-H., Newman, J. N. & Sclavounos, P.D. 1988 The analysis of wave interactions with tension leg platforms. In *Proc. OMAE Conference*, Houston, Texas.

[19] Lee, C.-H., Newman, J. N. & Yue, D. K. P. 1991 The computation of second-order wave loads. *Proc. 9th OMAE Conference.*

[20] Linton, C. M. & Evans, D. V. 1990 The Interaction of Waves with Arrays of Vertical Circular Cylinders. *J. Fluid Mech.* **215**, 549-569.

[21] Marthinsen, T. 1989 Hydrodynamics in TLP design. *Proc. 8th OMAE Conference.*

[22] Mei, C. C. 1989 *The applied dynamics of ocean surface waves.* World Scientific.

[23] Molin, B. 1979 Second-order diffraction loads upon three dimensional bodies. *Applied Ocean Research* **1**, 197-202.

[24] Newman, J. N. 1967 The drift force and moment on ships in waves. J. Ship Res. **11**, 51-60.

[25] Newman, J. N. 1977 *Marine Hydrodynamics.* M. I. T. Press, Cambridge, Mass.

[26] Newman, J. N. 1978 The theory of ship motions. *Adv. Appl. Mech.* **18**, 221-283.

[27] Newman, J. N. 1993 Wave-drift damping of floating bodies. *J. Fluid Mech.* **249**, 241-259.

[28] Nielsen, F. G. 1987 Approximation of the drift forces on submerged bodies in long waves. *Proc. of the 6th Intl Offshore Mech. and Arctic Eng. Symp.*

[29] Nielsen, F. G., Herfjord, K. & Løken A. 1990 Floating production systems in waves. Results from a comparative study on hydrodynamic coefficients, wave forces and motion responses. Norsk Hydro Research Center.

[30] Nielsen, F. G., Herfjord, K., Hunstad, G. & Olsen, G. 1994 Dynamic characteristics of a large catenary moored production platform. *Proc. 7th OMAE Conference, Boston.*

[31] Nossen, J., Grue, J. & Palm, E. 1991 Wave forces on three-dimensional floating bodies with small forward speed. *J. Fluid Mech.* **227**, 135-160.

[32] Ogilvie, T. F. & Tuck, E. O. 1969 A rational strip theory for ship motions - Part 1. *Report No. 013, Dept. of Naval Architecture and Marine Engineering, Univ. of Michigan, USA.*

[33] Ogilvie, T. F. 1983 Second-order hydrodynamic effects on ocean platforms. *Proc. Intl Workshop on Ship and Platform Motions, University of California, Berkeley.*

[34] Palm, E. & Grue, J. 1994 Wave forces on floating bodies in slow yaw-motion. *Proc. Intl OMAE Conference, Boston.*

[35] Papoulis, A. 1984 *Probability, random variables, and stochastic processes.* Second edition. McGraw Hill Book Company.

[36] Pinkster, J. A. & Oortrmerssen, G. van 1977 Computation of the first and second-order wave forces on oscillating bodies in regular waves. *Second Intl Conf. of Numerical ship Hydrodynamics*, University of California, Berkeley.

[37] Potter, M. C. & Foss, J. F. 1975 *Fluid mechanics.* Great Lakes Press.

[38] Press, W. H., Flannery, B. P., Teukolsky, S. A. & Vetterling, W. T. 1990 *Numerical recipes (FORTRAN version).* Cambridge University Press.

[39] Rottmann, K. 1985 Matematische Formel Samlung. Wissenschaftsverlag.

[40] Sclavounos, P. D. 1988 Radiation and diffraction of second-order surface waves by floating bodies. *J. Fluid Mech.* **196**, 65-91.

[41] Sclavounos, P. D. 1990 Responses of marine structures to sea loads. Class notes, 13.03 MIT.

[42] Sclavounos, P. D. 1990 The slow-drift oscillations of a floating body. *Proc. 5th Intl Workshop on Water Waves and Floating Bodies, Manchester.*

[43] Sclavounos, P. D. & Emmerhoff, O. J. 1992 Slow-drift simulations of multi-leg structures in regular and random waves. *Proc. 6th BOSS Conference, London*

[44] Sclavounos, P. D. 1994 Slow-drift oscillations of compliant floating platforms. *Proc. 7th BOSS Conference, Boston.*

[45] SWIM Version 2.0, user manual. MIT, 1993.

[46] Triantafyllou, M. S. 1978 Design of the dynamic positioning system of a drilling vessel. PhD. Thesis, MIT.

[47] Triantafyllou, M. S. 1982 A consistent hydrodynamic theory for moored and positioned vessels. *J. Ship Res.* **24**, 40-44.

[48] WAMIT Version 4.0, user manual. MIT, 1991.

[49] Wichers, J. E. W. & Sluijs, M. F. van 1979 The influence of waves on the low-frequency hydrodynamic coefficients of moored vessels. *Proc. Offshore Technology Conf., Houston*, OTC 3625.

[50] Zhao, R. & Faltinsen, O. M. 1988 Interaction of waves and current on a 2-D body in the free surface. *Applied Ocean Research* **10**, 87-99.

[51] Zhao, R. & Faltinsen, O. M. 1990 Interaction between current, waves and marine structures. *5th Intl Conf. on Numerical ship Hydrodynamics, 1989.* Washington: National Academy Press.